LAMINAR FLAME SPEED AND MARKSTEIN LENGTH MEASUREMENTS OF VARIOUS MULTI-COMPONENT LIQUID FUELS WITH DETAILED UNCERTAINTY ANALYSIS

A Dissertation

by

CHARLES LEWIS KEESEE

Submitted to the Office of Graduate and Professional Studies of
Texas A&M University
in partial fulfillment of the requirements for the degree of

DOCTOR OF PHILOSOPHY

Chair of Committee,	Eric L. Petersen
Committee Members,	Timothy Jacobs
	Waruna Kulatilaka
	Adonios Karpetis
Head of Department,	Andreas A. Polycarpou

December 2019

Major Subject: Mechanical Engineering

ABSTRACT

New laminar flame speed experiments have been conducted for various traditional and alternative kerosene-based liquid fuels. These fuels included: Jet-A, RP-1, Diesel Fuel #2, Syntroleum S-8, Shell GTL, and n-decane. Understanding the combustion characteristics of these fuels is an important step in developing new chemical kinetics mechanisms that can be applied to real fuels. The precise composition of these fuels is known to change from sample to sample. Additionally, their low vapor pressures cause uncertainties in their introduction into gas-phase mixtures, hence leading to uncertainty in the mixture equivalence ratio.

Multiple methods were implemented to help reduce and quantify the experimental uncertainty of these mixtures. One of these was an *in-situ* absorption technique. The diagnostic utilized a 3.39-μm HeNe laser in conjunction with Beer's Law. Other techniques included finding better syringes to inject the fuel to ensure all of the fuel entered the vessel. Also improved were the methods to fill the vessel switching from solely relying on the partial pressure to include measuring the mass of fuel injected. This addition also allowed for back-calculating the molecular weight of the injected fuel to verify the liquid fuel had vaporized and was behaving as an ideal gas.

The resulting spherically expanding, laminar flame experiments were conducted over a range of equivalence ratios from $\varphi = 0.7$ to $\varphi = 1.5$ at initial conditions of 1 atm and 403 K (all fuels except DF #2). Overall, the fuels showed similar behavior with all fuels having a peak flame speed between 56 cm/s and 60 cm/s, at an equivalence ratio between

$\varphi = 1.15$ and $\varphi = 1.25$. While this peak value is richer than typically seen in literature, it is shown that the average fuel molecule used throughout these studies is inconsistent. Therefore it is suggested that using fuel mole fraction as opposed to equivalence ratio is a better parameter when comparing results from different data sets. Analysis also showed a strong linear correlation between Markstein length and equivalence ratio. This was used to help verify the accuracy and acceptability of some of the data points.

ACKNOWLEDGMENTS

First and foremost I would like to thank my advisor, Dr. Eric L. Petersen. His continuous support and direction have significantly helped me through this project. I also want to thank my committee: Dr. Jacobs, Dr. Kulatilaka, and Dr. Karpetis (who took over following the passing of Dr. Mannan).

I would also like to thank all of my friends and colleagues at the lab both former and current. This particularly includes the laminar flame speed group: Anibal, Travis, Mattias, and Bill. The countless hours we spent working together setting up experiments or solving problems such as aligning optics, searching for leaks, or discussing general flame speed concepts have been immensely helpful. This project could not have been completed without them.

Finally, I would like to thank my family for their continued love and support. Especially my wife, Tammie, who put up with me coming home at night and wanting to discuss my most recent experiments. This work could not have been completed without all of your support.

CONTRIBUTORS AND FUNDING SOURCES

Contributors

This work was supervised by a dissertation committee consisting of Professors Eric L. Petersen, Timothy Jacobs, and Waruna D. Kulatilaka, of the Department of Mechanical Engineering and Professor Adonios Karpetis of the Department of Aerospace Engineering.

Additional analysis of the first three kerosene-based fuels was performed by Michael Gaskins and Juan Ramirez at TDI Brooks International. The GC-MS analysis of decane was performed by the Chemistry Mass Spectrometry Facility in the Department of Chemistry at Texas A&M. The five primary kerosene-based fuels used in this study were provided by Dr. Tim Edwards at the Air Force Research Laboratory in Dayton, OH.

The MATlab based code used for flame speed analysis was written by Dr. Travis Sikes.

All other work conducted for the dissertation was completed by the student independently.

Funding Sources

Graduate study was initially supported in part through the Post 9/11 GI Bill. Specific funding for the research was through the Qatar National Research Fund award NPRP8-1358-2-579 and the National Science Foundation via a Veteran's Research Supplement under grant number EEC-1560155.

NOMENCLATURE

φ	Equivalence Ratio
$S_{L,u}^{0}$	Laminar unburned, unstretched Flame Speed
P_b	Burned gas Pressure
ρ_b	Burned gas Density
T_b	Burned gas Temperature
P_u	Unburned gas Pressure
ρ_u	Unburned gas Density
T_u	Unburned gas Temperature
$\vec{V}_b$	Burned gas Velocity
$\vec{V}_0$	Unburned Gas Velocity
AFRL	U.S. Air Force Research Laboratory
POSF	AFRL Fuel designation, not an acronym
H/C	Hydrogen to Carbon Ratio
MW	Molecular Weight
ρ	Density
T_{cr}	Critical Temperature
P_{cr}	Critical Pressure
T_r	Reduced Temperature
P_r	Reduced Pressure
Z	Compressibility Factor

P	Pressure
V	Volume
n	number of moles
R_u	Ideal Gas Constant
T	Temperature
$t_{0.5}$	Half-life of species
NPT	National Pipe Thread
S_b	Stretched Burned Gas Flame Speed
S_b^0	Unstretched Burned Gas Flame Speed
L_b	Burned Gas Markstein Length
r_f	Radius of flame
σ	Density Ratio
m_{FUEL}	Mass of Fuel
$Syringe_{FULL}$	Mass of Syringe filled with fuel
$Syringe_{empty}$	Mass of Syringe Empty
N_{FUEL}	Moles of Fuel
I	Transmitted Intensity
I_0	Incident Intensity
σ_v	Absorption Cross Section
X_i	Mole Fraction of species i
X_{FUEL}	Fuel Mole Fraction
L	Path Length

$N_{O2,stoic}$	Stoichiometric number of moles of O2
U_{SL}	Total uncertainty
B_{SL}	Bias uncertainty
P_{SL}	Random Error
x_i	Variable i
u_i	Uncertainty in measurement i
a	Stoichiometric amount of O_2
b	Stoichiometric CO_2 following combustion
d	Stoichiometric H2O following combustion
$mass_{O_2}$	Mass of O_2
a_r	Markstein Length Correlation Coefficient

TABLE OF CONTENTS

Page

LIST OF FIGURES

Page

LIST OF TABLES

Page

CHAPTER I

INTRODUCTION

Kerosene-based fuels continue to be among the primary energy sources in the world. However there are still gaps in the research of the fundamental combustion chemistry of these fuels. This combustion chemistry needs to be better understood before moving on to study new, alternative fuel sources. Kerosene is especially complicated to study because it is a blend which can contain hundreds to thousands of different hydrocarbons. This complexity leads to difficulty in both repeatability of experiments and the development of a good chemical kinetics model that can be used for multiple kerosene-based fuels.

One of the key measurements used to validate chemical kinetics mechanisms is the laminar flame speed. Physically, the laminar flame speed is the speed at which an adiabatic, one-dimensional flame propagates through an infinite fuel-oxidizer mixture. A diagram of this is shown in Figure 1. However the ideal condition cannot be duplicated in laboratory conditions. Because of this limitation, there are a variety of techniques used to measure flames that simulate or otherwise approach this condition. The results can then be extrapolated to the one-dimensional condition of the physical definition. These include: the Bunsen Burner Method, the Heat Flux Method, the Counterflow or Stagnation method, and the spherical flame method. The spherical flame method is used for all experiments included in this study, and is described in detail later. The other methods are identified when used throughout the literature review. Since each method extracts laminar flame

speed in a different manner, the results from all these methods could vary slightly from method to method.

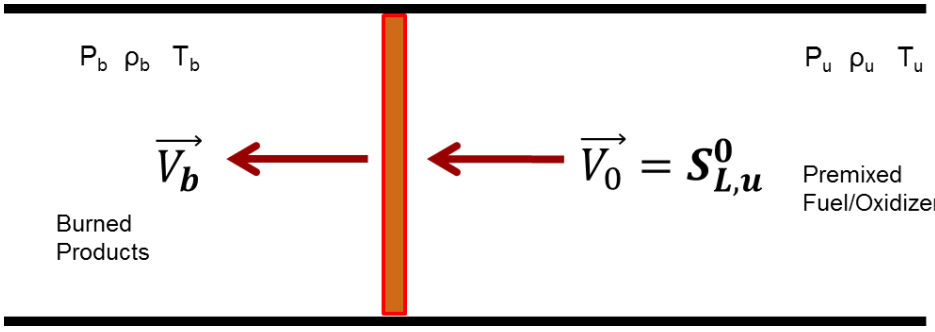

Figure 1. Ideal condition of an adiabatic, one-dimensional flame in the reference frame of the flame front.

Accurate knowledge of the laminar flame speed is key to the development and validation of chemical kinetics mechanisms. However, the laminar flame speed of kerosene-based fuels is not well known, with no consistent answers in the literature, making it difficult to accurately validate the chemical kinetics mechanisms and apply them to these fuels.

The actual chemical makeup of kerosene-based fuels varies from one production batch to the next, leading to additional complications in comparing results from different research groups. The primary distributer of fuel to research groups, at least in the United States, is the U.S. Air Force Research Laboratory (AFRL), which helps alleviate the problem somewhat. AFRL assigns what is known as a POSF number, which is a sequential number, to batches of fuel as they are received, as discussed by Edwards [1]. This number is used to identify a specific batch of fuel. When samples of fuel are shipped to various

research groups, the POSF number and other basic chemical information such as average molecular weight and percent hydrogen content (by weight) are provided, allowing researchers to know if they are using the exact same fuel as their counterparts.

Kerosene-based fuels are heavy liquid hydrocarbons. They have a very low vapor pressure. To measure laminar flame speed, all fuel and oxidizer components need to be in the vapor phase. Practically, the low vapor pressure requires heating of at least some portion of the experimental system to get the fuel into the vapor phase to conduct flame speed experiments. As pointed out by Ji et al. [2], this goal requires a careful balance of potential fuel condensation at cold spots and runs the risk of fuel cracking at hot spots in the experimental system. However there has arguably been no well-defined techniques utilized to address such concerns in laminar flame speed experiments. As is seen in the literature review, precision instruments are typically used to measure the amount of fuel in the system, by either measuring partial pressure, liquid volume, or mass flow rate. However, no technique has previously been utilized to measure the total gaseous fuel-air mixture in flame speed experiments of the type of interest to this dissertation.

The purpose of the present study was to conduct laminar flame speed experiments of kerosene-based fuels, new alternative fuels, and one of the key components of these fuels, taking into account true uncertainties involved. The corresponding results will add to the available data that can be used to develop chemical kinetics mechanisms. This dissertation also includes a detailed analysis of the types and sources of uncertainty that is inherent in these experiments, an area that up to this point has not been fully addressed.

Understanding and minimizing all of the sources of uncertainty in these measurements is key to moving toward consistent, repeatable results. Therefore, these sources were carefully addressed. These include finding better methods to inject the fuel into the vessel insuring that the amount of fuel thought to be in the vessel is actually in the vessel. Also included is the implementation of an *in-situ* laser absorption technique to help measure uncertainties in the equivalence ratio. Additional methods have also been implemented to measure the actual mass in the experiment vessel, and therefore the number of moles of fuel injected into the system as a means to more accurately determine the fuel-air mixture. As shown in this dissertation, the largest source of uncertainty is accurately knowing the average chemical formula of the fuel. Accounting for these differences when comparing results from different research groups appears to be very important.

This dissertation begins with a thorough review of the relevant literature including both developments of new chemical kinetics mechanisms and experimental studies. This literature review is followed in Chapter III by a discussion of the fuels used and their chemical composition. Chapter IV describes in detail the experimental setup used throughout this study. Chapter V provides a detailed look at the experimental process for the single component n-decane. Chapter VI provides a detailed uncertainty analysis. Flame speed results for all of the kerosene-based fuels are presented in Chapter VII, and Chapter VIII discusses different ways to analyze the data especially when comparing results to those of different research groups including chemical kinetics mechanisms. Finally, conclusions are presented in Chapter IX.

CHAPTER II

LITERATURE REVIEW

Previous fundamental combustion studies on liquid fuels typically fall into one of three categories. These categories are:

1) Purely experimental which compare new data to a surrogate fuel using a chemical kinetics mechanism already in existence.
2) Analytical studies focused on proposing new and potentially better surrogates for kerosene based on fuel properties. These studies typically also improved on or developed new chemical kinetics mechanisms.
3) Studies that conducted some combination of the previous two categories.

For clarity, this dissertation presents the literature simultaneously for the three categories described above, from oldest to newest; however all work published by a single research group is kept together. This exception includes studies that while done by different research groups were clearly directly related. As most studies have focused on Jet-A, that is the primary focus of this literature review, however when other fuels were tested they are also included in this review.

First it is important to understand what a surrogate fuel actually is. Surrogate fuels are blends of a few hydrocarbons that are commonly used to model the complex mixtures of hundreds of hydrocarbons typically found in kerosene-based fuels. Basic guidelines on

how to develop a good surrogate mixture were proposed by Edwards et al. [3]. Surrogate formulas typically fall into one of two categories, physical surrogates or chemical surrogates. A physical surrogate is a mixture that typically has the same physical properties, such as density, viscosity, thermal conductivity, etc., as the actual fuel. A chemical surrogate is designed to have the same chemical-class composition and same average molecular weight as the actual fuel [3]. Some of the first surrogates proposed sometimes had upwards of 15 components, while single-component surrogates such as n-decane or n-dodecane were also suggested. Most of the surrogates that have been proposed in recent years have contained between two and six components.

Jet Fuel Flame Speeds from the Literature

The work of Violi et al. [4] looked at finding a surrogate for JP-8, which is the U.S. military equivalent to Jet-A. One of the complications noted in their study is that these fuels consist of thousands of species, with few exceeding 1% by volume. There was also concern about the composition of the fuel changing over time. Various properties of the fuel were focused on to find a suitable surrogate, specifically: feasibility (known kinetic mechanism), simplicity (limit the number of carbon atoms per class of species), similarity (match physical properties), and cost. From these criteria, three surrogate blends were identified. One of these, identified as "Sur_1" was a six-component blend that was later used for comparison in the experimental study of Singh et al. [5]. This six-component blend consisted of: 30% n-dodecane, 20% n-tetradecane, 10% iso-octane, 20% Methylcyclohexane (MCH), 15% m-xylene, and 5% tetralin by volume. There is some

confusion about the use of volume fraction. For purely gaseous mixtures this would be the same as a mole fraction. With liquid fuels this is not the case. However, it is assumed that when they mean mole fraction in this case. This assumption is based on two factors: it is how the surrogate was used in [5], and all other studies by the same research group, discussed below specifically state mole fraction. The other two blends, "Sur_2" and "Sur_3" were not used or referenced beyond this initial study.

The experimental results of [5] were compared to "Sur_1" [4], using the chemical kinetic mechanism developed by Ranzi et al. [6]. In addition to looking at Jet-A, this study also investigated S-8 and n-decane. These experiments were all conducted using a spherical combustion chamber heated via a custom oven. The very low vapor pressure of liquid fuel required in the mixtures, on the order of 10 Torr, led to concern over significant changes in equivalence ratio due to slight deviations in the pressure gage used. Therefore the liquid volume of the fuel was used to determine equivalence ratio. This fuel was injected using a 24-inch-long needle that had a 1/16-inch diameter. This description appears to be that of a 14-gauge needle. Fuel condensation was not believed to be a concern because the fuel was injected directly into the heated vessel. Once the fuel-air mixture was prepared, it sat for ten minutes prior to firing the experiment to ensure total mixing. The unburned, unstretched laminar flame speed was calculated using a nonlinear method. A 12-component surrogate with an average formula of $C_{10.6}H_{20.2}$ was used to calculate the properties of Jet-A. Likewise, a seven-component surrogate with an average formula of $C_{11.4}H_{24.8}$ was used to calculate the properties of S-8.

Overall they found that the model over-predicted the flame speed for Jet-A by 10 to 15 cm/s, with an experimental uncertainty of about 4.5%. Their model analysis put the peak flame speed of 69.7 cm/s, with the experimental results putting the peak around 58.1 cm/s. An updated version of the chemical kinetics mechanism called the "Poll Mi mech 2" was published by Ranzi et al. [7] in 2011 which produced laminar flame speeds for Jet-A at 403 K, 1 atm closer to the experimental values (peak around 60 cm/s).

The research group of Dr. Violi proposed two new four-component surrogates for conventional jet fuel in the work of Kim et al. [8]. The first surrogate, labeled "UM1" is a blend of 38.44% n-dodecane, 14.84% iso-cetane, 23.36% decalin, and 23.36% toluene by mole fraction. The second surrogate, "UM2" is a blend of 28.97% n-dodecane, 14.24% iso-cetane, 31.88% decalin, and 24.91% toluene also by mole fraction. "UM1" was chosen because it provided a good match for temperature-independent properties, whereas "UM2" better matched the density and volume properties of the liquid fuel.

The following study of Kim et al. [9] expanded the surrogate to six components. This version was designed to adjust based on the specific kerosene fuel being evaluated. The six components included are: n-dodecane, n-decane, iso-cetane, iso-octane, decalin, and toluene. For all three fuels investigated, conventional Jet-A, S-8, and a coal-derived IPK, the surrogate mechanism still reduced to four components. This 4-component result was because two of the six had negligible concentrations. Interestingly, while the four components present in the new Jet-A surrogate are the same as UM1 and UM2 the concentrations are different. This difference was based on the derived Cetane number of the surrogate. The most recent work of Kim et al. [10] proposed yet another surrogate

mixture. This study was designed to account for larger hydrocarbon molecules that might not be currently available in chemical kinetics mechanisms. The added species included n-tetradecane and 1,2,4,5-tetramethylbenzene. As with the previous studies, the Cetane number of the component was the primary consideration. These studies were focused on developing a surrogate and did not present or compare to any new laminar flame speed data.

A two-component surrogate, labeled the "Aachen Surrogate," was proposed by Honnet et al. [11]. This surrogate consists of 80% decane and 20% 1,2,4 trimethylbenzene, by weight. This surrogate was based on the n-decane mechanism previously proposed by Bikas et al. [12]. The peak laminar flame speed for the "Aachen Surrogate" at 403 K and 1 atm was 68.1 cm/s and occurred around $\varphi = 1.1$.

The Aachen surrogate was used as the initial comparison point for the three successive studies conducted by Dr. Chih-Jen Sung's research group described in detail below. All of these studies presented laminar flame speed data that were collected on what appears to be the same Counterflow Twin-Flame Configuration setup. However, these studies also produced three different sets of results and don't appear to reference each other.

The first of these studies was published by Kumar et al [13], in 2011. The two fuels investigated were Jet-A and S-8. Laminar Flame speeds were measured at atmospheric pressure and three initial temperatures: 400, 450, and 470 K over a range of equivalence ratios from 0.7 to 1.4. The unstretched flame speed was determined using a linear extrapolation method. Experimental uncertainties were discussed with a less than 2%

uncertainty in equivalence ratio and a 5 K uncertainty in initial temperature. A twelve component surrogate was used to calculate equivalence ratio for Jet-A, whereas a ten component surrogate was used for S-8. Neither the composition of these surrogates nor their average molecules were specified.

The following year, 2012, another set of results was published by Hui et al. [14]. In addition to reinvestigating Jet-A and S-8, this study also looked at five additional alternative jet fuels, one of which was Shell GTL. While the range of equivalence ratios tested was the same as the previous study by the same group, only two temperatures, 400 and 470 K, were investigated in this latter study. Like the previous one, this study also used a linear extrapolation method to determine the unstretched flame speed. While admitting that this produced slightly higher results, this was done due to the lack of thermodynamic and transport properties for the alternative fuels studied. This particular study by the Sung group was the first one to provide average molecules for Jet-A POSF 4658 ($C_{10.174}H_{19.913}$), S-8 POSF 4734 ($C_{11.847}H_{25.502}$) and Shell GTL 5172 ($C_{10.26}H_{22.597}$). However, laminar flame speed results were only provided for Jet-A.

A third study by the same group was published in 2013 by Hui et al. [15]. This one investigated a large range of fuels at multiple temperatures and pressures. In addition to providing new results for laminar flame speeds for Jet-A and S-8, it also provided new results for some of the typical components used in surrogates such as n-decane, n-dodecane, and toluene. This study acknowledged the need to account for both fuel condensation and fuel cracking of the heavy hydrocarbon fuels. Unlike their previous investigations, in this one the authors used a nonlinear extrapolation method to determine

the unstretched laminar flame speed. The average molecule for Jet-A (POSF 4658) was stated as $C_{10.17}H_{19.91}$, with an average MW = 142 ± 20 g/mol, While this is essentially the same average molecule as used the previous year, the overall uncertainty in molecular weight is 14%.

In general, the results from the studies of Dr. Sung's group appear to be slightly faster than results reported by other groups. This difference was also noted when looking at the laminar flame speed data for the single-component fuel, n-decane, in the review conducted by Konnov et al. [16]. Typical results for n-decane showed a peak flame speed of 60 ± 2 cm/s at 400 K. The works of Kumar et al. [15,17] produced results 8 cm/s and 5.5 cm/s faster, respectively. This common result translates to a range of 9.2% to 13.3% faster than other experimental data, for decane, available in literature.

Single-component alkane flames ranging from C_5 through C_{12} were investigated by [2]. These laminar flame speed experiments were performed at atmospheric conditions over a wide range of initial temperatures and pressures using the counterflow configuration. Experimental results were compared to the "JetSurF 0.2" mechanism, which was current at the time. A syringe pump was used to introduce the liquid fuel into the system resulting in an estimated 0.5% uncertainty in equivalence ratio. Experimental results were calculated using both linear and non-linear methods with the linear method always returning slightly faster flame speeds. This difference became greater at rich conditions. In the results for dodecane, it was noted that their data were significantly slower than the results reported in [17]. It was also noted that the discrepancy appeared to be caused by more than the difference between linear and non-linear extrapolation. The

next study by Ji et al. [18] looked at both conventional and alternative jet fuels including fuels such as JP-7, JP-8, S-8, R-8 (a synthetic derived from animal and vegetable oil), and Shell-GTL in the same counterflow configuration used in the previous paper [2]. Experiments were conducted at 403 K and 1 atm over a range of equivalence ratios from $\varphi = 0.7$ to $\varphi = 1.5$. Results were then compared to model predictions of decane and dodecane using "JetSurF 1.0" mechanism.

A three-component surrogate for Jet-A was proposed by Dooley et al. [19]. This mixture of n-decane, iso-octane, and toluene was formulated to match the hydrogen-to-carbon (H/C) ratio and the derived Cetane number of the target fuel, in this case Jet-A (POSF 4658). A chemical kinetics model for this surrogate was developed by combining existing models for the pure components. However, no laminar flame speed data were presented in this initial study.

In a follow on study, Dooley et al. [20] proposed a four-component surrogate. The new surrogate, labeled "2nd Generation" consists of n-dodecane, iso-octane, 1,3,5-trimethylbenzene, and n-propylbenzene. The three-component surrogate from the previous study [19] is now labeled "1st Generation". This second study includes experimental laminar flame speed results for both generations of the surrogate with experimental results for Jet-A at 1 atm at both 400 and 470 K. It appears that in this collaborative work the laminar flame speed experiments were conducted by Chih-Jen Sung's group at the University of Connecticut, using linear extrapolation. The chemical kinetics mechanism for the "2nd Generation" surrogate was further refined in the work of

Malewicki et al. [21]. This study used shock-tube ignition delay time data as a comparison point for model validation.

Chong et al. [22] investigated laminar flame speeds of several liquid fuels including Jet-A1 and diesel using a jet-wall stagnation flame and particle imaging velocimetry (PIV) at 470 K. The primary difference between Jet-A and Jet-A1 is the freezing point [23]. This study was the first and only known to date to investigate the laminar flame speed of diesel fuel. They saw a significant difference, between 5 and 8 cm/s, when comparing their results for Jet-A to the results presented by Kumar et al. in their 2009 AIAA paper, which appear to be similar to the results they presented in [13]. The explanation given for the difference was the use of different batches of jet fuel.

Two different surrogate blends were proposed by Denman et al. [24] using the "JetSurF 2.0" mechanism. Fractions for both blends are given as mole fractions. "Blend 1," containing three components: 82.1% n-decane, 7.9% MCH, and 10% toluene, was formulated to match the H/C ratio of the jet fuel studied. The two-component "Blend 2" contained 59.9% n-decane and 40.4% toluene. It was designed to match to laminar flame speed and adiabatic flame temperature of real jet fuel in air. All flame speed experiments were carried out using the jet-wall configuration. Based on the way the liquid fuel was introduced to their system, uncertainty in equivalence ratio decreased at richer mixtures. At $\varphi = 1.2$, uncertainty was reported at ± 0.0035, whereas at the lean condition of $\varphi = 0.8$ the uncertainty was about 10 times greater at ± 0.034. Uncertainty in temperature readings was reported to be within 7 K.

The study of Moghaddas et al. [25] investigated the laminar flame speed of n-decane, believed to be one of the key components of jet and diesel fuel surrogates. They attributed the discrepancies in the literature data to a combination of flame stretch and experimental error. Because of this hypothesis, they paid close attention to flame instability, which was known to be greater at rich conditions. Therefore experiments were limited to lean and stoichiometric mixtures.

Laminar flame speed measurements of three, single-component fuels as well as two binary blends and one tertiary blend were reported in the work by Comandini et al. [26]. One species was chosen from each of the main hydrocarbon classes: n-decane, n-butylbenzene, and n-propylcyclohexane. This comprehensive study was the first to specifically look at mixtures of these three species. These experiments were conducted in a spherical bomb at 403 K and 1 atm. Mixtures were prepared using the partial pressure method, and results were compared to the "JetSurF 2.0" mechanism.

The study of Kick et al. [27] looked at several synthetic fuels. This work included both Gas-to-Liquid (GtL) and Coal-to-Liquid fuels (CtL). Experiments were conducted at stoichiometric and rich conditions using the Bunsen burner method. The fuel was vaporized at temperatures up to 600 K. Fuel cracking was determined to not be an issue below around 770 K. The vaporized fuel was then mixed with nitrogen and cooled prior to adding O_2 to prevent early ignition. Four factors were determined that limited the accuracy of this method: "temperature and mass flow rate of unburnt gases, determination cone angles, and pressure" [27]. It was also determined that flame speeds derived using this method would be different from results originated from stretch-corrected methods.

Dagaut et al. [28] investigated a GtL synthetic kerosene as well as a surrogate at 473 K. Experiments were conducted using a Bunsen burner flame at an initial temperature of 473 K, from $\varphi = 1.0$ to 1.5. Experiments were limited to rich and stoichiometric flames because flame angle could not be stabilized at lean conditions. These experiments were conducted on the same test rig and in the same manner as described in [27]. Mass flow rate and unburned gas temperature were identified as two of the key uncertainties in their measurements resulting in an overall total error of 5% in laminar flame speed. There was also a 2% uncertainty in equivalence ratio stated.

The recent study of Narayanaswamy et al. [29] combined three of their previous single-component mechanisms, [30-32], to develop a new chemical kinetics mechanism specifically tuned for their proposed surrogate Jet-A that consisted of: 30.3% n-dodecane, 21.2% m-xylene, and 48.5% MCH by mole fraction. This study compared experimental results from [5, 13, 14, 18] to their mechanism.

The study of Koniavitis et al. [33] used their newly developed technique that combines Rate-Controlled Constrained Equilibrium with Computational Singular Perturbation to reduce a chemical mechanism for kerosene. As a starting point, they used the mechanism developed in [29]. The main purpose of this study was to show that they could reduce a complex mechanism with their method. Results for their reduced mechanism are compared to results for the original mechanism, with the reduced model predicting a slightly slower flame speed. No experimental data were used for comparison in this study.

The single-component surrogate of n-decane and a binary surrogate mixture containing 80% n-decane and 20% benzene by liquid volume were proposed by Alekseev et al. [34]. Since the percentages were given in the paper as liquid volume as opposed to gas volume, these numbers need to be adjusted to either mole fractions or mass fractions. The resultant mole fractions are: 64.66% n-decane and 35.34% benzene. The heat flux method was employed to remove uncertainties caused by different stretch-correction methods. These experiments were conducted at 338 and 358 K and then temperature corrected to 403 K to compare their results to the data in literature. This study noted the results from the literature did not agree. It was pointed out that spherical flames consistently produced flames that were about 5 cm/s slower at the peak than heat flux or counterflow flames. However, they could not point out any clear cause of the discrepancy.

Wu et al. [35] studied Jet-A1, a surrogate blend, and pure components using a high-pressure Bunsen burner. The flame edge was captured during experiments using the OH* chemiluminescence technique and the kerosene-PLIF technique. Their experimental results were compared to the three-component surrogate model initially proposed by Dagaut et al. [36], consisting of 74% n-decane, 15% n-propylbenzene, and 11% propylcyclohexane by mole fraction. However for their study [36] converted these to weight fractions, resulting in values of: 76.7%, 13.2%, and 10.1% respectively. It was found that for the heavy hydrocarbon fuels OH* chemiluminescence was unable to capture the full flame edge at rich conditions due to flame tip opening. In these cases, the kerosene-PLIF technique was employed to track the flame edge.

A four-component surrogate for diesel fuel was proposed by Szymkowicz et al. [37]. This surrogate consisted of 37% n-hexadecane, 33% Heptamethylnonane, 18% decahydronaphthanlene, and 12% 1-methylnapthalene. These four components were selected from a pool of 13 components, representing each of the major molecular classes.

Summary Observations

While several groups have collected data for kerosene fuels, particularly Jet-A, there does not appear to be any consensus in the literature as to the correct laminar flame speed. While the data do show a trend that is moving to a slower flame speed, there is still a lot of scatter in experimental results. Different parameters are seen as key for developing a good surrogate model. Some of the more-recent chemical kinetics mechanisms are specifically tuned to run for a specific surrogate, which limits their usefulness when exploring new fuels. Unfortunately, the amount of experimental data used as comparison points for new models is not as extensive as it initially appears. While some groups have done independent experimental studies, most of the data used to compare models were taken from one of the many studies of Chih-Jen Sung's group which, as pointed out by [16], are suspected of being on the fast side. Previous groups have quantified their uncertainty in mixture equivalence ratio, biased solely on the accuracy of their instrumentation, and have not used any secondary diagnostic technique to verify the mixture equivalence ratio.

As discussed previously, every production batch of kerosene is different. This variation leads to the potential for laminar flame speed results to change over time and

from paper to paper. For most of the experimental studies discussed above, the Jet-A studied was POSF 4658, with an average molecule of $C_{10.17}H_{19.91}$. This Jet-A was a blend of several batches of Jet-A [8]. To the best of the authors' knowledge, POSF 4658 is no longer being distributed to research groups by AFRL. The current batch of Jet-A at the time of this dissertation is labeled POSF 10325 and has an average molecule of $C_{11.4}H_{22.1}$. When we requested Jet-A, we were automatically shipped POSF 10325. The full effects of a different batch of Jet-A have not been studied.

A summary of some of the proposed surrogates discussed above is shown in Table 1. Key components that tend to be proposed most often in surrogates are: decane, dodecane, and toluene. As shown, most of these surrogates are defined by mole fractions. Additional attention does need to be paid when the definition is based on liquid volume, as this of course is not same as a mole fraction.

Table 1. Summary of proposed surrogate blends for Jet-A and their components.

			Decane	Dodecane	Methycyclohexane	Toluene	n-tetradecane	m-xylene	o-xylene	tetralin	iso-cetane	decalin	1,2,4 trimethylbenzene	1,3,5 trimethylbenzene	iso-octane	n-propylbenzene	Benzene	propylcyclohexane	n-hexadecane
Mole Fraction																			
Violi "Sur_1" [4]				30.00%	20.00%		20.00%	15.00%		5.00%					10.00%				
Violi "Sur_2" [4]*				40.00%		20.00%			8.50%	8.00%		35.00%			3.50%				20.00%
Violi "Sur_3" [4]				73.50%	10.00%	10.00%									5.50%		1.00%		
Kim "UM1" [8]				38.44%		23.36%					14.84%	23.36%							
Kim "UM2" [8]				28.97%		24.91%					14.24%	31.88%							
Dooley "1st Gen" [19]			42.67%			24.31%									33.02%				
Dooley "2nd Gen" [20]				40.40%										7.30%	29.50%	22.80%			
Denman "Blend 1" [24]			82.10%		7.90%	10.00%													
Denman "Blend 2" [24]			59.60%			40.40%													
Narayanaswamy [29]				30.30%	48.50%			21.20%											
Alekseev [34]			64.66%														35.34%		
Dagaut [36]			74.00%										15.00%					11.00%	
Mass Fraction																			
Honnet "Aachen" [11]			80.00%										20.00%						

* The components in "Sur_2" as given in the paper [4] sum to 135%. Other references to this surrogate could not be found.

The average molecule, H/C ratio, and molecular weight of several of the proposed surrogates is shown in Table 2. As can be seen, the H/C ratio tends to range between 1.91 and 2.11. However, the average number of carbon atoms tends to range between 8 and 11. In most of the surrogates, this number is actually between 8 and 10 carbon atoms. These values are well below what the average carbon number for most jet fuels is (i.e., 12) as [20] pointed out.

Table 2. Average Fuel Molecule and H/C ratio for several of the surrogates.

Surrogate	Average Molecule	H/C	MW (g/mol)
Violi "Sur_1" (2002)	$C_{10.3}H_{20.5}$	1.99	144.371
Violi "Sur_3" (2002)	$C_{10.72}H_{22.36}$	2.09	151.290
Kim "UM1" (2014)	$C_{10.958}H_{21.1136}$	1.93	152.892
Kim "UM2" (2014)	$C_{10.687}H_{20.105}$	1.88	148.621
Dooley "1st Gen" (2010)	$C_{8.61}H_{17.27}$	2.01	120.818
Dooley "2nd Gen" (2012)	$C_{9.917}H_{19.426}$	1.96	138.688
Denman "Blend 1" (2012)	$C_{9.463}H_{19.968}$	2.11	133.782
Denman "Blend 2" (2012)	$C_{8.788}H_{16.344}$	1.86	122.022
Narayanaswamy (2016)	$C_{8.727}H_{16.788}$	1.92	121.737
Alekseev (2017)	$C_{8.57}H_{16.35}$	1.91	119.410
Honnet (2009)	$C_{9.77}H_{19.72}$	2.02	137.219

Figure 2 shows the laminar flame speed predictions of several of the surrogates for Jet-A, with their respective kinetics mechanisms. As can be seen, there is a marked variation among them. They do however have the same overall shape. Peak flame speed is predicted to be between φ = 1.05 and φ = 1.2, with a difference of about 15 cm/s between the fastest and slowest.

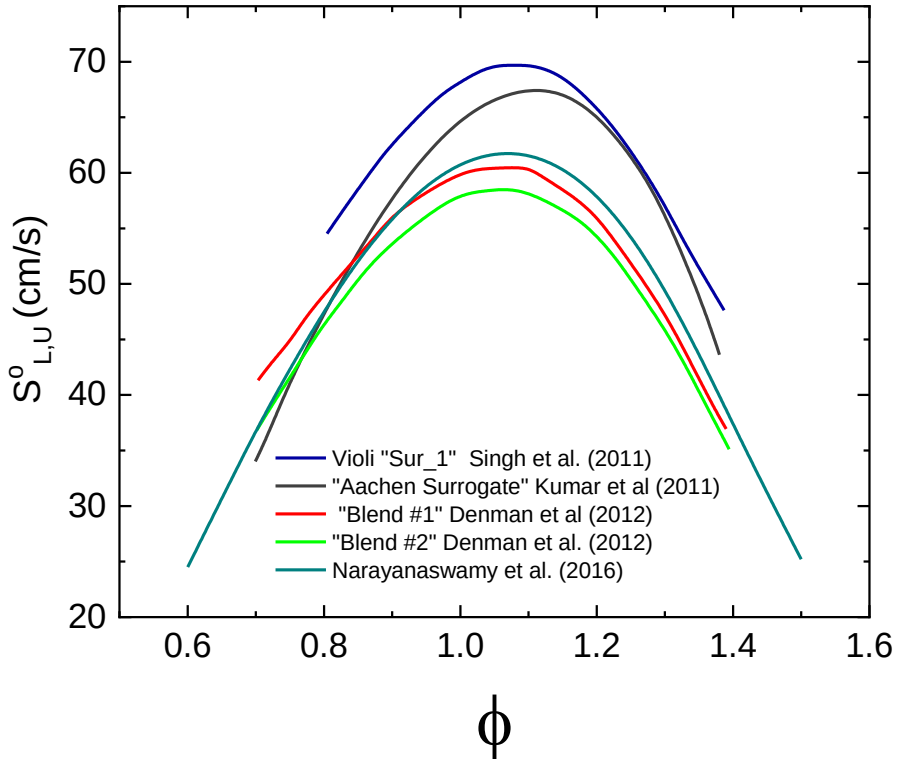

Figure 2. Laminar Flame Speed Predictions of several of the proposed surrogates and chemical kinetics mechanisms for Jet-A at 403 K and 1 atm.

A comparison of the experimental results for Jet-A, or similar fuels, is shown in Figure 3. Similar to the model predictions, there is a lot of scatter. On the lean side, the scatter is on the scale of 5 cm/s. However, there is significantly more scatter for rich mixtures, on the order of 20 cm/s between the different groups.

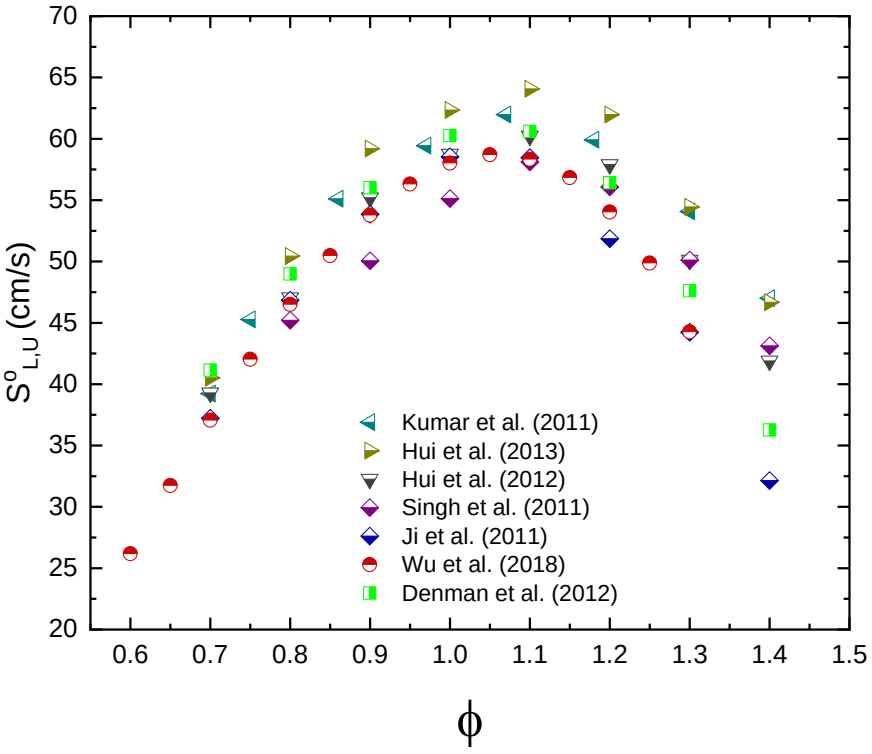

Figure 3. Experimental results for Laminar Flame speed experiments for Jet-A and JP-8 (Ji) conducted near 403 K and 1 atm.

Because of this discrepancy, more data are needed which contain a better understanding of the uncertainties. There also appears to be no agreement on the best way to define the kerosene-based fuel being tested. While some research groups used the measured average molecule of the fuel, other groups claimed the fuel was the surrogate they were attempting to match. When uncertainty was discussed, it was typically given as the minimal uncertainty based on instrumentation for gaseous mixtures but did not account

for the low vapor pressure of the fuel and the related difficulties. These critical but often overlooked items form an important part of the present dissertation.

CHAPTER III

FUELS

There were six different fuels included in this study. The first three of these were typical kerosene-based fuels. These were: Jet-A, RP-1, and Diesel Fuel #2. There were also two alternatively derived kerosene fuels which were Syntroleum S-8 and Shell GTL. The final fuel investigated was n-decane which is one of the key components in kerosene fuels, has been proposed as a single-component surrogate in the past, and is a convenient baseline fuel for method assessment.

All of the fuels used in this study, except for n-decane, were sourced through AFRL. As such, all of them are identified by a POSF number, which allows for a consistent comparison with the data that are available in the literature. A summary of some of the key fuel properties is shown in Table 3. These are the properties used to calculate equivalence ratio and fuel mole fraction throughout this study. The fuels are referred to by their common name (Jet-A, RP-1, etc.) unless they are being directly compared to data from a different study where understanding the batch of fuel is necessary.

Two batches of n-decane were used in this study. As a pure, single-component fuel with well-known properties, it is not important to identify the specific batch of fuel used. The original decane used was sourced from Sigma-Aldrich in 2011. Therefore a new batch of decane was obtained from Alfa Aesar to help verify the overall purity and repeatability of the experiments.

Table 3. Properties of Fuels included in this study.

FUEL	POSF #	Average Molecule	MW (g/mol)	H/C	ρ (g/mL) @ 20 °C
Jet-A	10325	$C_{11.4}H_{22.1}$	159	1.9385	0.803
RP-1	5235	$C_{12}H_{24.1}$	168	2.0083	0.809
Diesel Fuel #2	12758	$C_{13.1}H_{24}$	182	1.8321	
S-8	5018	$C_{11.8}H_{25.6}$	168	2.1695	0.757
Shell GTL	5729	$C_{10.15}H_{22.26}$	144.34	2.193	
n-decane	-	$C_{10}H_{22}$	142.29	2.2	0.73

Shown in are the major class compositions of the five real fuels included in this study. The data were taken directly from information provided by AFRL identifying the batch of fuel. The values shown in Table 4 are given as mass fractions. As these values are rounded to the nearest hundredth of a percent, the values may not add up to 100%.

Table 4. Major Component Classes of Fuels Investigated.

	% Weight				
Molecular Category	Jet-A (POSF 10325)	RP-1 (POSF 5235)	#2 Diesel Fuel (POSF12758)	S-8 (POSF 5018)	Shell GTL (POSF 5729)
Alkylbenzenes	12.90	0.15	14.41	0.16	0.26
Alkylnaphthalenes	2.33	-	-	<0.01	<0.05
Cycloaromatics	3.43	0.04	10.61	0.03	0.02
iso-Paraffins	29.45	35.07	22.10	75.88	55.1
n-Paraffins	20.03	0.46	12.77	23.37	44.0
Monocycloparaffins	24.87	40.41	23.33	0.50	0.59
Dicycloparaffins	6.78	21.66	11.52	0.05	0.07
Tricycloparaffins	0.21	2.19	<0.01	<0.01	-
Diaromatics		<0.01	4.92		
Triaromatics			0.35		

As can be seen, even though these fuels have similar average molecules, their compositions are very different. Jet-A has just under 60% iso- and n-paraffins, and about 30% cycloparaffins, whereas S-8 is almost exclusively (>99%) straight-chain paraffins. The key components of these fuels were initially described as falling into five major categories in Edwards [38]. These included: n-paraffins, iso-paraffins, cycloparaffins, aromatics, and olefins. Looking first at all three types of paraffins, as seen in Table 4, it is easy to see the differences in the three. All three are characterized by single bonds throughout. The difference between iso-paraffins and n-paraffins is the placement of additional methyl radicals in the molecules. For the cycloparaffins, a majority of the carbon atoms form a ring with additional methyl radicals attached on the outside. The monocyclo- , dicyclo-, and tricyclo- referenced in Table 4, refer to the number of methyl radicals attached on the outside of the ring. The general category of "aromatics" listed in [38] was broken out into five separate categories as seen in Table 4. These include: Alkybenzenes, Alkylnaphthalenes, Cycloaromatics, diaromatics, and triaromatics. By far, the most common of these are "Alkybenzenes" which for this purpose include benzene. An example of one of the most common of these species (toluene) is included in Figure 4.

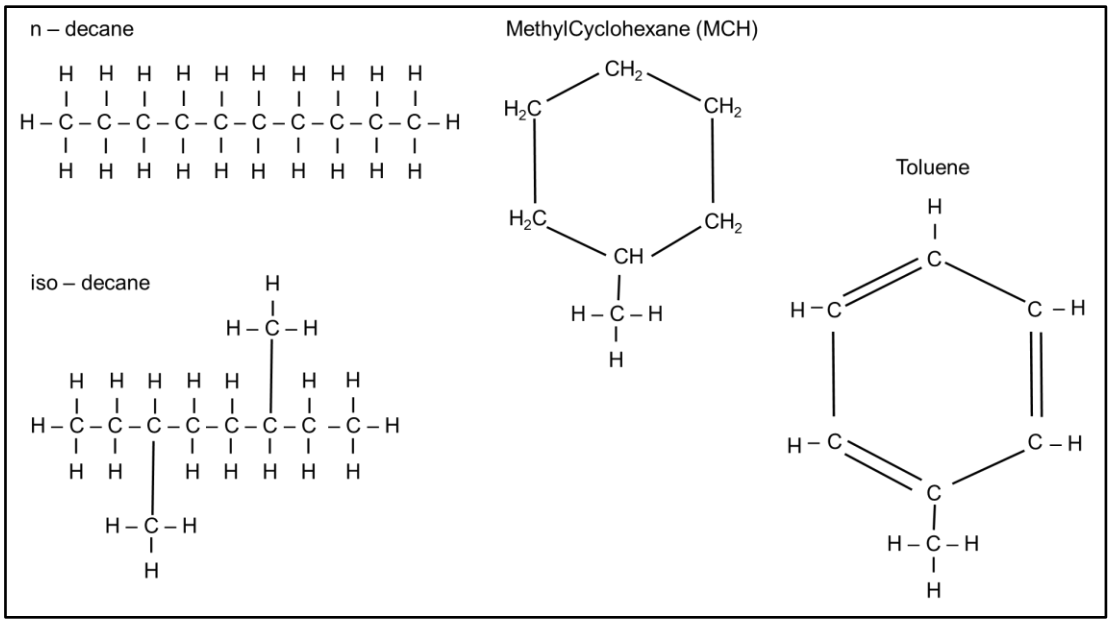

Figure 4. Sample molecules for some common fuel components. These diagrams are based on information in [38] and Turns [39].

Fuel Behavior

Known Average Molecule

As was seen in the literature review, and is discussed in significant detail later, there are several different average molecules, and therefore molecular weights, used for these kerosene-based fuels. The average molecules used throughout this study were provided along with the fuel when it was received from AFRL and are assumed to be correct. These values were obtained using a GC X GC mass spectrometer analysis.

Ideal Gas versus Real Gas

When using the partial pressure method, one of the major assumptions is that all components are in the gas phase and behave as an ideal gas. When dealing with liquid fuels, this is a major assumption that needs to be verified repeatedly.

The well-known ideal gas law is only applicable at high temperatures and low pressures, as described in Çengel et al. [40]. What constitutes high temperature and low pressure are of course relative to the gas to which they are being applied. These are based on the gas' critical temperature, T_{cr}, and pressure, P_{cr}. The critical point is defined as the point where the saturated liquid and vapor states are the same. The reduced temperature, T_r, and pressure, P_r, shown in equations 3.1 and 3.2, are used to help determine if the gas is an ideal gas. Typically if $P_r << 1$ or $T_r > 2$ the gas can be assumed to be ideal [40]. The liquid fuel is injected into the test vessel and vaporizes because the total pressure is below the fuel vapor pressure at the vessel temperature. However, it is important to ensure that there are no lingering real gas effects due to being too close to the saturation point. A way to account for this is to add the compressibility factor, Z, to the ideal gas law as shown in equation 3.3.

$$T_r = \frac{T}{T_{cr}} \tag{3.1}$$

$$P_r = \frac{P}{P_{cr}} \tag{3.2}$$

$$PV = ZnR_uT \tag{3.3}$$

Typically the compressibility factor ranges between 0 and 1, where a compressibility factor of 1 indicates an ideal gas. The compressibility factor can be quickly obtained using a Nelson-Obert Generalized Compressibility Chart.

For all fuels, except Diesel Fuel #2, Z was calculated to be over 0.96 at 403 K. These values are based on the reported MW of the fuel, the experimentally determined vessel temperature, and the volume of the vessel.

Vapor Pressure

The vapor pressure of a gas is the pressure at which a gas starts to condense at a given temperature. An easy way to think of this is the analogous dew point of water in air [40]. If the partial pressure of the fuel gets too high, and therefore the mole fraction increases, the air will not be able to hold it in vapor form and the fuel will condense. However, if the partial pressure of the fuel stays below the vapor pressure then it will remain a vapor. Finding this temperature and pressure combination is useful so the vessel does not have to be heated to a higher temperature than is necessary.

The vapor pressure for Jet-A is reported to be ≈ 3.6 psia (182 Torr) at 403 K [1]. The increase in vapor pressure as a function of temperature for Jet-A is shown in Figure 5. For our experiments, the partial pressure of Jet-A ranges from 6.5 Torr at $\varphi = 0.7$ to 13.9 Torr at $\varphi = 1.5$. Therefore, while there might be some uncertainty in the vapor pressure, the fuel should stay in vapor form for all conditions being tested provided the temperature is uniform and there are no cold spots in the system. A detailed analysis of the temperature inside the vessel is provided in Chapter 4.

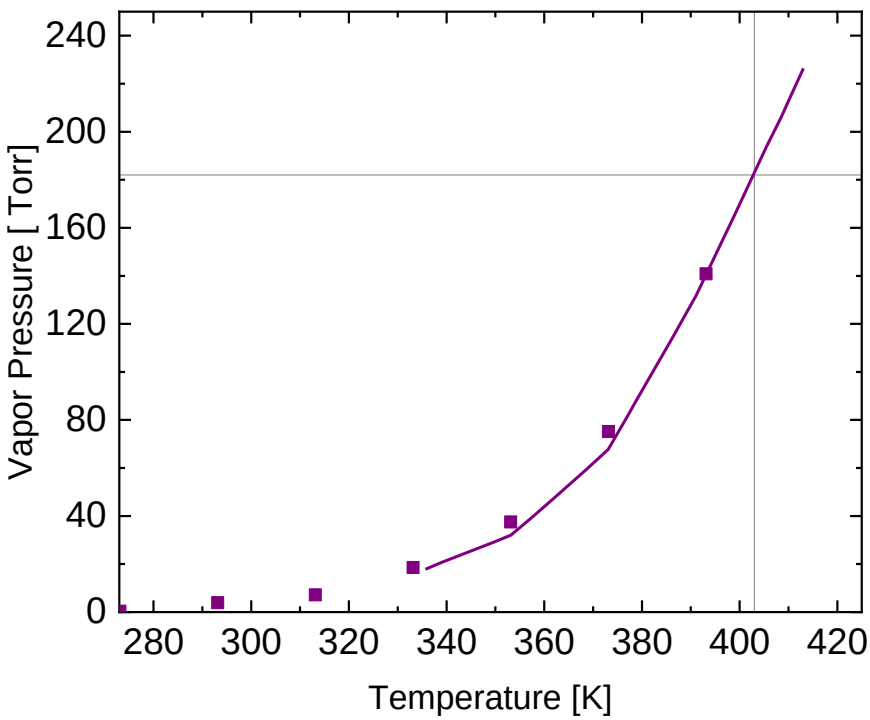

Figure 5. Vapor Pressure Data for Jet-A (POSF 10325) adapted from [1].

Fuel Cracking

Another concern was that the fuel would crack, or break down into smaller parts, due to the elevated temperature in the test vessel. Widegren et al. [41] investigated the decomposition kinetics of Jet-A. The focus of this study was higher temperatures starting at 648 K. Based on the calculated Arrhenius parameters, the decomposition half-life for Jet-A is shown in Figure 6. Therefore, Jet-A should not decompose at the temperature of the present vessel, 403 K, in our experimental timeframe. Fuel cracking does not appear

to become a concern until the temperature reaches about 640 K. Similar results were seen for RP-1 by Andersen et al. [42].

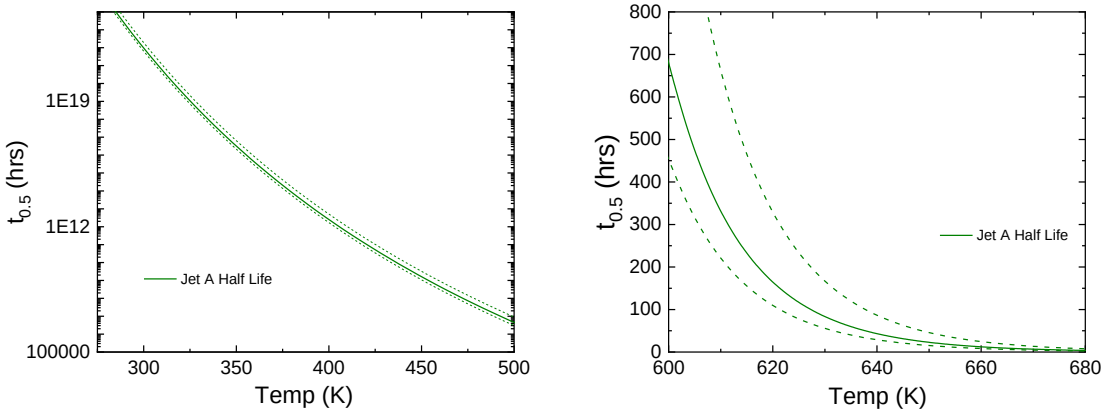

Figure 6. Arrhenius plot showing the half-life time for Jet-A. The graph on the left is a semi-log plot showing the temperature range of our experiments. The plot on the right shows the higher temperature range where Jet-A will decompose. Plots are based on the equations presented in [41]. Dashed lines indicate the 50% uncertainty in rate constant.

CHAPTER IV

EXPERIMENTAL SETUP

High-Temperature High-Pressure Vessel

Physical Dimensions

Experiments were conducted in the high-temperature, high-pressure (HTHP), stainless steel, constant-volume vessel at Texas A&M University. The design of this vessel is described in detail in Krejci et al. [43]. This vessel has an internal diameter of 31.8 cm and an internal length of 28 cm. The window diameter is 12.7 cm. This optical aperture allows the flame to be measured from ignition to the edge of the window at near-constant-pressure conditions.

A diagram of this vessel and the key components of the connected manifold are shown in Figure 7. Remotely controlled pneumatic valves separate the vessel from the gaseous fill and exhaust lines. A 0-100 Torr pressure gauge is mounted as close as possible to the vessel to monitor the partial pressure of the liquid fuel added. Needle valves were used at all other locations on the heated portion of the line. While these took longer to open and close than ¼-turn valves, they were necessary because the o-rings in the ¼-turn valves would melt after about 1 to 2 weeks at the high temperature of 400 K. This o-ring failure caused leaks and increased inaccuracy in the system.

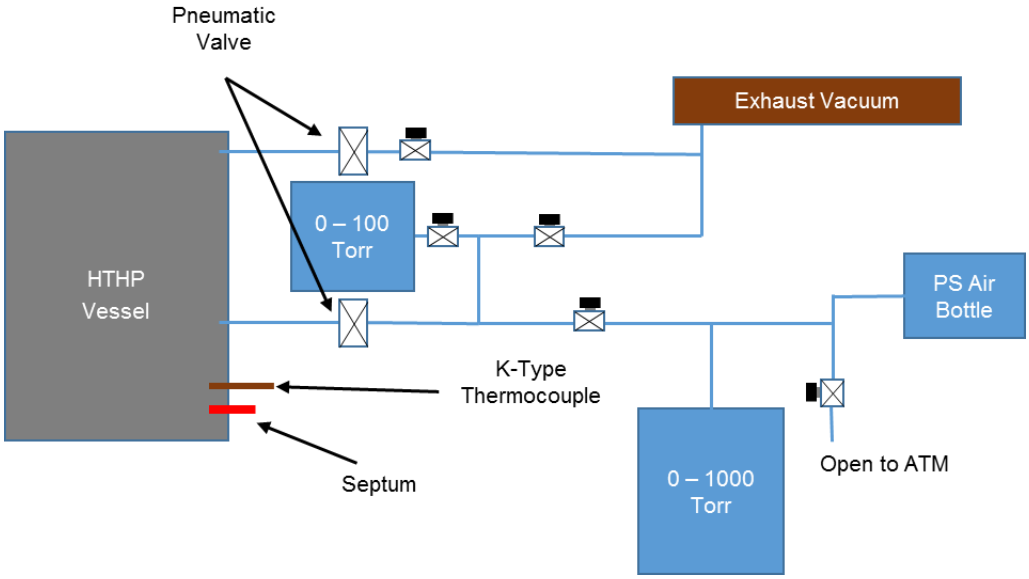

Figure 7. Diagram showing the Vessel setup with lines, valves, and pressure gauges.

Leak Detection

As with any pressure vessel, this system is prone to small leaks on occasion. Therefore it is important to limit and control these leaks. When dealing with a heated system, leak checking becomes more difficult. Some leaks will develop at higher temperatures but are not detectable at ambient conditions. At room temperature, the primary method to find leaks is to raise the pressure of the vessel above 1 atm, and use soapy water, looking for bubbles. However, this approach does not work when the vessel is at 403 K as the water will boil off quickly. Likewise, the alternate method of using acetone, on a vacuumed chamber, and looking for a pressure rise does not work because the acetone will evaporate. Therefore a high-temperature leak detector fluid *Leak-Tec*®

Formula #415 was purchased. This oily fluid was designed for use between temperatures of 210 and 415 degrees Fahrenheit (372 – 486 K).

However, there were also numerous places on the vessel that this technique would not work because they could not be seen. These include the o-rings on the endcaps and windows, and the electrodes. The electrodes set in a bore hole about 4 inches inside the vessel. The top electrode bore hole is plugged so it is not a likely source of a leak. The primary suspect is the electrode.

The electrode is a modified commercial ignitor, an Auburn F-68, which is similar to an automotive spark plug. As this plug could not initially hold a vacuum, it was sealed using a high-temperature epoxy. However, heating and cooling cycles often led to failure of the epoxy. Therefore it makes sense that leaks could develop overtime. To visualize the electrode and check it for leaks, a modification was designed for the manifold. This modification required fabricating a pipe about 1 foot in length tapped on both ends with ½-in female NPT threads. This leak check system is shown in Figure 8.

Figure 8. Ignition spark plug tester on the manifold. A) Shows the tester in its normal configuration with a plug at the end. B) Shows the tester being used to test the ignition spark plug.

Vessel Volume Calculation

As is discussed in more detail later, exact knowledge of the internal volume of the vessel became very important. The initial volume estimate was calculated to be 24.53 L based on the original technical drawings. A more-precise estimate was experimentally calculated using a known mass of steam vapor and the resultant pressure.

An initial mass of 1.5g of steam was injected into the vessel which resulted in a pressure of 80 Torr. This method assumed that steam would behave as an ideal gas since the vessel was at the high temperature and total pressure was low. The temperature of the vessel was at 403 K. Calculated from this was a vessel volume of 26.6 L. However, this test also included the portions of the line and valves to the 0 – 100 Torr pressure gauge, as shown in Figure 7. Therefore, the measured value included some uncertainty due to

possible condensation, and as such could be slightly high. Since there is about an 8% difference between these two values, a final definitive test was used to determine the volume of the vessel.

This final test required a direct measurement of the volume of the vessel. This measurement was accomplished by first cooling the vessel back to room temperature. The plug from the top electrode hole was removed, and the vessel was filled with water. The water poured into the vessel was measured in a 1-L beaker graduated at 50-mL increments. The volume of the vessel was determined to be 25.8 L. The water was then siphoned out, the end cap removed, and the vessel thoroughly dried. This procedure was repeated twice, with nearly identical results (within 50 mL). This method looked at only the vessel and did not include any of the lines past the pneumatic valves that lead to the pressure gauges. This is a similar procedure, filling the vessel with water, to the one described in Singh [44] when determining the volume of their spherical vessel to use fuel volume to more accurately measure liquid fuels.

Heating Procedure

The vessel was slowly heated from room temperature to 403 K to ensure a constant temperature throughout with a heating jacket. This procedure usually took about 3 to 4 days raising the set temperature of the heating jacket 20 ℃ every 8 to 12 hours. However it was necessary to verify that uniform heating was present.

The lines leading up to the vessel were heated with a HTS/Amptek Silicone Extruded Duo-Tape, 312 Watts, heating tape. These lines were heated daily to between

423 K and 478 K. This line heating was done in incremental steps between 20 and 30 degrees. This elevated temperature was used to ensure that there were no cold spots in the lines in which the fuel could condense. It had been determined from previous experience in the laboratory that the lines and valves were the most likely place fuel would condense. However, the lines were cooled at the end of each day as a safety precaution, so the heating procedure was repeated daily. The lines have a very small surface area and mass, and therefore were able to be heated quickly.

The initial belief was that the heating jacket would heat the vessel to a constant, homogenous temperature. To verify this constant heating, 5, K-Type thermocouples were placed in the vessel at the locations shown approximately in Figure 9. These locations included known potential cold spots such as against the windows.

The vessel was then heated in the same manner as it would be when conducting flame speed experiments. The only difference being the vessel was kept at atmosphere as opposed to vacuum. This atmospheric condition was due to the port that had been removed to install the thermocouples. The readings of each of the 5 thermocouples and the vessel thermocouple, mounted in the wall, were recorded at various time intervals throughout the heating process.

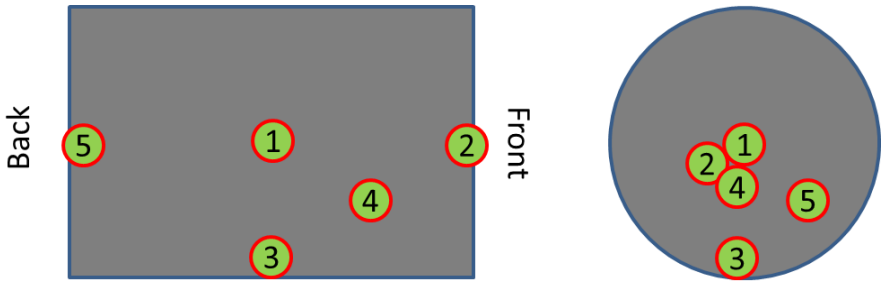

Figure 9. Diagram showing the placement of 5 Thermocouples in the vessel for heating test.

Figure 10, shows the results for the heating check. As can be seen, there were some fluctuations evident during the initial heating, but once an equilibrium temperature had been reached the thermocouples all read within 2 degrees of each other. The K-Type thermocouple mounted to the wall tended to read a slightly higher temperature than the ones placed inside the vessel. However this was found to be within the known ± 2 K uncertainty of a K-Type thermocouple.

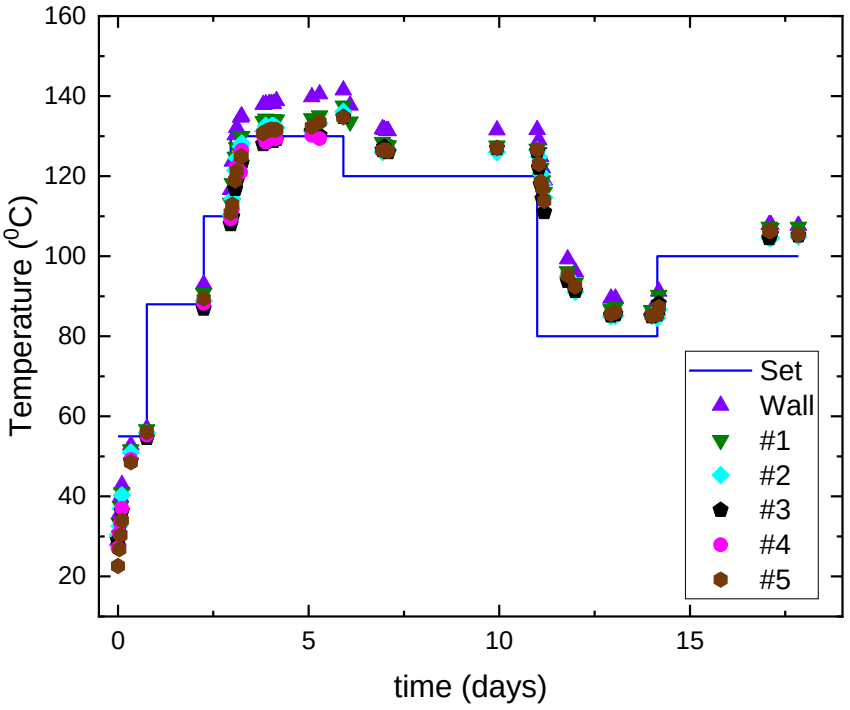

Figure 10. Time Study showing the readings of the five thermocouples compared to the wall thermocouple and the set point of the heating jacket over a period of several days.

As expected, the vessel achieved a temperature higher than the set temperature of the heating jacket. While this difference is inconvenient, it is not a problem. The set point of the jacket was adjusted so the thermocouples inside the vessel read the desired temperature. Based on these experiments, the reading of the vessel K-Type thermocouple mounted in the wall was determined to be correct. The temperature inside the vessel was also determined to be homogenous throughout.

Spark Plug Adjustment

The initial ignition system relied on two electrodes [43]. There was the sparkplug mounted in the bottom of the vessel, and a grounding rod mounted in the top of the vessel. However, there were multiple problems with this configuration. Insulation failures due to the high temperatures, and leaks required the electrode to be serviced regularly. Reinstalling the electrode and aligning the tips, with the vessel closed and at temperature, was practically impossible. This re-alignment procedure required the vessel to be cooled and opened any time the electrode needed repair. As a remedy, a single electrode that contained its own grounding rod was designed. A picture of both configurations is shown in Figure 11.

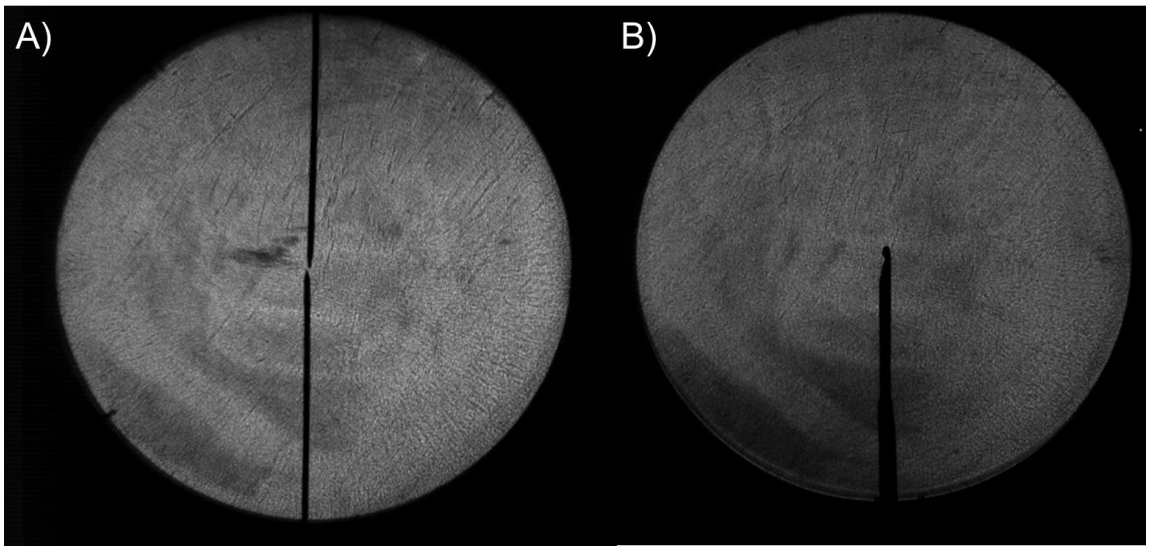

Figure 11. Different electrode configurations. A) Shows the previous electrode setup with the electrode on the bottom and the grounding rod on top. B) Shows the current, single-electrode setup.

0 – 100 Torr Pressure Gauge

The final adjustment to the experimental setup was to move the 0 – 100 Torr pressure transducer. While it had been relied on during the partial pressure experiments, it was not needed for the mass-based measurements (discussed later). There was also the suspicion that fuel was condensing in the lines and valves leading to the transducer, leading to inaccurate readings. However, with the single sparkplug system, the previous top electrode port could be used to mount the pressure gauge. Therefore, a fitting was designed that allowed for it to be mounted directly on the vessel. The diagram of this final configuration is shown in Figure 12.

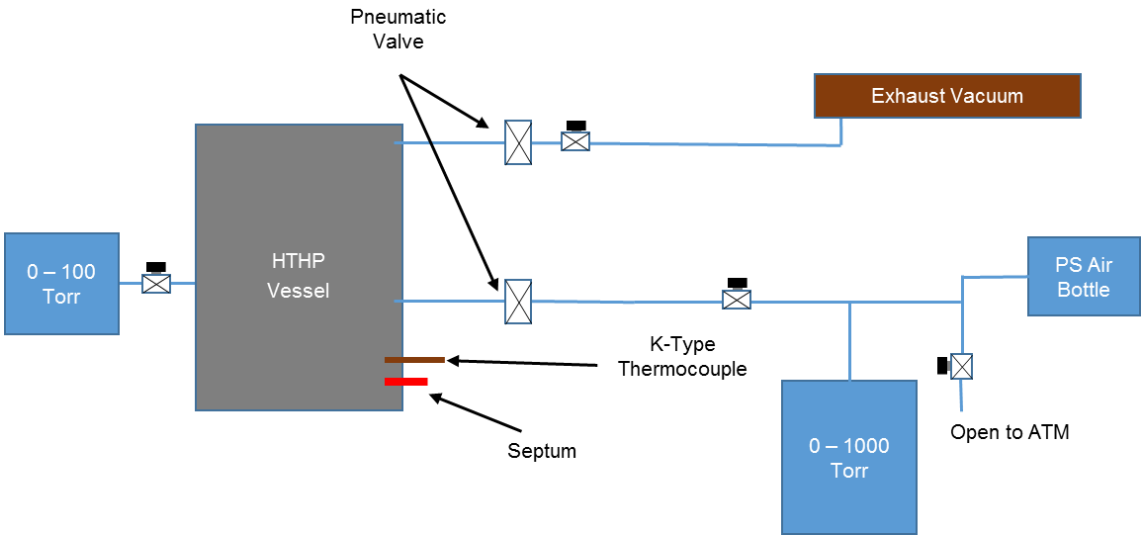

Figure 12. Diagram showing the current setup of the vessel with gauges and valves. The 0 – 100 Torr pressure gauge is now mounted directly on the vessel, and the lines leading to the vessel have been simplified.

Experimental Procedure

Filling Procedure

The procedure for filling for a given mixture was based on the desired equivalence ratio, and from that the mole fractions of the components. The full procedure for calculating equivalence ratio is described in Appendix A. From these mole fractions, either the partial pressures or the necessary mass loading of fuel could be calculated. A brief discussion of the filling methods is given below, with a more-detailed description highlighting the pros and cons of each method provided in the next chapter.

The vessel was pulled down to a near-perfect vacuum. Ideally, this level would be less than 0.1 Torr. Liquid fuel was then injected into the vessel via a septum. When the total pressure stabilized at the appropriate partial pressure for the fuel, the vessel was closed off, and the line was vacuumed back down. The line was then flushed with atmospheric air multiple times to ensure that all remaining fuel had been removed from the line. The oxidizer components of O_2 and N_2 were then added using the partial pressure method.

The mass-based method was similar. However, since a known mass of fuel was injected into the vessel, and none of the lines were exposed to the fuel, there was no need to flush the lines with air. This direct-injection method allowed for experiments to be conducted quicker as there was not time spent flushing the lines.

Schlieren Imaging

Experimental data were collected using the schlieren setup shown in Figure 13. With this setup, the density gradient at the edge of the flame becomes visible and can therefore be tracked. This system used a high-speed camera (Photron Fastcam SA1.1) with the frame rate of the camera set at 10,000 frames per second. This speed allowed for at least 100 frames to be available for data analysis for each experiment after wall and ignition effects have been removed.

For the schlieren imaging setup, the light from a mercury arc lamp is collimated through a lens (focal length 800 mm). The beam of light is then reflected by a flat mirror at 45 degrees to pass through the vessel. The collimated light is then reflected by another 45-degree mirror and passed through another lens (focal length 800 mm). A knife edge is placed at the focal point to remove excess light. The light then enters the high-speed camera where the schlieren image is captured.

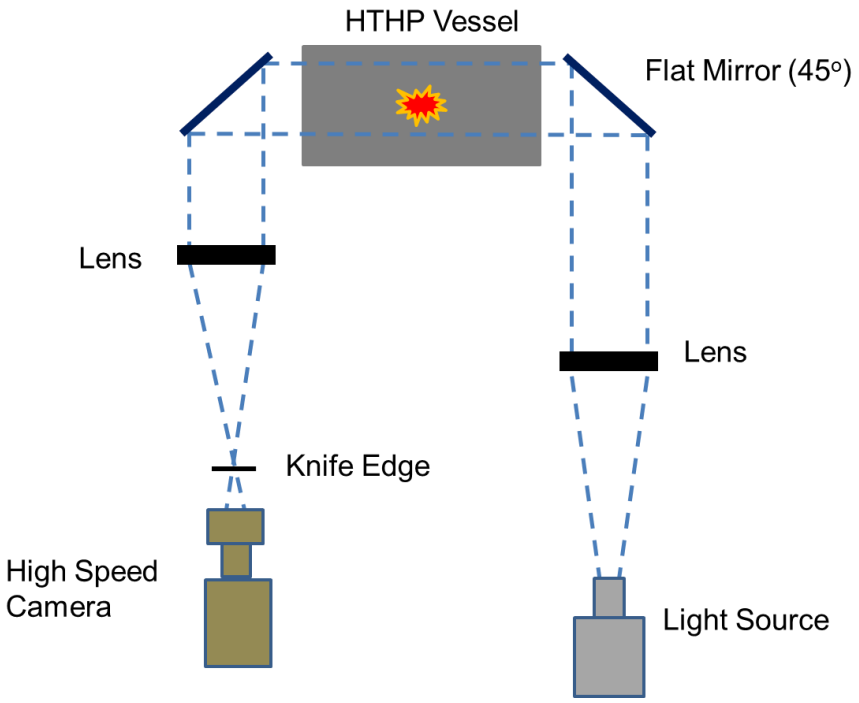

Figure 13. Schlieren setup for the HTHP vessel.

Flame Speed Analysis Program

A MATlab-based edge detection program, outlined in Sikes et al. [45], is used to track the edge of the flame and thus determining the burned, stretched flame speed. The second part of the analysis program is then applied to extract the unburned, unstretched laminar flame speed and the burned gas Markstein length using the appropriate non-linear equation as outlined by Chen [46]. The method used is based on the Markstein length, L_b, of the flame. If the Markstein length is positive, then nonlinear method I, Equation 4.1, should be used. A negative Markstein length requires the use of nonlinear method II, Equation 4.2. This result is then divided by the density ratio, Equation 4.3, to achieve the unburned, unstretched laminar flame speed, Equation 4.4.

$$S_b = S_b^0 - S_b^0 L_b \left(\frac{2}{r_f}\right) \tag{4.1}$$

$$ln(S_b) = ln(S_b^0) - S_b^0 L_b \left(\frac{2}{r_f S_b}\right) \tag{4.2}$$

$$\sigma = \frac{\rho_u}{\rho_b} \tag{4.3}$$

$$S_{L,u}^0 = \frac{S_b^0}{\sigma} \tag{4.4}$$

When analyzing spherical flames, it is necessary to remove both ignition and wall affects. Additional energy from the spark will accelerate the flame initially, whereas the pressure rise as the flame gets closer to the wall will decrease the flame speed. The images are also analyzed for signs of instability. If the flame becomes too wrinkled and can no longer be assumed to be spherical, those images will not be included in analysis. Sample images for all fuels and S_b versus stretch plots used for this analysis are provided in Appendix E.

Markstein Length

The Markstein Length, L_b is one of the key parameters usually calculated and presented in laminar flame speed research. It is a very good indicator of the overall stability of the flame and can be linked to turbulent flame structures. In general, a flame with a larger, positive Markstein length will be more stable, whereas a flame with a smaller

and potentially negative Markstein length will be less stable. Monteiro et al. [47] described the Markstein length as the slope of the S_b versus stretch plot. Burke et al. [48] described it as an indication of the flame's response to the strain rate. Thus, for a positive Markstein length the flame speed will decrease as stretch increases, whereas for a negative Markstein length the flame speed will increase with stretch.

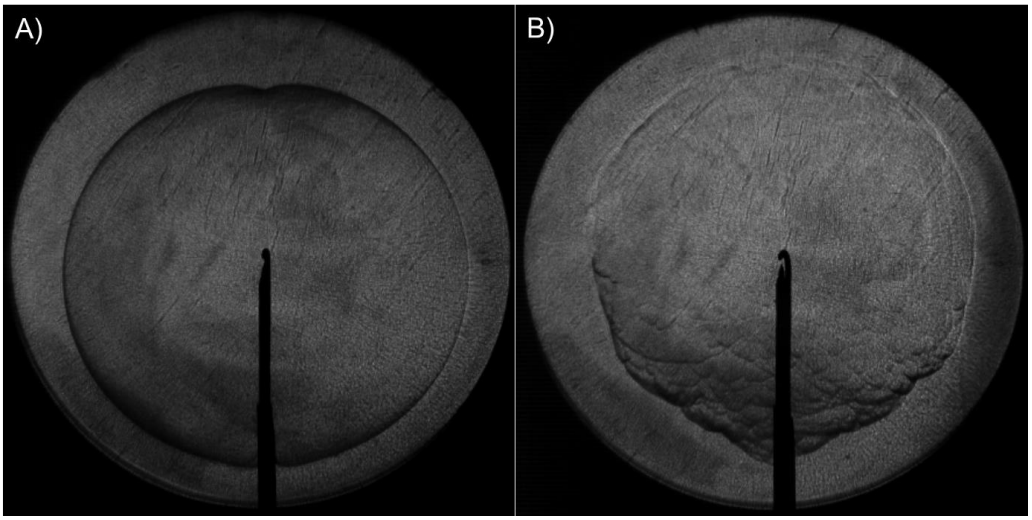

Figure 14. Examples of flames with a positive and negative Markstein Length. A) Is an example of a stable flame with a positive Markstein length, L_b = 0.2137cm, taken from a Jet-A flame at φ = 0.995. B) Is an example of an unstable flame with a negative Markstein length, L_b = -0.060 cm taken from a decane flame at φ = 1.575.

Figure 14 shows examples of two flames from the current study. While the exact value of the Markstein length is not immediately evident, its positive or negative nature is usually very easy to quickly determine. On the left is a flame with a positive Markstein length. The flame appears to be very round with a clearly defined edge. In contrast, the flame on the right has a negative Markstein length. Cellular structures can be seen forming,

especially near the bottom of the flame. The overall structure of the flame also no longer appears to be round.

Nonetheless, the Markstein length is a not always the easiest parameter to use for data analysis. As noted in [46], the results can vary by up to 300% between different groups. Part of this might be due to the overall small physical values for the Markstein length. For example, in the present data set the Markstein length typically ranged from around 0.17 cm for lean and stable mixtures to around -0.06 cm at richer and less stable conditions.

Experimental Timeline

The experiments included in this study were conducted over a period of two and a half years. Improvements and updates to the experimental process were implemented during that time to produce a better and more accurate experiment. As such, in the presentation of the data that follows results are not always presented in chronological order. However, knowledge of the order of events shows how a better experimental procedure was developed. For completeness, a timeline of events is provided in Figure 15.

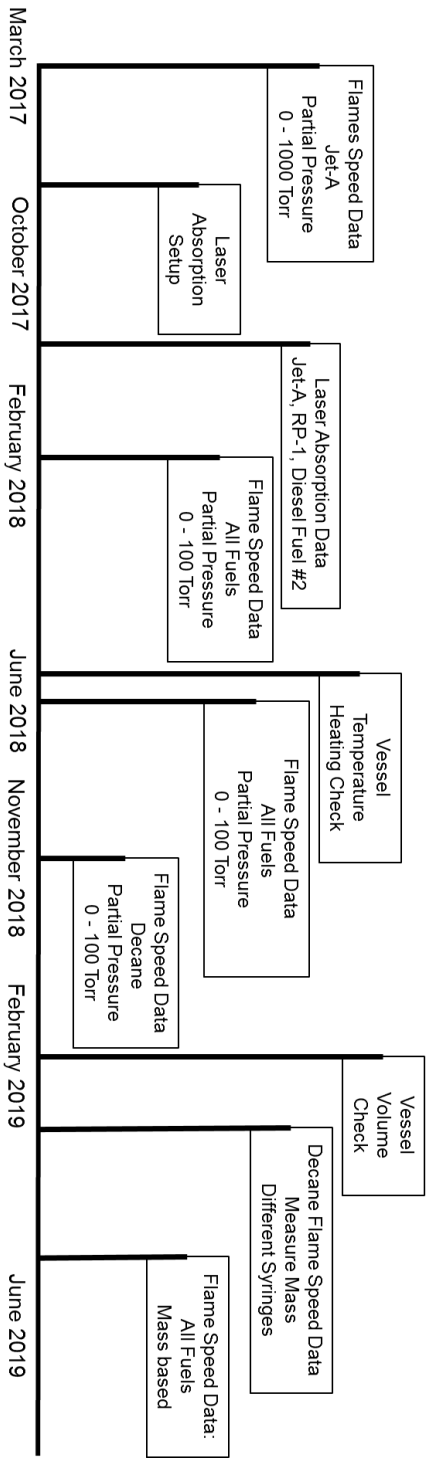

Figure 15. Timeline showing the overall order of experiments and updates to the procedure used throughout this study.

CHAPTER V

DECANE STUDY

Decane is useful to study because it is known to be one of the key components of the real fuels that are discussed later. It is also a pure fuel with a known chemical formula, $C_{10}H_{22}$, thus removing average molecular formula as a cause for any uncertainty in the fuel's overall behavior. The molecular weight of decane, *MW*, is 142.29 g/mol. The density, ρ, at room temperature is 0.730 g/mL, and the normal boiling point of decane is 447.25 K. From vapor pressure calculations of higher order hydrocarbons, at various temperatures in Maxwell [49], the vapor pressure of decane at 403 K is approximately 182.4 Torr. The partial pressures of the fuel in the range of equivalence ratios being tested are on the order of 10 Torr, well below the vapor pressure at the experimental temperature. Therefore decane within the test vessel should stay in the vapor phase.

Since there is no uncertainty in the fuel composition, decane is useful to quantify the uncertainty and repeatability in the experimental setup. This approach helped to determine the minimum error bars around φ that should be included when dealing with the practical, complex fuels. This study of decane was used to refine the procedure used to fill the vessel throughout this study. These results were then compared to results available in the literature.

Partial Pressure Method

Initial experiments were conducted using the typical partial pressure method to fill the vessel. This partial pressure method is the technique that has historically been used at Texas A&M (for mostly gas-phase fuel) and therefore was a reasonable initial approach for the liquid-fuel experiments. This method assumes that all of the fuel is in the vapor phase once it is injected into the vessel, to obtain an accurate pressure reading. This method also requires the fuel filling a small portion of the lines in addition to the vessel to reach the 0-100 Torr pressure transducer. Therefore, this portion of the line is heated well above the experimental temperature to ensure that no cold spots are present that could lead to local fuel condensation. This technique requires the pressure transducer to be accurately calibrated, as pressure is the only verification of the mixture equivalence ratio.

As can be seen by the initial results shown in Figure 16, the flame speed for decane produces a very good and fairly repeatable curve. However, the data show a noticeable shift from that available in the literature, toward richer equivalence ratios. Since this is a pure fuel with no question as to the molecular formula, then MW uncertainty should not be the reason. In other words, Figure 16 indicates that the true mixture in the vessel is at a leaner equivalence ratio, so there is likely a lower fuel-to-air ratio than expected (to shift the flame speed data to the left). Either fuel is condensing somewhere between the introduction point and the vessel interior, or extra air is entering the vessel causing a higher partial pressure reading than is accurate. For this reason, additional and more-refined methods of introducing liquid fuel into the vessel were explored.

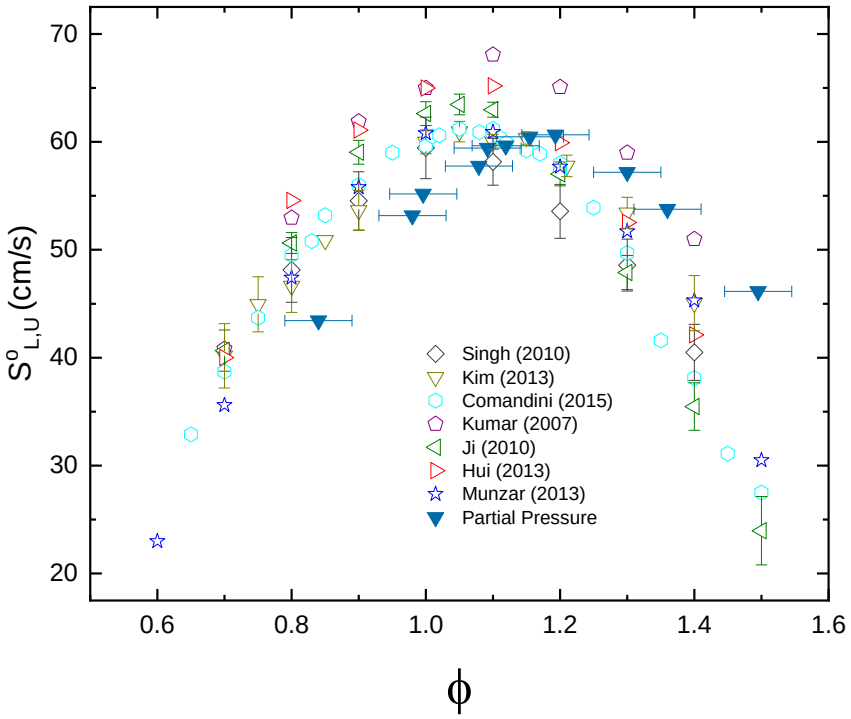

Figure 16. Laminar Flame speed data for Decane at 403 K and 1 atm using only the Partial Pressure Method compared to literature data.

Mass-of-Fuel Measurement

The first of these changes was to measure the mass of the fuel that was injected into the vessel as opposed to relying on the partial pressure. The mass of fuel remains the same in liquid or gaseous form and therefore can easily be converted to a number of moles and thus a mole fraction in the gas phase. All this requires is accurately knowing the molecular weight of the fuel. However, unlike the partial pressure method this technique requires knowing the exact volume of the vessel. The determination of the volume of the vessel was discussed fully in Chapter IV With the ideal gas law, Equation 5.1, the number

of moles of an ideal gas the vessel can hold at any given temperature can be determined. The pressure of the vessel is given as *P*. The vessel volume is shown as *V* and the temperature as *T*. The ideal gas constant, R_u, to help keep units consistent is defined as 62.36 Torr L mol^{-1} K^{-1}. The final term, *n*, represents the number of moles.

$$PV = nR_uT \tag{5.1}$$

As discussed in the previous chapter, the volume was calculated to be 25.8 L. This known volume results in the vessel being able to hold 0.780227 moles of an ideal gas at 403 K and 760 Torr. From this calculated number of moles and the previously determined mole fractions, X_{FUEL}, can be used to determine the mass of fuel that should be injected into the vessel to achieve a given equivalence ratio.

Table 5. Volume and mass values for n-decane over a range of equivalence ratios.

Φ	X_{FUEL}	n_{FUEL}	V (mL)	mass (gram)
0.8	0.0107	0.0084	1.63	1.19
0.85	0.0114	0.0089	1.73	1.26
0.9	0.0121	0.0094	1.83	1.34
0.95	0.0127	0.0099	1.93	1.41
1	0.0134	0.0104	2.03	1.48
1.05	0.0140	0.0109	2.13	1.56
1.1	0.0147	0.0115	2.23	1.63
1.15	0.0153	0.0120	2.33	1.70
1.2	0.0160	0.0125	2.43	1.78

Table 5 shows the liquid volume and mass of n-decane necessary to achieve equivalence ratios from φ = 0.8 to 1.2. As can be seen, an increase of 0.1 mL or 0.07 grams

of fuel results in an increase of φ = 0.05. The syringe used in this study was graduated to 5 mL at increments of 0.2 mL. The scale used to measure the mass of the fuel gave readings to 0.01 grams. Based on the values in Table 5, liquid volume alone would not provide the necessary precision to calculate equivalence ratio. However, the precision of the mass measurement is sufficient to calculate equivalence ratio.

To accomplish these tests, the dry syringe was initially weighed and the mass recorded. The syringe was then filled with decane to a volume around the experimental equivalence ratio. The volume measurements were for informational purposes only and not used to calculate φ. After the fuel had been added to the syringe and any air removed, the full syringe was weighed and the mass recorded. The liquid fuel was then injected into the evacuated and closed off vessel via the septum. The syringe was then weighed one final time and the mass recorded. The mass of fuel added to the vessel was then calculated as shown in equation 5.2. It was also found that there was typically about 0.1 gram of fuel remaining in the syringe after filling. This observation is an additional indication that liquid volume alone is not an ideal method to use.

$$m_{FUEL} = Syringe_{Full} - Syringe_{empty} \tag{5.2}$$

Fuel Analysis

One of the concerns was the age of the n-decane initially used in this study. The fuel had been received by the laboratory in August 2011, partially used, and had been sitting in the flammable storage cabinet ever since. Even though it had been properly stored, if there had been any decay of the decane over the intervening 8 years, this would affect the overall equivalence ration and therefore the placement of the data points.

To verify the purity, GC-MS analysis on a sample of n-decane was performed by the Chemistry Department. The analysis concluded that the sample was still 99% pure. While that test was being conducted, a new batch of decane was procured. This new batch of decane was used for the remainder of the experiments

Septum Setup

One of the key points of uncertainty in the vessel was the septum. The septum is a small, LB-2 rubber disc that the needle is inserted through when injecting the liquid fuels. This point also needs to be able to hold a vacuum. After repeated punctures, the septum can develop a leak. Therefore it was necessary that it to be replaced frequently. To help reduce any related chance of a local leak, a ¼-turn valve was installed between the vessel and septum holder as shown in Figure 17. While this reduced leaks in the septum, it also increased the standoff between the septum and the vessel wall. The septum holder has a length of about 1.5 inches. The ¼-turn valve and additional tubing had a length of 2.5 inches. Therefore, the 2-inch needles would end in the middle of the ¼-turn valve. The vessel wall thickness is 4 inches, so even with the 6-inch needle, the end of the needle would still be within the wall with the ¼-turn valve installed. The concern that fuel was

condensing in this portion of the septum configuration led to the search for longer needles, and the eventual removal of the ¼-turn valve from the septum as shown in the current setup in Figure 17. However, a needle longer than 6 inches was still required to ensure that the fuel successfully made it all the way inside the vessel.

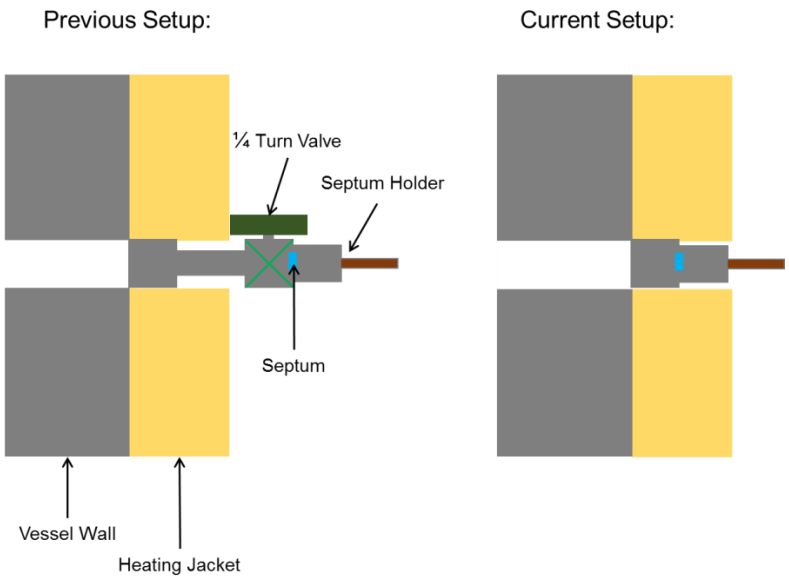

Figure 17. Diagram showing previous and current septum configurations.

Different Syringes

Different syringes and needles were used to inject fuel into the vessel. The initial syringes used were 5-mL FORTUNA Optima glass syringes with a Luer lock connection as shown in Figure 18. These syringes were graduated at 0.2-mL intervals. Initially these syringes were used with a 2-inch-long, 23-gauge needle. One of the concerns was the fuel not getting all the way into the vessel. Therefore, a longer needle was needed to ensure

that all the fuel made it into the vessel and that none remained in between the septum and the vessel.

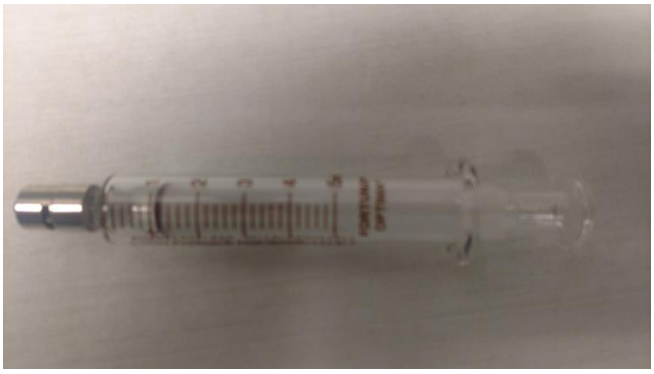

Figure 18. 5-mL FORTUNA Optima syringe with Luer Lock connection.

The longest needle immediately commercially available at an economical price was a 6-inch needle; however, the smallest diameter available was 20 gauge. With this configuration, the fuel was sucked out of the syringe as soon as it punctured the septum. This event was completed before the needle could be completely inserted into the vessel. Therefore there was no benefit from the longer needle.

The next configuration that was attempted was a 4-inch-long, 22-gauge needle. While this was an improvement over the previous configuration, there were still some potential problems present. A concern that was present even from the initial configuration was air entering the syringe from behind the plunger. This possibility continued to be a reasonable cause for uncertainty. There was also a concern of fuel leaking out through the Luer lock connection.

A new syringe system was needed to solve all of these potential causes of uncertainty. This eventual solution was achieved with a custom-made Gastight Model 1005 Luer Tip Cemented Needle syringe with a 10-in-long, 23-gauge needle as shown in Figure 19. This syringe had the needle mounted to the barrel of the syringe, so there was no potential for leaks at that point. Also, there were better seals on the plunger to prevent air from leaking into the barrel of the syringe. The long needle ensured that the injected fuel made it all the way into the vessel.

Figure 19. 5-mL Gastight syringe with cemented 10-in-long, 23-gauge needle.

This syringe and needle preformed exactly as expected. There was no indication of any air leaking in from behind the plunger or fuel leaking out from the base of the needle. The needle was fully inserted into the vessel and allowed for pressure being applied to the plunger prior to any significant amount of fuel exiting the syringe. Looking in through the window of the vessel, one could clearly see the stream of fuel entering the vessel at the desired time and location.

Different Fill Techniques

One of the concerns was that the fuel might be freezing when it was injected into the vessel that was initially under vacuum. This possibility of severe expansion was due to the large pressure differential between the liquid fuel in the syringe at 1 atm and room

temperature, and the vessel the elevated temperature and very low pressure of < 0.5-Torr. It was possible that the fuel or parts of it could freeze or crystalize as it left the syringe and not fully return to gas phase prior to the experiment being conducted.

Since the amount of fuel in a mixture was measured by mass, and not partial pressure, and primary standard air was being used, the addition of air to the vessel could be split to help counter this effect and decrease the pressure differential. Initially, 400 Torr of air was added to the vessel prior to the fuel. This created a much lower pressure ratio of 1.9 between the atmosphere and the vessel, as opposed to around 1900 when the vessel was completely evacuated. However, the initial results were not very good. It was evident that something was wrong as the resultant flame speeds were about 15 cm/s off of the expected value.

This unforeseen problem was most likely due to the low vapor pressure of decane, which as stated previously is around 182 Torr. Since the vessel was initially at 400 Torr, the fuel stayed a liquid during filling. This new problem resulted in an inaccurate measurement of the equivalence ratio. There was also evidence of fuel pooling in the bottom of the vessel as seen in one of the analysis videos following the initial flame propagation.

To counter this effect, the initial addition of air was lowered to 125 Torr. This pressure is a value slightly below 75% of the fuel vapor pressure. The resultant pressure ratio is 6.08 between the atmosphere and the vessel. The results from this technique looked much better and were overall similar to the previous results, while also reducing the likelihood of any fuel freezing due to the expansion of the stream when entering the vessel.

Laminar Flame Speed Results

The full Texas A&M University (TAMU) data for n-decane are shown in Figure 20. Highlighted are the different methods used to prepare the mixture as discussed above. The data are also compared to the results of the chemical kinetics mechanism of [7]. Two things are important to note: the shift of the curve when compared to the mechanism and the scatter in the data. The scatter in the data is addressed more in the next section, when the results are compared with those of other groups. The shift indeed appears to be caused by fuel condensing somewhere in the vessel or lines effecting the overall equivalence ratio.

For the data points where the extra ¼-turn valve was present, the same shift was present as previously seen with the partial pressure data. These data, with the valve installed, show a peak flame speed around $\varphi = 1.2$, whereas when the valve is removed the peak shifts closer to the expected value of $\varphi = 1.1$. Therefore, it appears that fuel was indeed condensing in the ¼-turn valve. Based on the mass of fuel required for a given equivalence ratio (discussed in Mass of Fuel Measurement), the loss of a couple of drops of fuel could easily account for this difference.

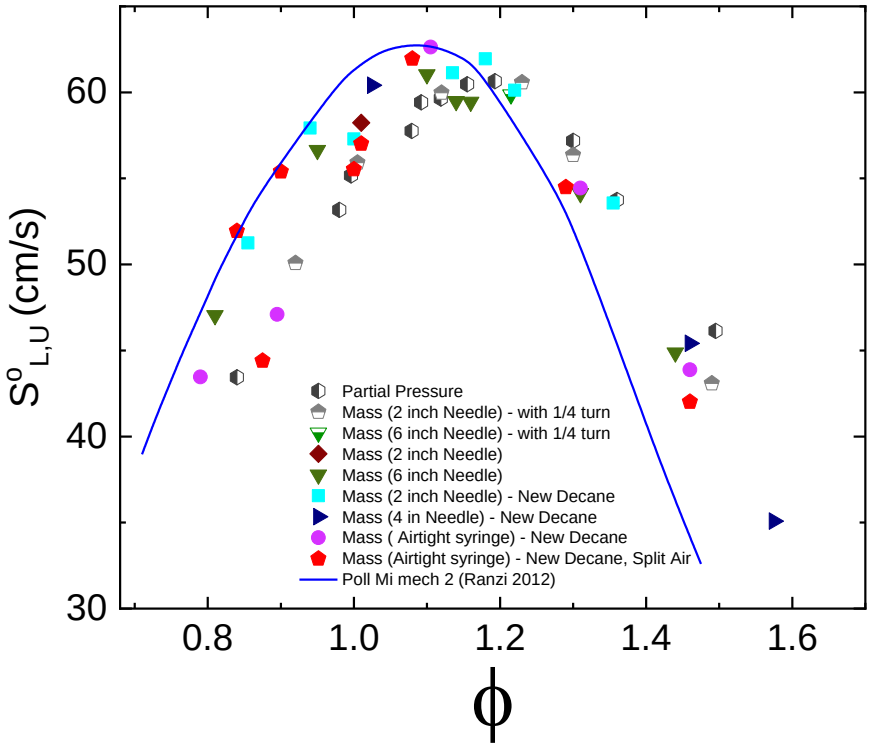

Figure 20. Full Decane flame speed data at 403 K and 1 atm. Data points are shown broken down by the different methods used to measure the injected fuel into the vessel.

Figure 21 shows the mass-based laminar flame speed results of the current study, with the ¼-turn valve removed, compared to those available in the literature at 403 K and 1 atm. This plot includes all methods from the literature used to determine laminar flame speed. The studies of [15, 17] used a counterflow, twin flame configuration. Similarly, the study of [2] also used a counterflow, twin flame configuration. The work of Munzar et al. [50] used a stagnation flame configuration. The remaining studies all used a spherical flame technique similar to the present configuration. The error bars, when shown, are taken directly from the literature studies. Overall, the curves appear very similar, with the

present data peaking at a slightly richer equivalence ratio, closer to φ = 1.1, as opposed to φ = 1.05. There is also significantly more scatter at rich mixtures than at lean mixtures. The two points near φ = 0.9, in the current data set that appear significantly slower are believed to be inaccurate data points that should be removed as is discussed in the next section.

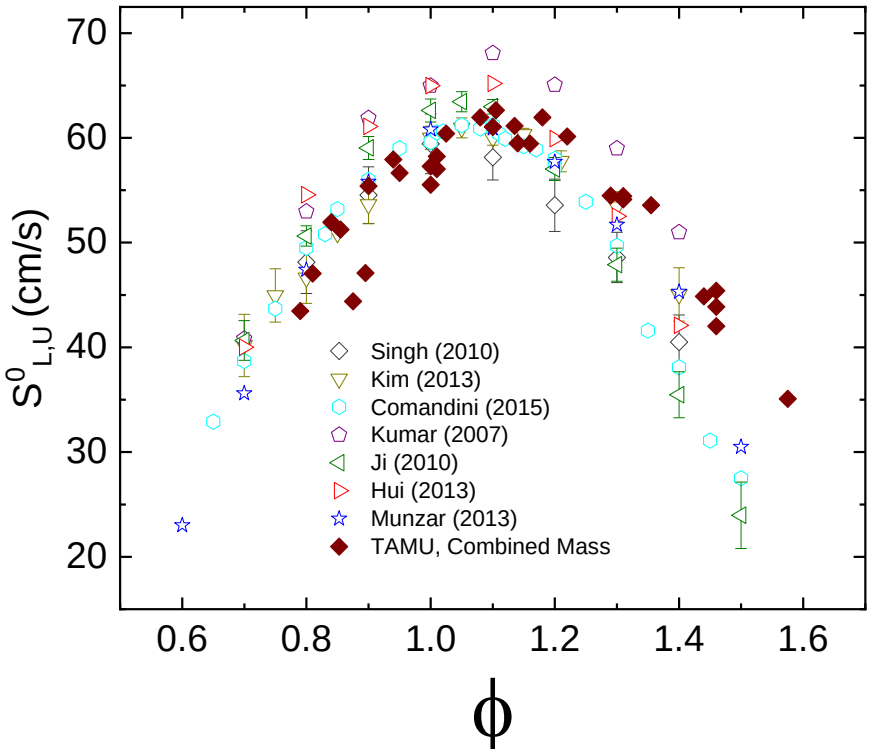

Figure 21. Laminar Flame Speed data based on mass injected compared to all decane studies available in literature. All experiments were conducted at initial conditions of 403K and 1 atm.

However to best validate our techniques, it is important to only compare to experimental results gathered using a similar method. Therefore, the results shown in Figure 22 are only for spherical flames.

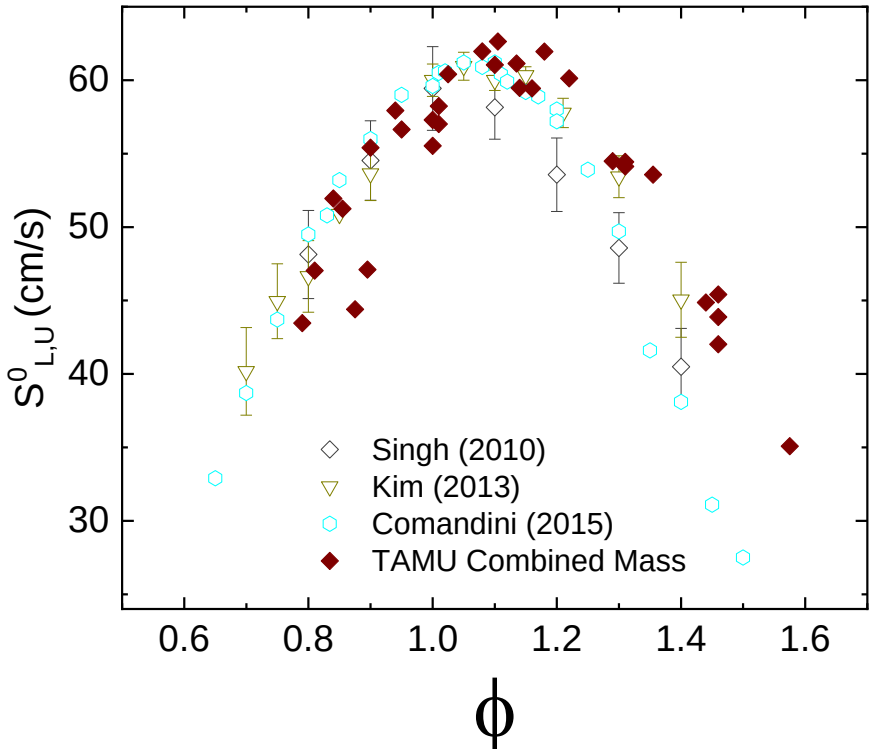

Figure 22. Mass-based laminar flame speed data compared only to the literature studies that used the spherical flame technique.

The scatter in laminar flame speed seen in the present data is on the order of 3 – 5 %. This level is based on the repeatability of the experiments. It is on the same order as

the uncertainty reported by [5], of less than 10%, and Kim et al. [51] of 1.1 – 7.2%. There was no uncertainty in flame speed reported by [26].

Our data most closely match the work of [51], with our results being typically slightly faster. At $\varphi = 0.8$, we are 0.85% faster while at $\varphi = 1.3$ we are 1.85% faster. Both of these results are within the stated uncertainty. The results around $\varphi = 1.4$ also appear very similar.

The comparison to the results of [26] are not as good. For lean mixtures, our results are slightly slower. For example, at $\varphi = 0.8$ we are 5.2 % slower. However, at rich mixtures our flame speeds are significantly faster. At $\varphi = 1.3$ there is an 8.9% difference. This difference grows to around 30% at $\varphi = 1.45$. At rich mixtures however, the results of [26] are slower than all of the other spherical laminar flames from the literature. For example, at $\varphi = 1.4$ the results of [26] were about 6% slower than the results of Singh et al. and about 17% slower than [51].

One of the major goals of the decane study was to determine the acceptable amount of scatter and repeatability in the data. As shown, most groups reported their uncertainty in flame speed being between about 3% and 10%. While this number might seem high, especially when compared to gaseous fuels, it is reasonable to assume that the uncertainty for real, multicomponent fuels will be similar or even greater.

Markstein Correlation

The burned-gas Markstein length is a parameter that is frequently reported in laminar flame speed studies. However, these results are almost never the primary focus of

the study. For most hydrocarbons, in general, the Markstein length decreases at richer mixtures. Singh et al. [52] pointed out that this trend was opposite to what is seen in H_2/Air flames. So a trend along these lines was to be expected. However as seen in Figure 23, a very strong linear trend was detected. It was determined that a linear fit to these results might be useful in helping to determine the acceptability of data points.

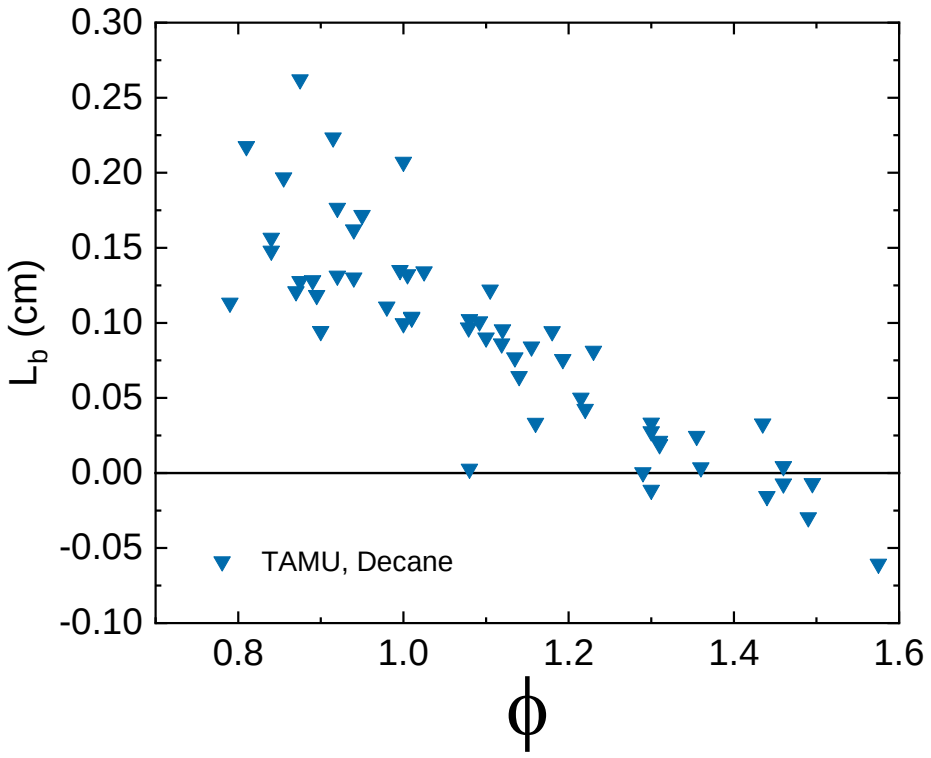

Figure 23. Complete Markstein length data for n-decane at 403 K and 1 atm. A strong linear trend was noticed for L_b as a function of φ.

The linear correlation of the burned-gas Markstein length as a function of equivalence ratio is shown in Equation 5.3, with L_b in cm. This equation is a linear fit based on the stoichiometric and rich data because there appeared to be significantly more scatter in the data for lean mixtures. This correlation is added onto the Markstein length plot in Figure 24.

$$L_b = -0.28105\varphi + 0.40227 \tag{5.3}$$

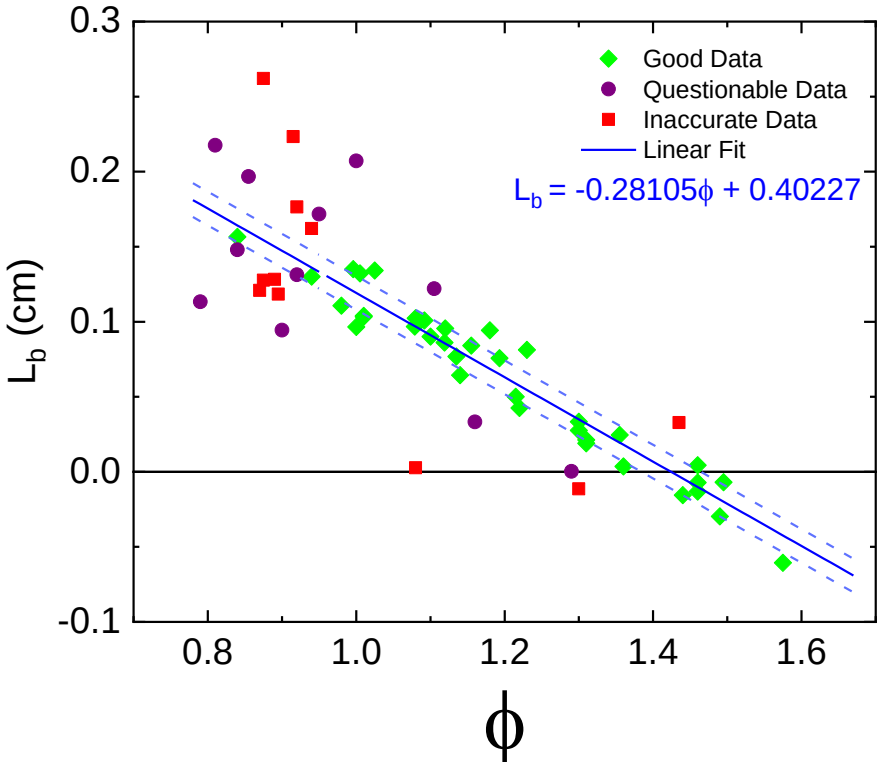

Figure 24. Burned-gas Markstein length for decane-air mixtures at 1 atm and 403 K. Solid line shows the linear correlation for the data with the dashed lines showing the uncertainty limits. Data points are color coded based on the quality of the data.

The dashed lines shown are based off of a ± 0.04 uncertainty in φ. This value comes from the experimental uncertainty in the equivalence ratio. Data points falling outside the dashed lines are not automatically rejected. However, if the flame speed is found to be significantly outside what is expected or from the trend displayed in the entire data set, these points will be rejected. The flame speed plot based on this analysis is shown in Figure 25.

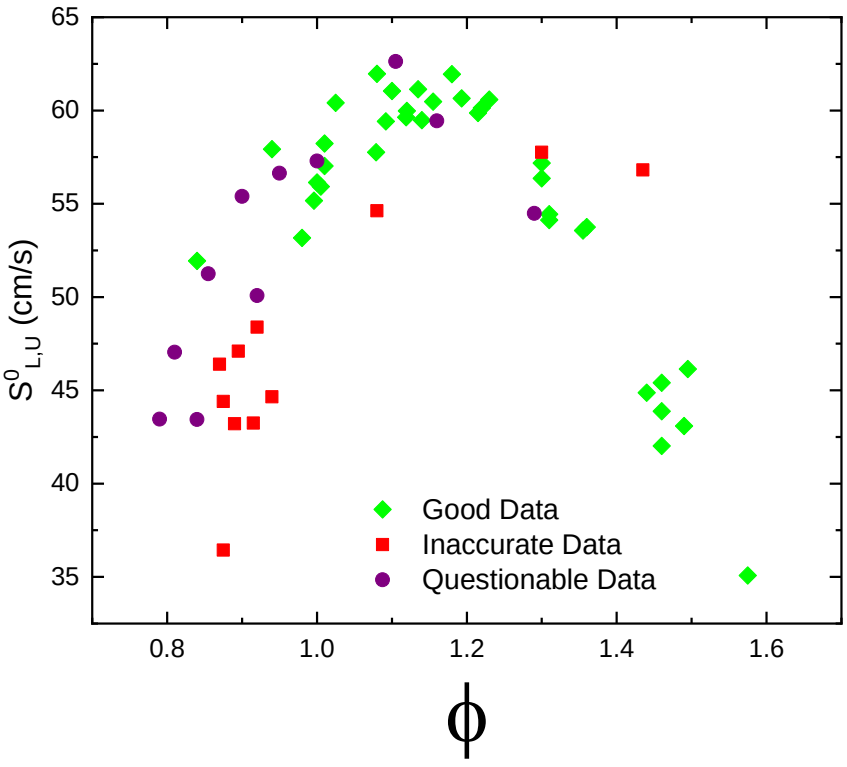

Figure 25. Flame Speed data for decane focusing on the quality of the data based on Markstein length analysis. This includes all data points collected including the data collected based on the partial pressure method.

This correlation appears to be useful in helping to analyze the data for decane. As such, the linear fit was applied to the other fuels in this study, with adjustments to account for the different average molecules. This adjustment is described in detail in Appendix B.

Conclusions

The detailed study of decane helped to improve and validate the current experimental procedures. Different methods for filling the vessel, including using different syringes and needles, were tested to ensure that all of the fuel was entering the vessel and vaporizing. The final n-decane data are shown, complete with error bars, which are discussed in detail in the next chapter in Figure 26.

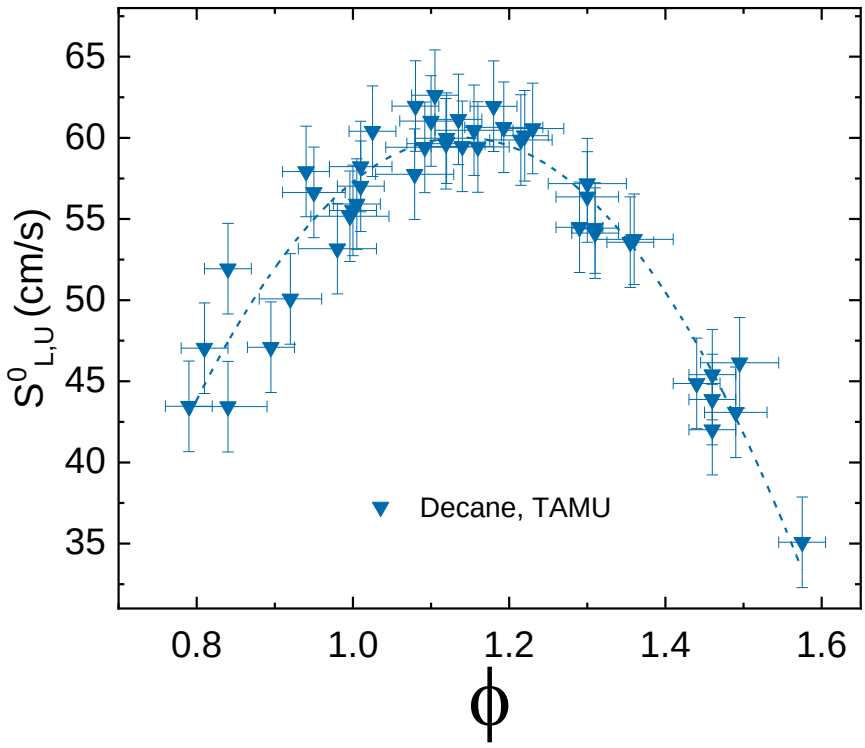

Figure 26. Complete, acceptable laminar flame speed data for n-decane at 1 atm and 403 K. Therefore the points that were red in Figure 25 have been removed. Dashed line shows a trend line through the data and is not a model prediction.

A typical practice when presenting laminar flame speed data is to average several data points together. This sometimes makes overall trends easier to visualize, but it often makes the final data points look much more orderly without showing the actually data variation. As seen in Figure 27, the 45 data points shown previously are now reduced to 10 data points. In this method, data points are grouped around a common equivalence ratio. For example, the six data points ranging from φ = 1.44 to φ = 1.495 are grouped together at an average equivalence ratio of φ = 1.4675. Overall error bars in both flame

speed and equivalence ratio are based on a combination of the standard deviation around the averaged point value and the total uncertainty discussed in the next chapter.

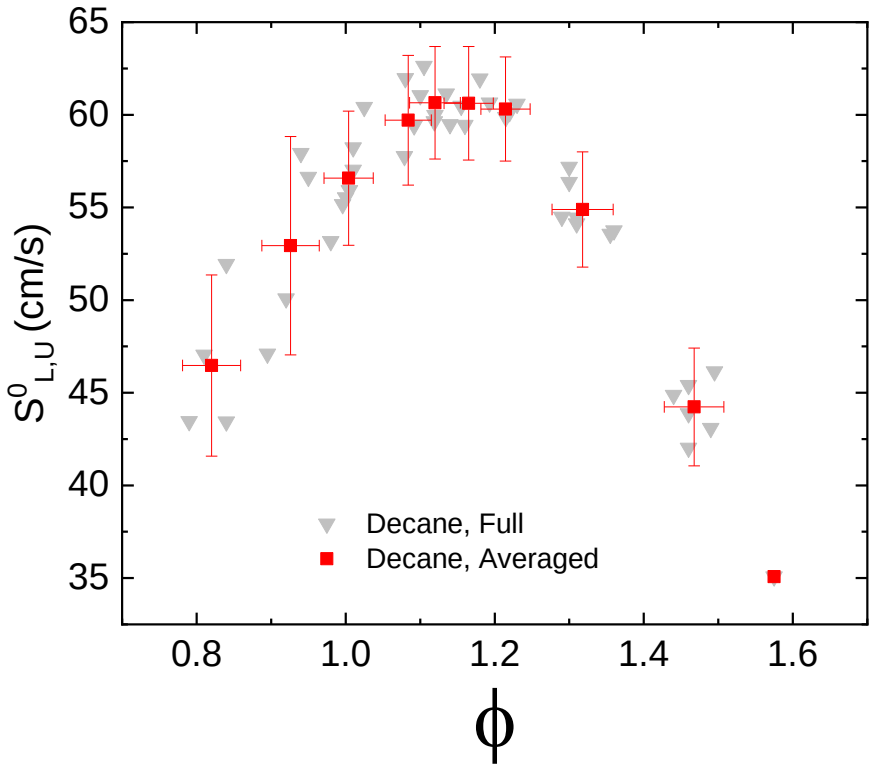

Figure 27. Decane results showing the averaged-points curve. Original data points are shown as light gray triangles, with averaged points as red squares.

CHAPTER VI

UNCERTAINTY ANALYSIS

As with any engineering analysis, understanding and quantifying the uncertainties in these experiments is very important. There are uncertainties in the chemical composition of the fuel, which must be fully known and understood. Then there are experimental uncertainties which fall in two distinct categories: first, uncertainty in the equivalence ratio or the amount of fuel in the mixture; and second, uncertainty in the measured laminar flame speed. Each of these is discussed in more detail below.

Uncertainty in Fuel Composition

One of the leading causes of uncertainty is the average molecule and hence the average molecular weight of the fuel. This parameter leads to an uncertainty in the overall equivalence ratio. In other words, if you are uncertain about what the fuel is then you cannot accurately determine where you are compared to the stoichiometric ratio. As noted in [14], the molecular weight of their Jet-A (POSF 4658) was given as 142 ± 20 g/mol. This value amounts to an uncertainty of just over 14%. This uncertainty in φ would indicate that an experiment thought to be at $\varphi = 1.0$ could in reality be anywhere from $\varphi = 0.86$ to $\varphi = 1.14$. As is shown later, this is the primary reason that using the fuel mole fraction as opposed to equivalence ratio is so important when comparing different data sets involving complex fuel blends like kerosene.

The molecular weight, average molecule, and composition information for the fuels used in this study were provided by AFRL and were obtained using multidimensional gas

chromatography (GC x GC). An attempt was made by the author to confirm and validate the chemical composition of the first three fuels (Jet-A, RP-1, and DF #2) via TDI Brooks International, located in College Station. Unfortunately, the methods they used were only able to capture the n-paraffin species. This limitation amounted to them only being able to investigate about 20% of Jet-A, 0.46% of RP-1, and 12.77% of Diesel Fuel #2. The analysis on each of the fuels was conducted twice with different results, which gives some indication of the repeatability of determining the average properties in general. For example, the concentration of n-decane in the sample of Jet-A was found to be between 6% less and 1% greater than the AFRL value. The full comparison of these results is given in Appendix C.

Uncertainty in φ

This section discusses how differences in the filling technique affect the overall equivalence ratio. For the purpose of this analysis, the single-component fuel decane is used, thus removing any uncertainty in the fuel molecule and allowing for the focus to solely be on the experimental procedure.

Partial Pressure Method

Initial experiments were conducted using the partial pressure method, which relies on percentage of fuel and air in the mixture measured as a pressure. This method is independent of the size of the vessel because pressure fractions, mole fractions, and volume fractions are all the same for ideal gas mixtures. This partial pressure approach allows for the same experiments to be conducted in different experimental configurations using the same ratios.

When dealing with purely gas mixtures, the only sources of uncertainty in these experiments should be the thermocouples and the pressure transducers used. However, other uncertainties are added into the testing when dealing with liquid fuels such as vaporization, condensation, and the way the fuel is injected into the vessel.

The partial pressure method has traditionally been used to make mixtures at TAMU. Partial pressures for the fuel components for some of these studies are shown in Table 6 [53-56]. As can be seen in Table 6, the fuel partial pressures get closer together with larger hydrocarbons. Whereas an error in filling to 0.5 Torr would be unnoticeable for a syngas or methane mixture, it will be very significant for a decane mixture. Because of this enhanced sensitivity to small changes in partial pressure, it was important to have instrumentation as accurate as possible.

Table 6. Fuel partial pressures for gaseous and liquid fuels when filling to 1 atm.

ϕ	Coal Syngas 60% CO 40% H_2	Methane CH_4	Propene C_3H_6	Isobutene C_4H_8	Decane $C_{10}H_{22}$
0.7	172.73	52.05	24.05	18.18	7.14
0.8	191.19	58.91	27.36	20.71	8.15
0.9	208.54	65.64	30.65	23.22	9.16
1	224.85	72.24	33.90	25.71	10.16
1.1	240.23	78.72	37.12	28.19	11.16
1.2	254.75	85.07	40.32	30.65	12.16
1.3	268.48	91.31	43.49	33.09	13.16
1.4	281.48	97.44	46.63	35.51	14.15
1.5	293.81	103.45	49.74	37.92	15.14

Two pressure gauges were used during this study. The first was a Baratron 631D, with a range of 0 – 100 Torr and with a readout to the hundredth of a Torr. This gauge was only

used to measure the partial pressure of the liquid fuel added. The other pressure gauge used was a Baratron 626A, with a range of 0 – 1000 Torr. The display readout was to a tenth of a Torr. The K-type thermocouple, used to measure the temperature inside the vessel, has a display readout to the tenth of a degree.

When filling at a constant temperature, a 0.1-Torr difference in fuel partial pressure will result in an $\varphi = \pm 0.01$ difference. An extreme error of 0.5 Torr in fuel partial pressure would result in an error of equivalence ratio between $\varphi = 0.04$ and $\varphi = 0.05$. In contrast, a rather extreme fluctuation of ±3 K during filling would result in a fairly small error of $\varphi = \pm 0.01$.

It is also important to know how much effect an error in filling air will have on the mixture. Fortunately, the mixtures are not as sensitive to errors in filling with air. For example, with decane, a major error of 5 Torr when adding air, either above or below the target value of 760 Torr, would only result in a shift of $\varphi = \pm 0.006$. An error of 2 Torr would cut this value by a third to $\varphi = \pm 0.0012$. This reduced sensitivity when adding air (or any other gas) is not meant to be a license to be reckless while filling. However, it does indicate that a small pressure rise, post filling the vessel prior to ignition, as fuel re-vaporizes should not have a significant impact on the equivalence ratio.

There was also the question as to what was actually being added to the vessel when adding the fuel. In earlier experiments, it was noticed that air was leaking in through the syringe with air pockets forming in the syringe. This leakage led to uncertainty into if just fuel or some fuel-air mixture had been added to the vessel showing the resultant pressure. This is a big factor that led to the need for better airtight syringes discussed in the previous chapter.

Overall, the uncertainty in φ when using the partial pressure method was estimated at φ = ± 0.05. The residual uncertainty due to the instrumentation accounts for a small portion, at most 20%, of this. However, the instrumentation uncertainty assumes that all of the fuel added is immediately in the vapor phase and behaving as an ideal gas.

Two major factors contribute to the remaining uncertainty: air being added with the fuel (making the mixture leaner than expected) or liquid fuel vaporizing later (making the mixture richer than expected). The possibility of the fuel remaining in liquid form is discussed in more detail in the section regarding Laser Absorption. Because of these factors, it was determined that solely relying on the partial pressure method when preparing these mixtures did not provide sufficient accuracy.

Mass-Based Method

The next method used to prepare a mixture explored injecting a known mass of fuel into the vessel. While this method allows one to know exactly how much fuel is added to the vessel, and can thus calculate equivalence ratio, another source of uncertainty is added. This additional uncertainty is based on accurately knowing the volume of the vessel which leads to how many moles of the ideal gas fuel-air mixture it will hold at a given temperature and pressure. The mass of fuel added can be converted to number of moles if the molecular weight of the fuel were known. As discussed earlier, the volume of the HTHP vessel used in this study was measured to be 25.8 L using water and a 1-L beaker graduated at 50-mL increments. Using the ideal gas law, at ideal temperature (403 K) and pressure (760 Torr) the vessel will hold 0.7802275 moles of an ideal gas mixture.

However, the total number of moles will change if the volume measurement is inaccurate, or it the temperature or pressure change. To determine the effects these parameters would have on calculating the total number of moles, a matrix was formulated based on temperature, pressure, and volume. For this calculation, the volume of the vessel was adjusted ± 200 mL from the measured value. The temperature was adjusted ± 5 K from the experimental condition. Finally, the final total pressure was adjusted ± 5 Torr. These values were set beyond what would experimentally be accepted. This conservative approach provided an absolute maximum experimental uncertainty. This method looked at varying each of the three parameters individually, and then together. Results for the extreme cases, with the highest and lowest total moles, are shown in Figure 28.

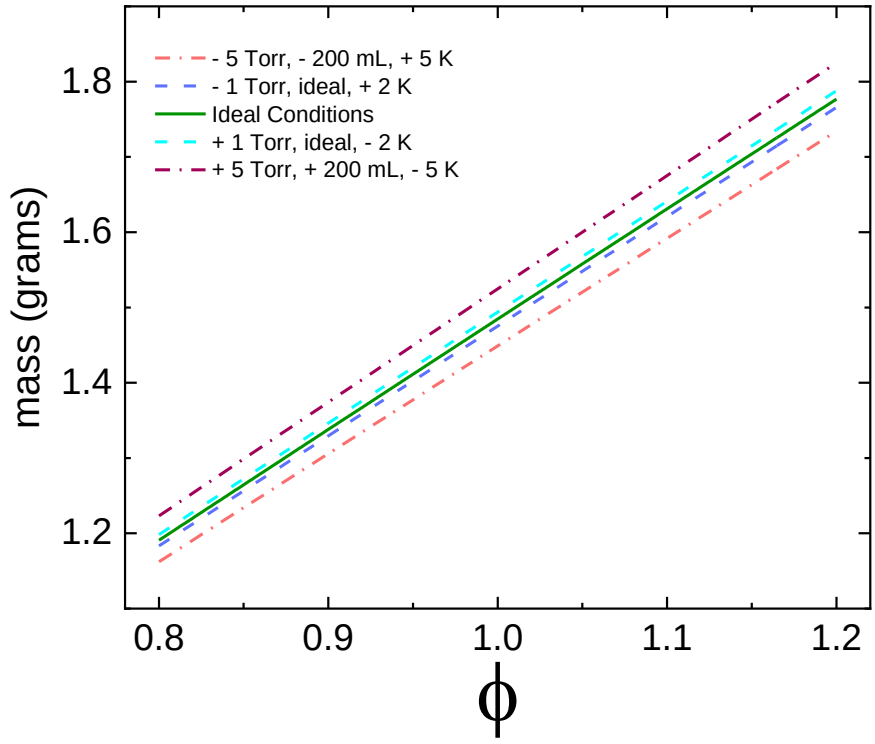

Figure 28. Effect of Temperature, Pressure, and Vessel Volume on the total number of moles the vessel can hold, leading to X_{FUEL} and therefore φ.

A detailed study focusing on just the vessel volume around φ = 1.0 is shown in Figure 29. An increase or decrease of 50 mL in the volume of the vessel will result in a 0.1313% change in the number of moles of ideal gas the vessel can hold. An extreme error in the measurement of the volume of the vessel of 200 mL would result in a 0.6583% increase or decrease in the moles of an ideal gas that the vessel could hold.

To put this this into a measurable perspective, for decane at φ = 1.0, 403 K, 760 Torr, the mass of fuel added should be 1.48 grams. A 200-mL error in the volume of the vessel

would result in a mass loading of 1.50 grams at the larger volume, and a loading of 1.47 grams at the smaller volume. These loadings would result in a range of φ = 0.99 and φ = 1.01, with the original volume and number of mole assumptions.

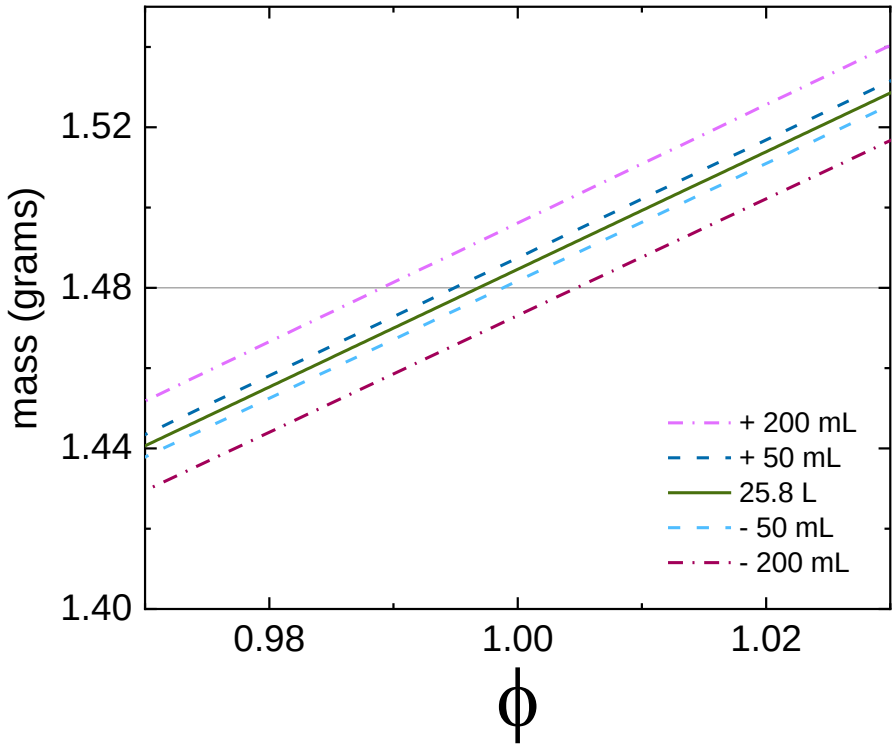

Figure 29. Mass loading for decane focusing on a variation of just vessel volume, around φ = 1.0.

The scale used to measure the mass of the fuel was an OHAUS Scout Pro SP202, with a range of 0 – 200 grams. Since the mass of fuel used in these experiments was on the order of one to two grams, all measurements were taken at the low end of the scale's range. The

accuracy of the scale was verified using a 12-Piece Test Weight Test Set with Calibration Certificate. The scale displayed mass to the hundredth of a gram. Hence, the accuracy of the scale was of the same order of magnitude as the residual uncertainty for mass loading at a given φ due to the uncertainty in the volume of the vessel.

Once injected, there are two sources of uncertainty with the fuel. The first of these is whether all of the fuel made it all the way inside the vessel. As discussed in the section on syringes in Chapter 5, longer syringe needles were used, increasing from 2 inches to 10 inches. This increase allowed for the tip of the needle to be all the way inside the vessel and allowed for clear visualization of the fuel entering the vessel. The second concern is whether the fuel vaporized completely or stayed in liquid form. This is the same concern as was previously seen with the partial pressure method.

Air is added to the vessel using the same partial pressure method as before. This will result in the same uncertainty as associated with addition of air discussed in the previous section.

The overall uncertainty in φ when using the mass-based method is $\varphi = \pm 0.03$. The major benefit of this technique is knowing exactly how much fuel was injected into the vessel. The uncertainties being: did the fuel make it all the way into the vessel (this concern was eliminated with the use of longer syringe needles), and did the fuel stay in vapor form. Only about one-third of this is the result of the instrumentation, a 50% decrease in the uncertainty from the partial pressure method.

Combined Method – Verification of Molecular Weight

Additional tests were done that combined the benefits of the partial pressure and the mass-based methods. To accomplish this, the 0 – 100 Torr gauge was mounted directly on the vessel, which allowed for the measurement of the molecular weight of the fuel as it was added to the vessel. This set of tests helped to verify the chemical composition of the fuel and ideal gas behavior in addition to knowing exactly how much fuel had been injected into the vessel.

To accomplish this, the molecular weight of the fuel was estimated based on a modified form of the ideal gas law shown in Equations 6.1 – 6.3. From the known mass of fuel injected into the vessel and the resultant partial pressure, the molecular weight can be calculated. This calculation is also dependent on the measured vessel temperature and the known vessel volume.

$$PV = N_{FUEL} R_u T \tag{6.1}$$

$$PV = \frac{m_{FUEL}}{MW} R_u T \tag{6.2}$$

$$MW = \frac{m_{FUEL} R_u T}{PV} \tag{6.3}$$

Based on these calculations, the molecular weights for RP-1, S-8, Shell GTL, were calculated to be within 3.3% of the values reported by AFRL. This result is well within the uncertainty in MW of 15% reported in [15, 20]. These results are shown in Figure 30.

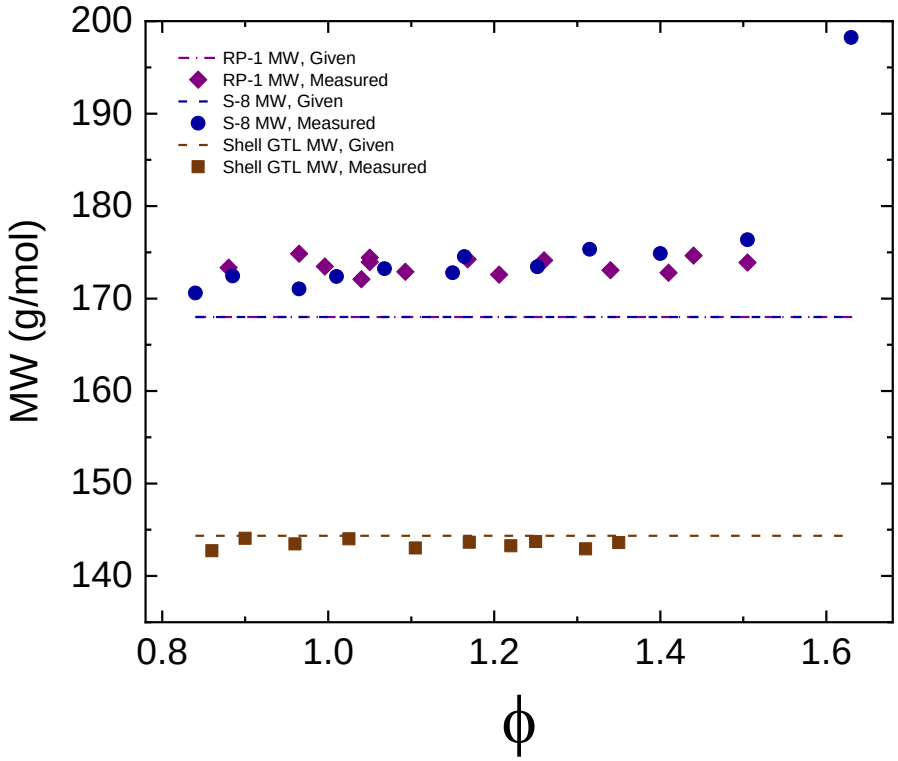

Figure 30. Calculated molecular weights of RP-1, S-8, and Shell GTL, compared to the provided values from AFRL. Throughout the range of tested equivalence ratios, these typically fell within 3.3% of each other.

This process also showed that the temperature for the diesel fuel experiments needed to be increased higher than previously thought. The reported molecular weight for diesel fuel #2 was 181.53 g/mol. When checked at 413 K the calculated molecular weight was 240 g/mol, or 31.86% greater than expected. The temperature was increased in 5-degree increments, as seen in Figure 31, to bring the calculated molecular weight closer to the reported molecular weight. This process increased until the vessel temperature was 448 K, when the average MW = 190.16 g/mol ± 1.5 g/mol. This is 4.75% greater than the value reported by AFRL but is a

value well within what appears to be the acceptable uncertainty in molecular weight for such a fuel.

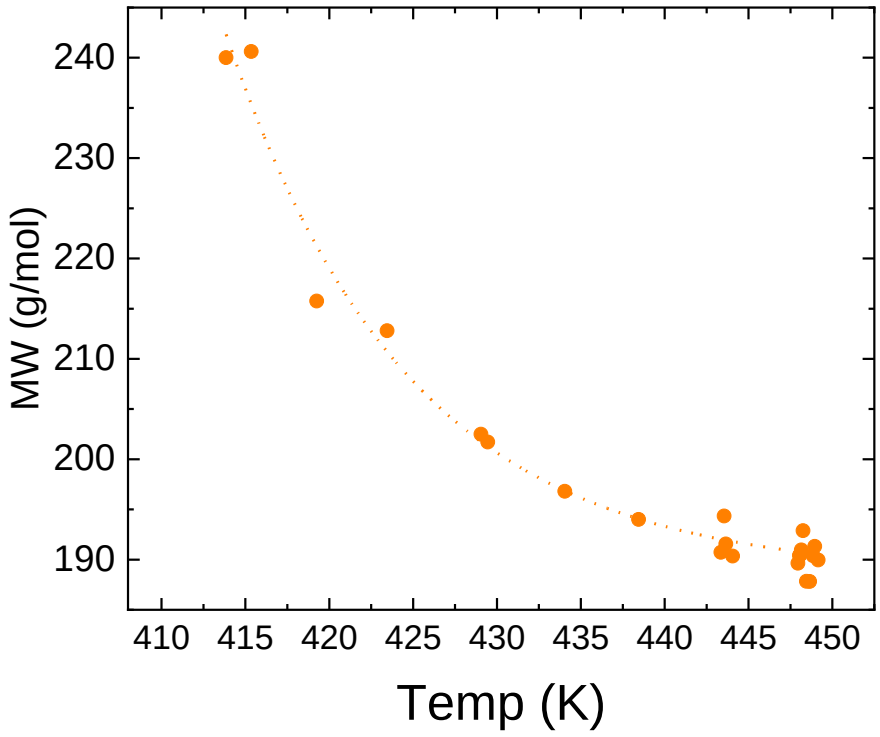

Figure 31. Effect of temperature on the measured Molecular Weight of Diesel Fuel #2. Symbols indicate data points. Dotted line is a curve fit through the data.

The overall uncertainty in φ using the combined method remains at φ = ± 0.03. Using both methods simultaneously is primarily designed to verify the fuel. At best, the calculated molecular weights were within 3% of the reported values. Therefore, this method is also attempting to account for uncertainties in the reported molecular weight. This uncertainty in fuel chemical composition was not measurable with any of the prior configurations.

Laser Absorption

Background

Beer's Law

One of the major concerns when working with these low-vapor pressure liquid fuels is condensation somewhere in the system which leads to uncertainty in the equivalence ratio from test to test. To help prevent and quantify the resulting uncertainty, the procedure for filling the flame speed vessel was tested and verified using an *in-situ* laser absorption technique to monitor directly the gas-phase fuel concentration within the vessel. To this end, a 3.39-μm HeNe laser used in conjunction with Beer's Law, Eqn. 6.4, was used to verify fuel mole fraction, leading to the equivalence ratio.

$$\frac{I}{I_0} = EXP\left[-\sigma_v \frac{X_i P}{R_u T} L\right] \tag{6.4}$$

The 3.39-micron wavelength corresponds to the C-H stretch vibrational mode that is typical of all hydrocarbons. The only two species-dependent terms in the equation above are the absorption cross section, σ_v, with units of m^2mol^{-1}, and the mole fraction X_i. Since O_2 and N_2 do not absorb at 3.39 μm, the only mole fraction of concern is the fuel mole fraction, X_{FUEL}. The transmitted intensity, I, and incident intensity, I_0, of the laser are the two measured parameters in the equation. The pressure, P, and the temperature T, are experimentally determined parameters, and R_u is the ideal gas constant. The only term that is adjustable is the tested area path length, L.

Therefore, with a known absorption cross section for the fuel, the mole fraction can be calculated from Eq. 6.4, and thus the equivalence ratio can be verified. The equation used to convert a known mole fraction to equivalence ratio is shown in Eq. 6.5. This equation assumes that the average molecule is used to represent the fuel blend, and therefore the stoichiometric amount of oxygen is known for that fuel. This equation also assumes that the fuel is being mixed with primary standard air with a molar N_2/O_2 ratio of 3.76.

$$\varphi = \frac{\frac{4.76}{\frac{1}{X_{FUEL}} - 1}}{\frac{1}{N_{O_2,stoic}}} \tag{6.5}$$

Relevant Literature

Most of the research and data on absorption cross sections of the relevant fuels comes out of the research group of Dr. Ronald Hanson at Stanford University. Even with a typical uncertainty of around 5%, these data are very useful as a starting point in calculating equivalence ratio given the absorption cross section.

The study of Klingbeil et al. [57] investigated and measured the absorption cross section of several hydrocarbons including: methane, n-decane, n-dodecane, Jet-A, and gasoline at various temperatures and pressures. All experiments were conducted in pure nitrogen as opposed to air. Shown in Figure 32 are the results for absorption cross section for Jet-A at various temperatures at 1 atm. Stated uncertainty in the absorption cross section was 4.2%. After fitting a third-order polynomial to their results, we can interpolate the absorption

cross section for Jet-A to our experimental condition of 403 K. The result is an absorption cross section of 45.39 m^2mol^{-1}.

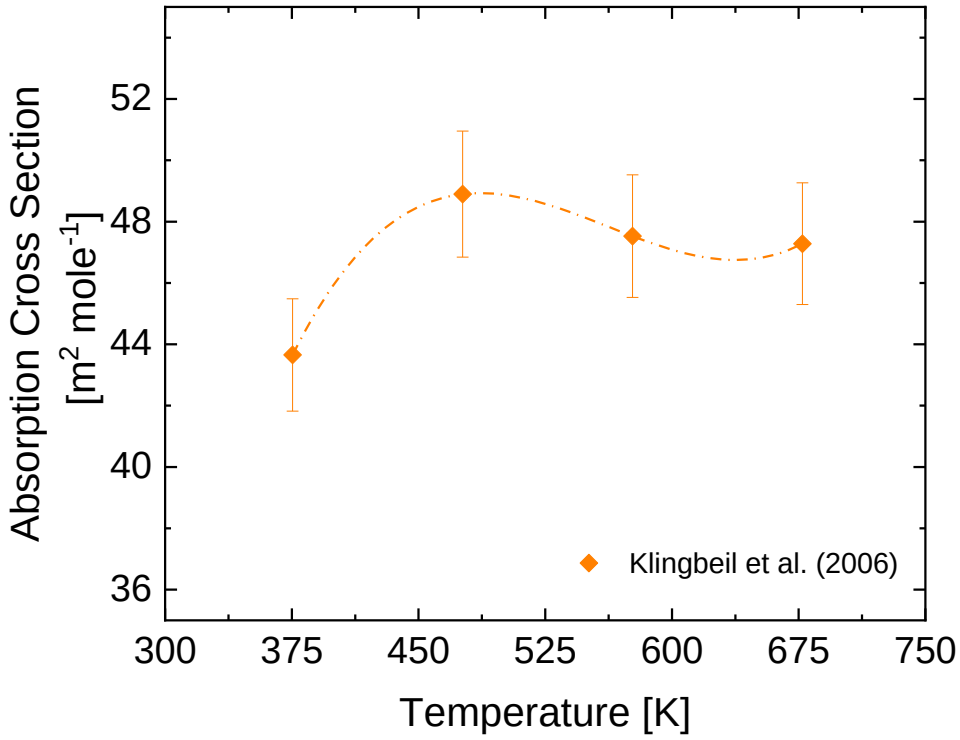

Figure 32. Absorption cross section versus temperature for Jet-A. Dashed line is a curve fit to the experimental data used to interpolate the absorption cross section at 403 K.

The follow on study of MacDonald [58] investigated several additional large hydrocarbons and hydrocarbon blends: dodecane, RP-1, MCH, and iso-Cetane. A temperature-dependent polynomial equation was provided for each fuel to calculate the absorption cross section at the 3.39-μm wavelength. The polynomial for RP-1 is given in Equation 6.10.

The resultant absorption cross section is 56.7 m^2mol^{-2}. No uncertainty was specified with this equation. A reasonable assumption would put it on the same order, 4-5% as was seen in [57].

$$\sigma_v(T) = 35.9 + 0.0818T + (-8.02 \times 10^{-5})T^2 + (1.31 \times 10^{-8})T^3 \qquad (6.10)$$

There are no published absorption cross section data available for Diesel fuel #2. As the average molecular weight and molecular formula for diesel fuel are similar to those for Jet-A and RP-1, an estimated starting point would be a similar absorption cross section.

Experimental Setup

It was desired to have I/I_0 in the range between 40 and 70%. Based on the absorption cross section data for Jet-A calculated by [57], this target range required the path length through the vessel to be around 3.75 cm. (Note that if the pathlength were taken to be the entire vessel inner diameter, the absorption would be at 100%.) To achieve this short path length through the vessel, the electrodes were removed and guide rods with windows on the ends were installed. Unfortunately, this setup prevented flame data from being collected at the same time. This portion of the setup is shown in Figure 33.

The desired dimensions also required navigating the 3.39-μm laser from the tabletop through the beam splitter, and then vertically about 3 feet to get it above the vessel, over to the center of the vessel, down through the vessel, then turned one last time. Overall, the beam was

reflected by 5 mirrors between the laser and the final intensity, *I*, detector. A simplified schematic of the optical configuration is shown in Figure 34.

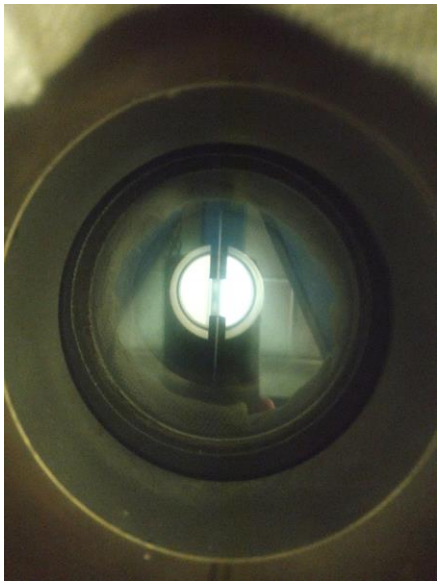

Figure 33. Laser guide rods as seen looking through the vessel window.

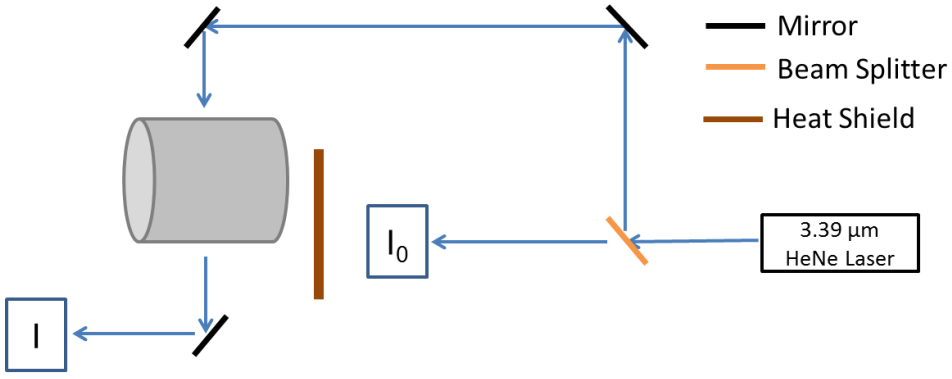

Figure 34. Diagram of setup for laser absorption experiments.

One of the complications of this setup was tracking the IR laser beam. Initially the beam was tracked and the mirrors aligned using a sight card that would show a dot where the beam was hitting. This method proved to be ineffective after the beam had been reflected by a couple mirrors as it was difficult to keep the card steady long enough to get a strong dot. The most effective way to align the laser was to carefully remove the IR laser and replace it with a red (632 nm) laser with an identical beam diameter. The mirrors were then adjusted to maneuver the laser beam through the vessel and to the intensity detectors. The red laser was then removed and the IR laser replaced. This laser replacement was done with care to ensure that none of the other components of the optical set up were disturbed.

Experimental mixtures were prepared in exactly the same manner as for a flame speed experiment, following the partial pressure method as these tests were conducted early on in the study. For all experiments, the HeNe laser was turned on and allowed at least one hour to warm up prior to any data collection. The J10D Series Indium Antimonide detectors used to record both I and I_0 were filled with liquid N_2, and I_0 was set equal to I using a polarizer. The readings of both detectors were monitored throughout the filling process. Once the filling was complete and the pressure stabilized at 760 Torr, readings for I and I_0 were recorded every 3 to 4 minutes for about 25 minutes. The average and standard deviation of these readings were then calculated.

One of the complications of this diagnostic was keeping the J10D Series Indium Antimonide detectors cold enough. While they were both cooled with liquid N_2, they were both placed within a foot of the vessel which was sitting at 403 K. This proximity to the heated

vessel caused the liquid N_2 to boil off quickly. Refilling the detectors during an experiment would significantly alter the measurement. To help reduce this effect, a heat shield, shown in Figure 35, which consisted of a piece of plywood covered with aluminum foil, was placed between the vessel and I_0 detector. This design proved to be effective in allowing for experiments to be completed prior to the detectors overheating. The *I* detector was located below and slightly farther away from the vessel, so it was not as affected as much.

Figure 35. Heat shield between the heated vessel and the J10D Series Indium Antimonide detector. Also visible are the HeNe laser tube and a couple of the mirrors used to pass the laser beam through the vessel.

Jet-A

Figure 36 shows the results for I/I_0 versus φ for Jet-A/air mixtures. These mixtures were prepared in the manner described above over a range of equivalence ratios. The laser absorption values shown are the average values over a period of about 20 minutes. As expected, I/I_0 decreased as the mixture became richer, as the greater amount of fuel absorbed more of the laser. The results for Jet-A are reasonably close to the predicted values of [57].

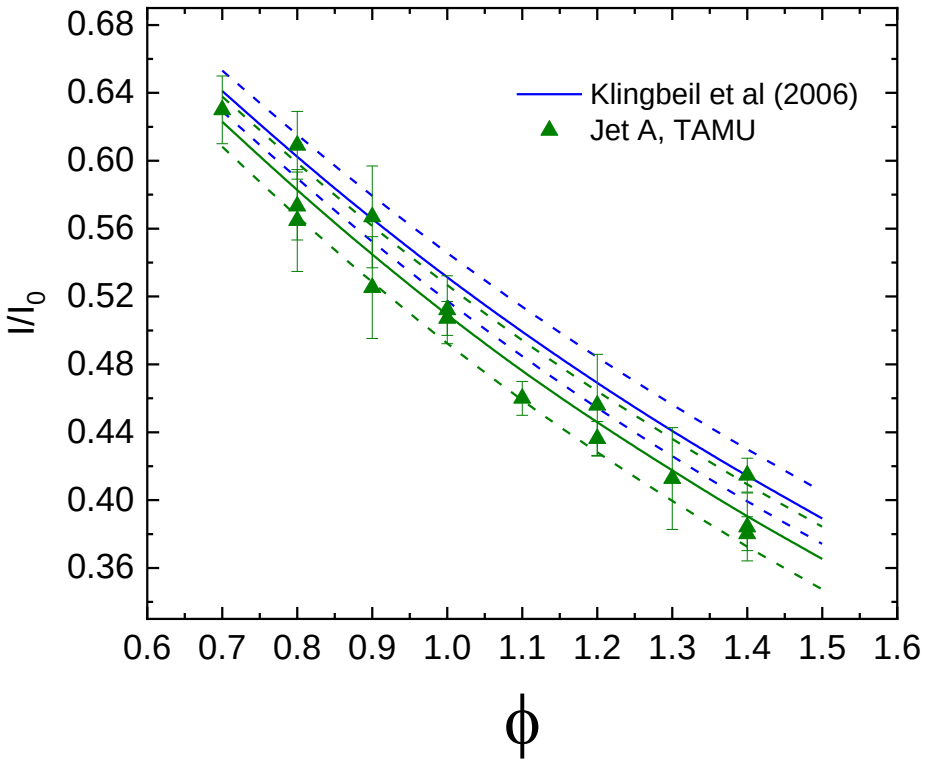

Figure 36. Laser absorption results for Jet-A at 403 K and 1 atm. Triangles are data points. Solid lines are predicted values for I/I_0. Dashed lines show the uncertainty predictions for I/I_0.

Based on the data collected, an absorption cross section was calculated for the Jet-A currently being used. This calculation resulted in a $\sigma_v = 48.23$ m^2mol^{-1}. The predicted values for I/I_0 with this absorption cross section with a 5% uncertainty are shown by the green solid and dashed curves respectively in Figure 36. There was a 4.2% uncertainty calculated in $\sigma_v = 45.39$ m^2mol^{-1}, evaluated in [57]. These predicted values are shown by the blue curves, with the dashed curves giving the range of uncertainty. There is a 6% difference in the two calculated absorption cross sections.

RP-1

Figure 37 shows the laser absorption data for RP-1. The absorption results were compared to the predictions calculated by [58]. The data showed very good agreement with the predictions, although results were still around 3% lower overall. The experimental data also proved to be much more repeatable than they were for Jet-A. Similar to Jet-A, the absorption cross section was calculated based on the experimental data. This value of $\sigma_v = 57.7$ m^2mol^{-1} is less than 2% greater than the value of 56.7 m^2mol^{-1} calculated in [58]. Based on scatter in the data, experimental uncertainty is predicted to be 5%.

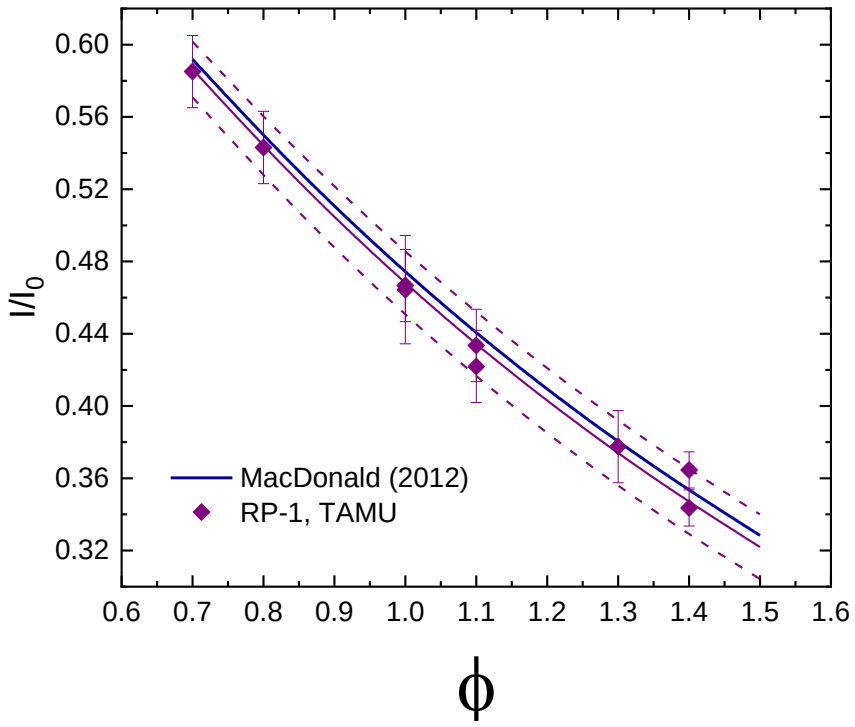

Figure 37. Laser absorption results for RP-1 at 403 K and 1 atm. Diamonds are data points. Solid lines are predicted values for I/I_0. Dashed lines show the uncertainty predictions for I/I_0.

Diesel Fuel #2

There were no model predictions to compare with the Diesel Fuel #2 experimental laser absorption data. As diesel fuel has the widest variation in average chemical formula, and therefore the largest variation in absorption cross section, this lack of models is understandable. The data still proved to have a fairly constant and repeatable absorption cross section on the same order as was found for Jet-A and RP-1. The laser absorption results are shown in Figure 38. These data were collected at 403 K. While condensation was seen at richer

conditions, there was no indication of any condensation at the lean, stoichiometric, and slightly rich conditions shown in Figure 38. Based on the more recent analysis with MW, this was clearly not the case.

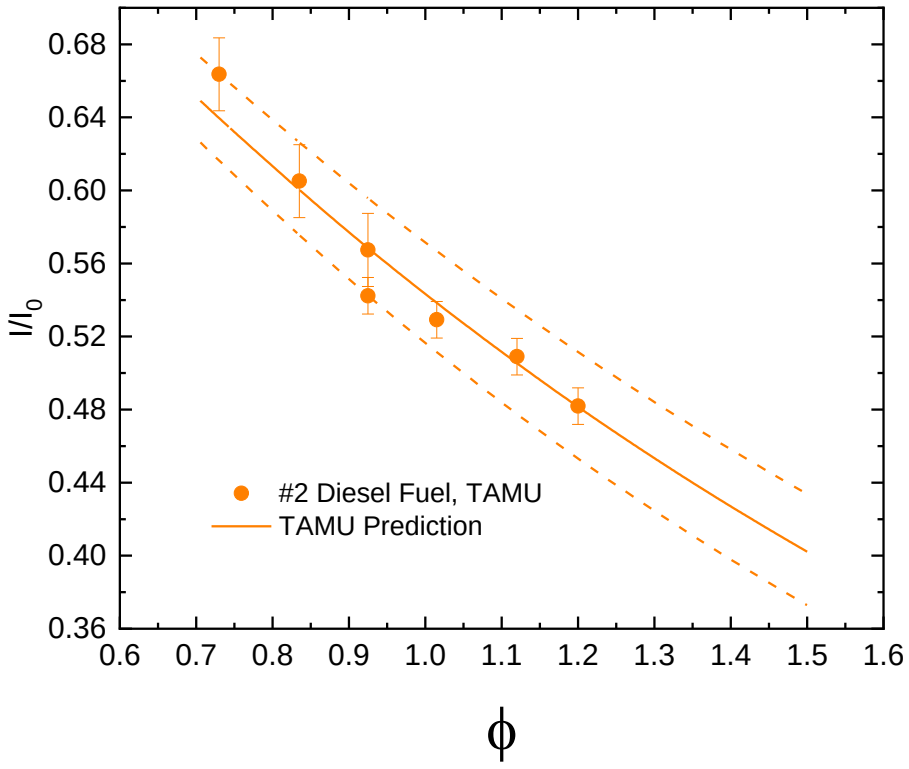

Figure 38. Laser absorption results for Diesel Fuel #2 at 403 K and 1 atm. Circles are data points. The solid line represents the predicted values for I/I_0. Dashed lines show the uncertainty predictions for I/I_0.

Data Analysis over Time

The laser absorption measurements also showed that the fuel condensed while filling the vessel with air. This phenomenon could be seen in the first five minutes after air was added to the mixture. Shown in Figure 39 are recorded values for I/I_0 over time for each fuel at sample equivalence ratios. Time started for these measurements once the vessel had been completely filled to atmospheric pressure. As shown, I/I_0 decreased by about 20-25% over the first five minutes. The value of I/I_0 remained relatively stable over the next 20 minutes. This stability at longer times indicates that the fuel condensed somewhere in the vessel and was therefore not absorbed by the path of the laser. As the air added to the vessel heated up, the fuel re-vaporized and the absorption reached steady state. Because of this observation, during actual flame speed experiments the fuel/air mixture was allowed to sit in the vessel for at least 10 minutes prior to ignition.

Conclusions

Overall, the laser absorption analysis was useful in verifying that the fuel was vaporizing. However, it still left an uncertainty around $\varphi = \pm 0.05$. This number was due to the roughly 5% uncertainty in absorption cross section. Nonetheless, this method showed the importance of giving the fuel and air mixture time to heat up and the fuel to return to vapor state following filling. This was seen as I/I_0 significantly decreased in the first five minutes following the addition of air. Because of this, at least 10 minutes and usually between 15 and 20 minutes elapsed between fully filling the vessel and conducting the experiment. Experiments conducted prior to the 5 minute mark would run the risk of having fuel still in

liquid form somewhere in the vessel, and therefore not being at the correct equivalence ratio. Finally, the laser absorption measurements of the fuel concentration also showed the repeatability of the fuel introduction (and equivalence ratio evaluation) methods using an independent assessment of the amount of fuel that was being put into the vessel.

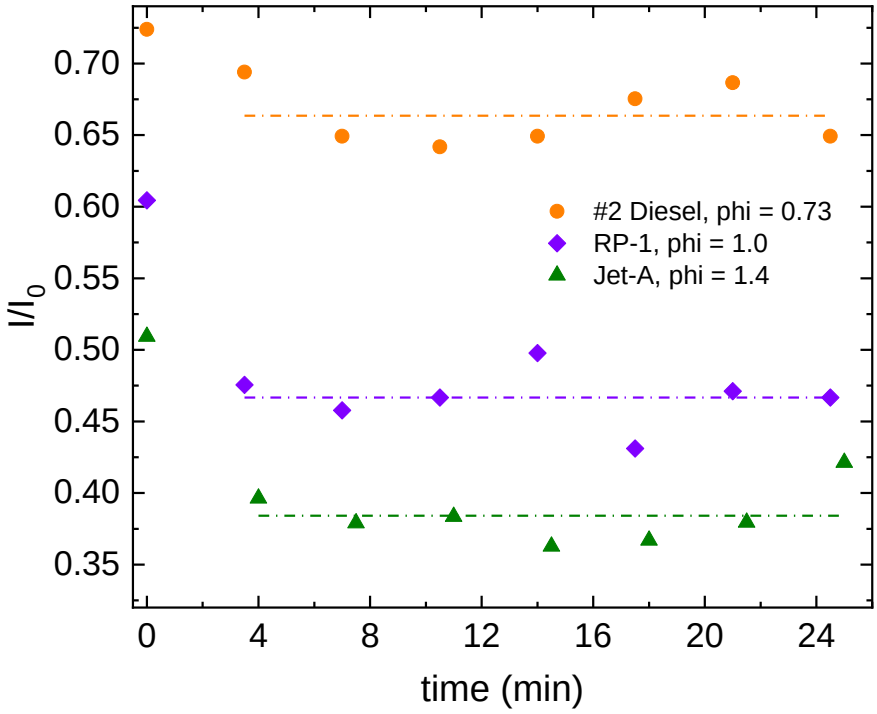

Figure 39. Laser absorption results over time for selected experiments at different equivalence ratios. Symbols indicate actual values of I/I_0. Dashed lines are the average values (as shown on previous Figures).

Uncertainty in Flame Speed

Density Ratio Analysis

As discussed in Chapter 4, the unburned, unstretched laminar flame speed is calculated by dividing the burned, unstretched laminar flame speed by the density ratio, σ, of the unburned to the burned gases. These values are calculated from equilibrium chemistry. However these estimates require the use of a chemical kinetics mechanism and (primarily) the corresponding thermochemical data set. Figure 40 shows the density ratios for several of the proposed surrogates for Jet-A across the range of equivalence ratios tested. The equivalence ratios tested the "Narayanaswamy mechanism" [29] has the smallest density ratio, whereas the single-component, $C_{11}H_{22}$, using the "JetSurF 2.0" mechanism has the largest density ratio. This single component was chosen because it most closely matched the average molecular formula and therefore molecular weight of the Jet-A used in this study. At $\varphi = 0.65$, there is a 0.98% difference between these two values. At $\varphi = 1.5$, this difference has grown to 1.95%. This difference amounts to an uncertainty of 1 cm/s for rich mixtures and would be the minimum uncertainty for the unburned flame speed.

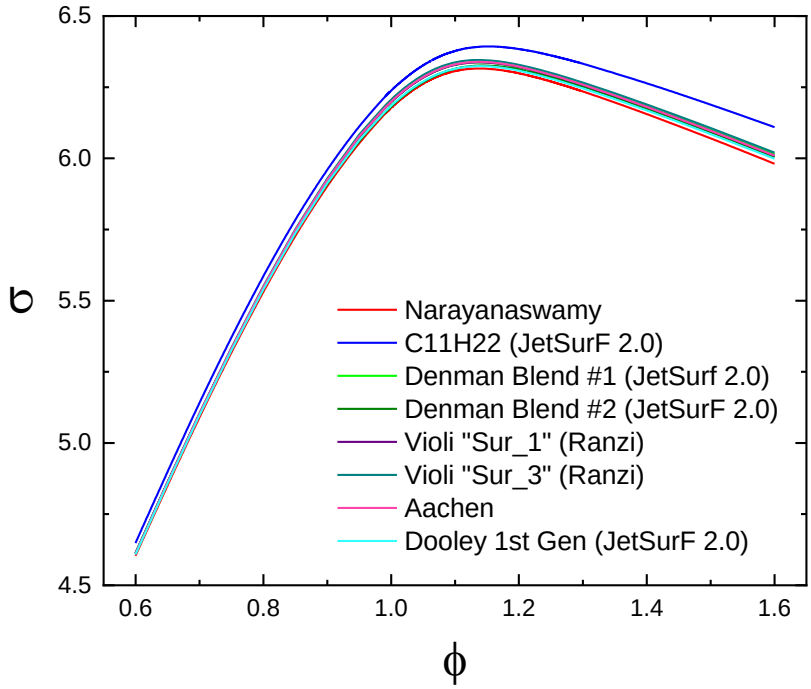

Figure 40. Density Ratios for various surrogates for Jet-A at 1 atm and 403 K.

Kline and McClintock Method

Additional uncertainty analysis was carried out using the method of Kline and McClintock as outlined in Moffat [59], and used in previous studies. This method calculates the total uncertainty, U_{SL}, as a combination of the bias error, B_{SL}, and the random error, P_{SL}. This procedure is shown in Equation 6.11. The terms in this equation are discussed below.

$$U_{SL} = (B_{SL}^2 + P_{SL}^2)^{0.5} \qquad 6.11$$

Bias uncertainty is a systemic error parameter affecting the accuracy with which experiments can be conducted. Using some of the chemical kinetics mechanisms as a tool for calculating laminar flame speed, the bias uncertainty aims to determine how much small differences in experimental equivalence ratio or temperature can impact laminar flame speed.

The general equation for laminar flame speed as a function of temperature and equivalence ratio is shown in Equation 6.12. The nine coefficients for this equation were determined using the "Narayanaswamy Mechanism" [29] for Jet-A. The mechanism was run at various temperatures of 385, 388, 403, 420, 430, 450, 473, and 500 K. A surface was than fit to the results, and the coefficients calculated using the surface-fitting tool in MATLAB. The resultant graph is shown in Figure 41. From looking at the surface fit, it is easy to see the strong effect temperature has on flame speed. The same procedure was used with the chemical kinetics model of [7] to fit a surface for the pure fuel, decane. The resultant coefficients are provided in Table 7.

$$S_{L,u}^{0} = (a + b\varphi + c\varphi^{2} + d\varphi^{3} + e\varphi^{4})\left(\frac{T}{403K}\right)^{(p+q\varphi+r\varphi^{2}+s\varphi^{3})} \qquad 6.12$$

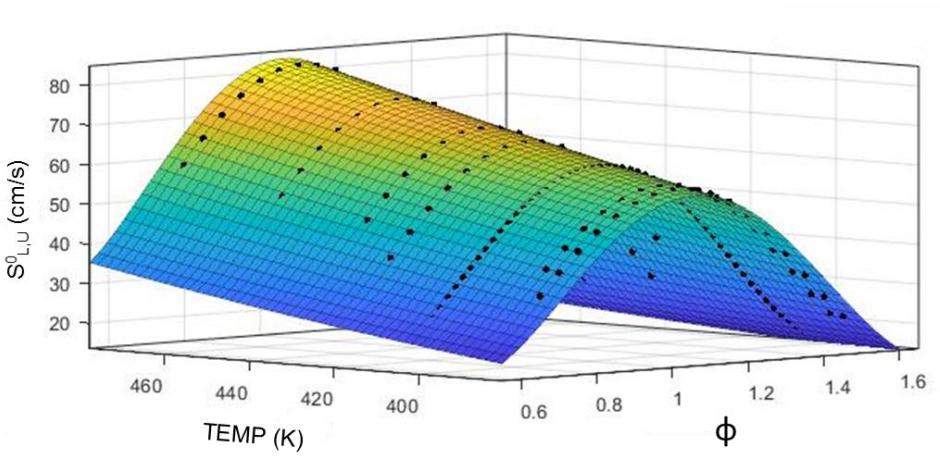

Figure 41. Surface fit of Narayanaswamy mechanism for Jet-A based on equation 6.12.

Table 7. Coefficients of flame speed equation (Eqn. 6.12) for two sample fuels.

Surrogate	a	b	c	d	e	p	q	r	s
Narayanaswamy	198.3	-1024	1928	-1360	318.7	9.608	-19.02	14.54	-3.468
Decane	367.3	-1596	2632	-1734	392.6	10.39	-21.52	17.12	-4.3

The bias uncertainty is calculated from the partial derivatives of Equation 6.12 as shown below. Overall, both the three-component Narayanaswamy blend (30.3% dodecane, 21.2% m-xylene, and 48.5% MCH) and decane have similar results.

$$B_{SL} = \sqrt{\sum_{i=1}^{n} \left(\frac{\partial S_{L,u}^{0}(x_i)}{\partial x_i} u_i \right)^2} \qquad 6.13$$

For both surrogates, the average B_{SL} = 1.01 cm/s with values ranging between 0.8 cm/s and 1.25 cm/s. These differences appear to be greater the further away from the ideal condition of φ = 1.0, 403 K the data point is. This value is small because the uncertainty in φ was set at its minimal instrumentation-only value of φ = ± 0.1. This choice is justifiable because error bars in φ are being shown separately.

The random error, P_{SL}, is based upon the differences in the repeated data points throughout the data set. Figure 42 shows the experimental results for n-decane and Jet-A over a small range of equivalence ratios between φ = 0.94 and φ = 1.06. Essentially, these are all of the repeats of the stoichiometric condition.

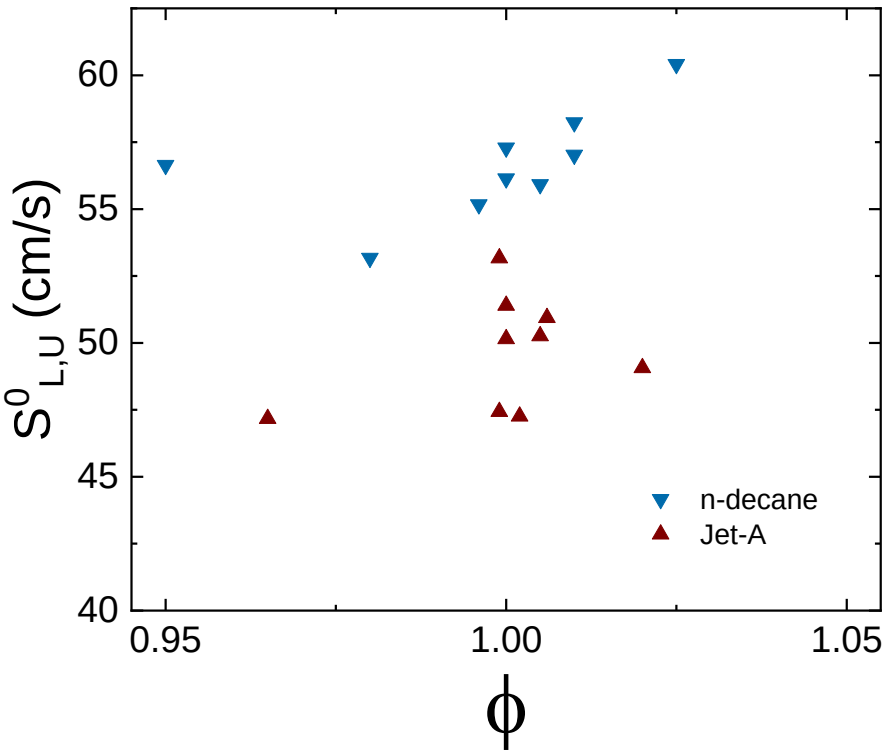

Figure 42. Laminar Flame Speed Results for n-decane and Jet-A near φ = 1.0 at 403 K and 1 atm.

Decane at φ = 1.0 ± 0.01 was repeated six times with an average flame speed of 56.6 cm/s with standard deviation of 1.11 cm/s. Likewise, Jet-A at φ = 1.1± 0.01 was repeated six times with an average flame speed of 50.8 cm/s with a standard deviation of 1.3 cm/s. All of these points were determined to be good data points during Markstein length analysis, which is discussed in the next chapter. Based on these values and to account for larger deviation at both lean and rich equivalence ratios, the estimated random error is set at twice the standard deviation, P_{SL} = 2.6 cm/s.

Based on this analysis, the average overall uncertainty for all fuels is ± 2.79 cm/s. A majority of this error comes from the random error calculation based on the repeatability of experiments.

Conclusions

It is very important to fully understand all the sources of uncertainty present in the system. There is some uncertainty tied to the calculation of the flame speed due to the density ratios used. However, this value appears to be very minor, on the order of 1 – 2% of the overall flame speed. Repeatability of data is also a common source for uncertainty. However, when looking at repeated points of both the pure fuel decane, and Jet-A, it has been shown that the results are fairly repeatable, with a variation of about 4.25%.

The uncertainty in φ was reduced from $\varphi = 0.05$ to $\varphi = 0.03$ when using the mass-based method for filling as opposed to the partial pressure method. The laser absorption technique could initially only determine $\varphi = \pm 0.05$ due to the uncertainty in the absorption cross section. However, the laser absorption measurements showed the importance of waiting at least 10 minutes after filling to allow the mixture to fully heat up and any condensed fuel to return to vapor phase. The composition of the fuel was verified to within 3% by measuring the molecular weight of the fuel.

The uncertainty in laminar flame speed was determined to be ± 2.79 cm/s. The chemical kinetics mechanism used to calculate the density ratios was shown to affect flame speed by 1 cm/s at most.

These overall effects on the uncertainty in both equivalence ratio and laminar flame speed are shown as percentages in Figure 43. Overall, 2/3 of the uncertainty in equivalence ratio is due to the nature of the fuel, with the remaining 1/3 due to the accuracy of the instrumentation used. As for the calculated laminar flame speed, 93% of the uncertainty is due to the repeatability of the experiments. Hence, if one were to use only the bias error (i.e., the error due to measurement precision) to estimate the uncertainty, they would seriously underpredict the true measurement uncertainty for liquid-fuel laminar flame speeds such as herein.

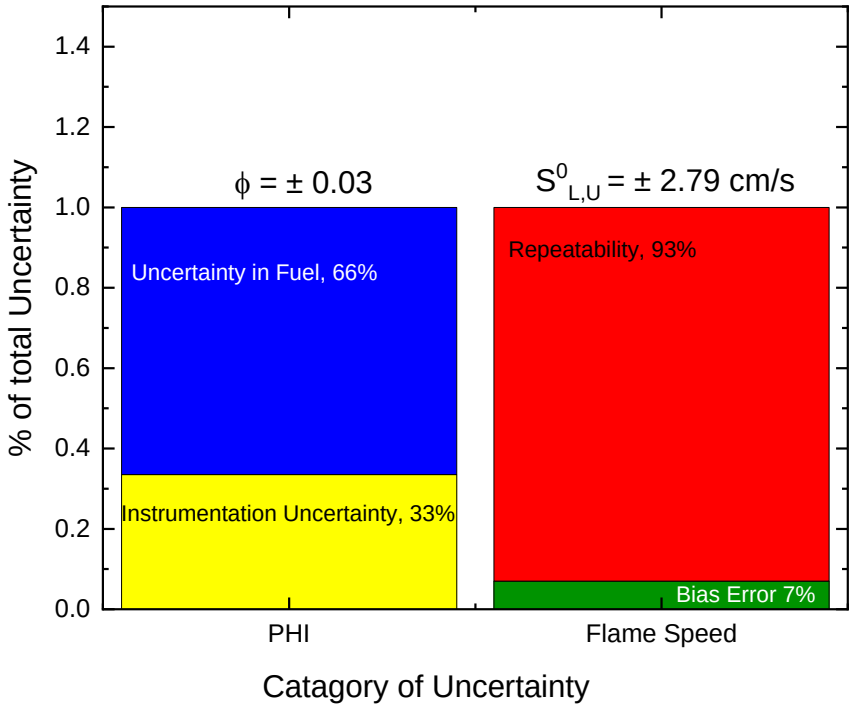

Figure 43. Breakdown of the sources of uncertainty showing their overall impact on the total experimental uncertainty.

CHAPTER VII

FLAME SPEED RESULTS

This chapter presents laminar flame speed results for the fuels contained in this study. The focus is to present the results and highlight noticed trends as well as analysis of good, questionable, and bad data points using the methods outlined in the previous chapters, partially based on Markstein length analysis. Comparison to other research groups' data sets and chemical kinetic mechanisms are covered in Chapter 8.

Jet-A

As discussed previously, the Jet-A used for all flame speed experiments in this study was sourced from AFRL, identified as POSF 10325. The average molecule for this fuel was specified as $C_{11.4}H_{22.1}$. At room temperature, the density of the fuel was reported as 0.803 g/mL, and the molecular weight was given as 159 g/mol. The fuel was a clear liquid.

Three different sets of data were collected for Jet-A. The first of these utilized a 0-1000 Torr pressure transducer to measure the partial pressure of the fuel. This initial data set consisted of eleven data points ranging in equivalence ratio from $\varphi = 0.84$ to $\varphi = 1.38$. These data are referred to as "2017" in the figures that follow. These were also the very first liquid fuel points collected, the results of which partially led to the decision to conduct the laser absorption measurements described in the previous chapter. The second set of data were collected using the previously discussed 0-100 Torr pressure transducer. This change was done to obtain better precision in measuring the amount of fuel injected into the vessel. This data set consisted of 15 points ranging from $\varphi = 0.8$ to $\varphi = 1.4$. These data are referred to as "2018"

in the figures that follow. The final data set for Jet-A was collected measuring the mass of fuel injected into the vessel. This data set consisted of 13 points ranging from φ = 0.905 to φ = 1.33. These data are referred to as "2019" data in the figures that follow.

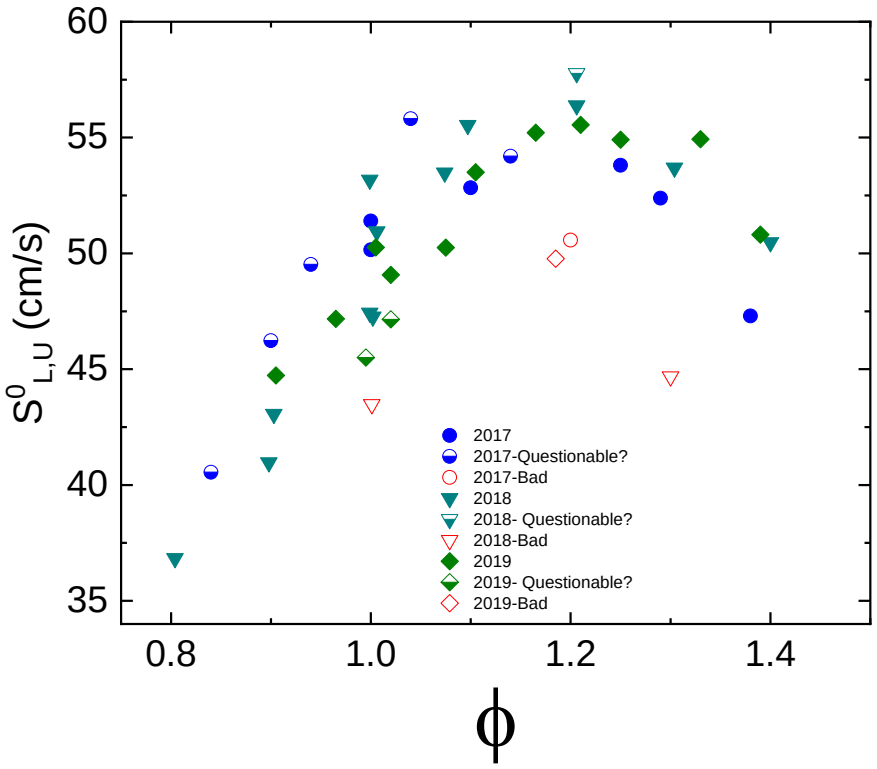

Figure 44. Complete laminar flame speed results for Jet-A. Data are color coded by year and method with indications on the acceptability of the data. Phi is based on average molecule ($C_{11.4}H_{22.1}$) provided by AFRL.

The results for all three data sets are shown in Figure 44. For each study, the results are divided into three different categories: Good, Questionable, and Bad. These designations are discussed in more detail below. Overall, the results for all three curves show fairly good

agreement. All three saw a peak flame speed around 55 cm/s at φ = 1.2. However, there was also some significant scatter in the results, such as a 10 cm/s difference in measured flame speeds around φ = 1.0. The 2017 data has the least-defined curve, and also appears to have the most scatter. This poorer quality makes sense due to the less-accurate pressure gauge used to measure the partial pressure of the fuel.

With the large amount of data collected, other trends sometimes become apparent, such as when the measured flame speed results do not appear reasonable. Examples of this would be the points labeled as "bad" in the 2017 and 2019 data sets located around φ = 1.2. Both of these points measured a laminar flame speed around 50 cm/s, which is about 9% below the expected data based on the other results.

To help determine the accuracy of the data, a Markstein length correlation, similar to the one discovered for n-decane, was used. The correlation for Jet-A is shown in Equation 7.1. An uncertainty of φ = ± 0.1 was applied to help determine if data points were acceptable or not.

$$L_b = -0.30688\varphi + 0.43925 \tag{7.1}$$

As can be seen in Figure 45, most of the data follow the same trend. However, there are some data points that are clear outliers, looking again at the two data points around φ = 1.2. Based on the correlation, the Markstein length should be around L_b = 0.070994 cm. The measured Markstein lengths for the two data points are L_b = -0.0189 cm for the 2017 data point and L_b = 0.18 cm for the 2019 data point. These L_b are both clearly outside of the

acceptable limits. Since neither the laminar flame speed nor the Markstein length are within reasonable limits, the points were rejected as bad data.

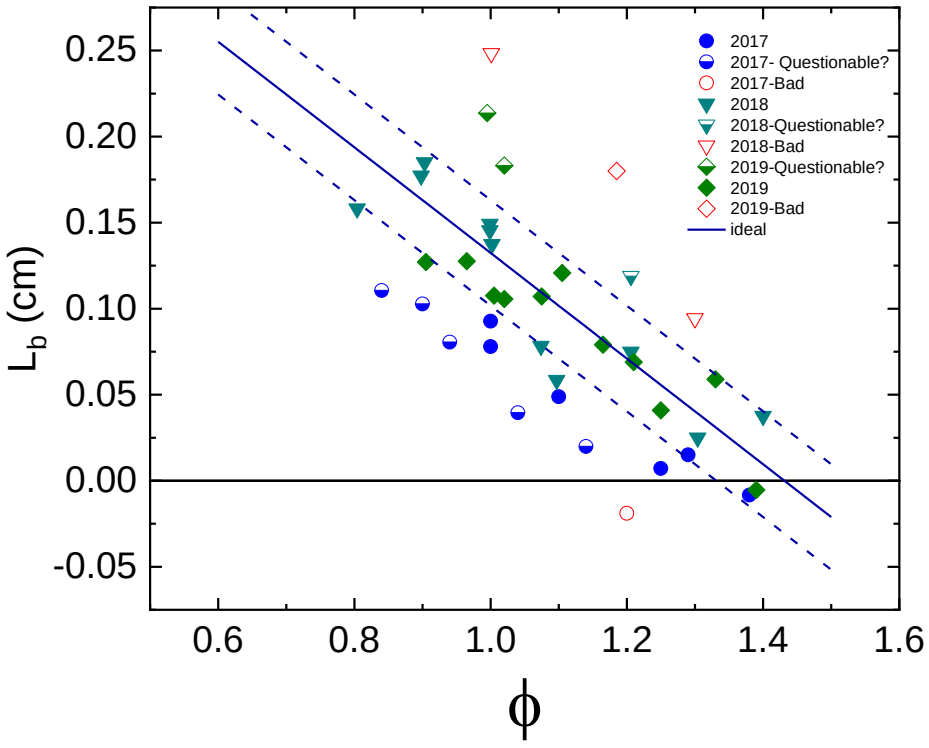

Figure 45. Burned gas Markstein Length results for Jet-A. Symbols show the experimental results by year, method, and acceptability of the data. Solid line indicates the linear correlation for the Markstein length with dashed lines showing the uncertainty interval.

In contrast, there were several data points that fell almost exactly on the correlation line. An example includes the 2019 data point at $\varphi = 1.075$ which had a measured Markstein length of $L_b = 0.1071$ compared to the predicted value of $L_b = 0.10954$. The flame speed of 50.25 cm/s is also within the acceptable range.

Overall, the Markstein length data look very good. The “2017” data appear consistently to produce a slightly smaller Markstein length. The “2018” and “2019” data show better agreement, with the results almost right on top of each other. The Markstein length remained positive for almost all mixtures investigated. A slightly negative value was only measured at the very richest conditions tested, and therefore nonlinear method I was used for analysis almost exclusively. This positive Markstein length trend also indicates that the flames remained very stable throughout all equivalence ratios tested.

After analyzing all of the data together, a final data set was assembled including only data points determined to be acceptable. These data are compiled in Figure 46. The dashed line shown is a trend line to help better see the overall shape of the curve. As before, the peak flame speed is around 56 cm/s near $\varphi = 1.18$. Error bars shown are based on the uncertainty analysis discussed in the previous chapter.

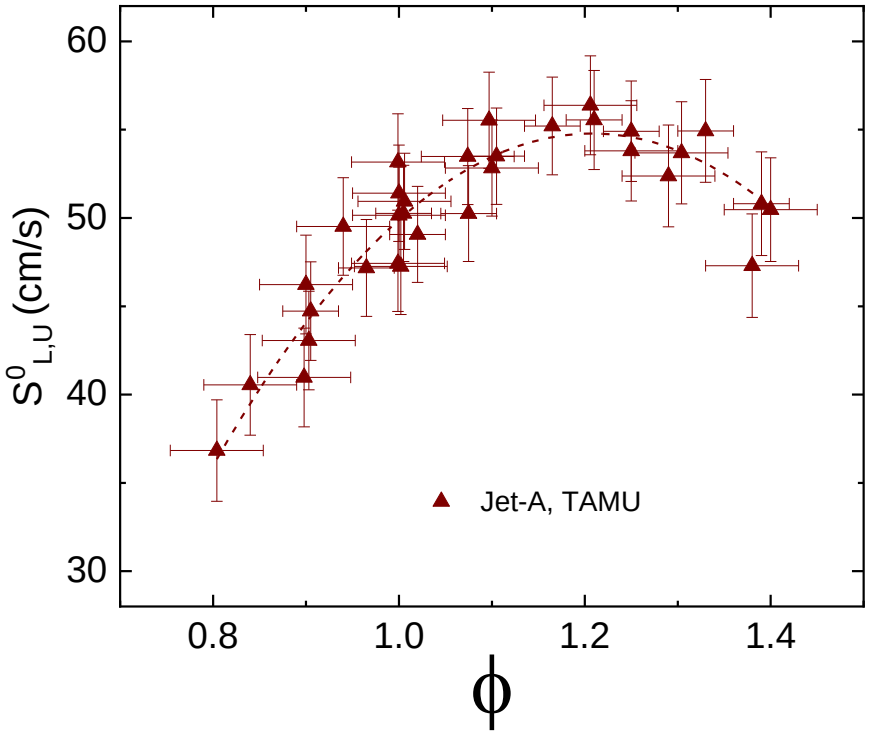

Figure 46. Final data set for Jet-A at 403 K and 1 atm. Dashed line is a trend line through the data. Phi is based on average molecule ($C_{11.4}H_{22.1}$) provided by AFRL.

RP-1

The RP-1 used for all experiments was identified as POSF 5235, with an average chemical formula of $C_{12}H_{24.1}$. The molecular weight for the fuel was listed as 168 g/mol, with a density at room temperature of 0.809 g/mL. In appearance, the fuel had a slightly pink color to it.

The initial data set for RP-1 was collected using the 0-100 Torr pressure transducer to measure the partial pressure of the fuel. This initial data set contained 12 points ranging from

φ = 0.904 to φ = 1.4. For the following discussion, these data are referred to as the "2018". When the data set was repeated using the mass-based method, 14 points were taken ranging from φ = 0.88 to φ = 1.505 and are referred to as "2019". The combined results are shown in Figure 47. Overall, the flame speed trend looks good, with a peak value between φ = 1.1 and 1.2. The peak flame speed was found to be 56.8 cm/s. As can be seen, the results were fairly repeatable as evidenced by the four points around φ = 1.1 that returned flame speeds within 1 cm/s of each other.

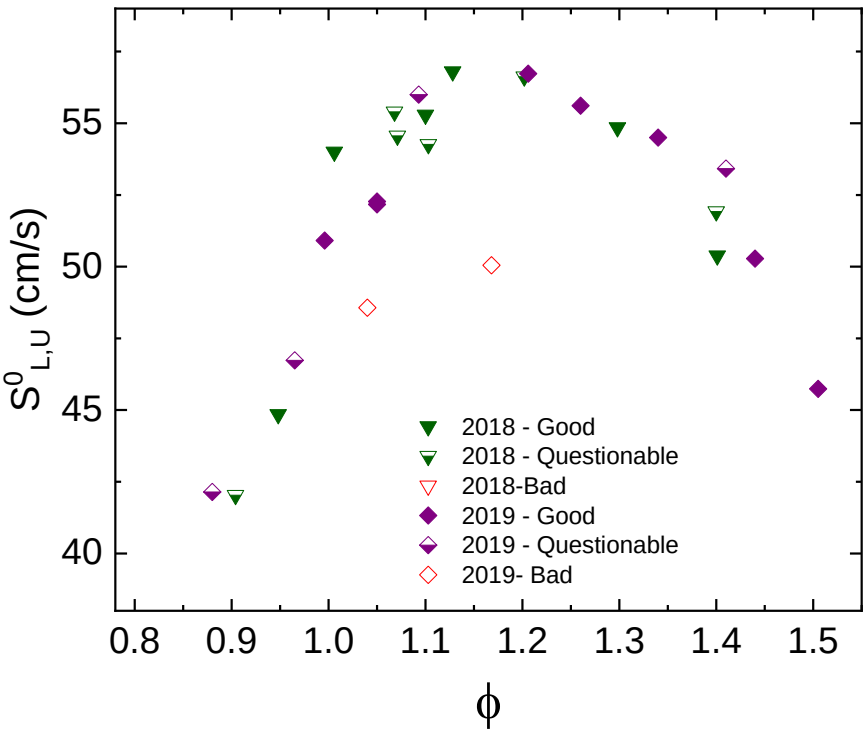

Figure 47. Complete laminar flame speed results for RP-1. Data are color coded by year and method with indications on the acceptability of the data. Phi is based on average molecule ($C_{12}H_{24.1}$) provided by AFRL.

There were far fewer “questionable” or “bad” data points for RP-1 when compared to the results with Jet-A. However, two points from the 2019 appear to have significant errors. The first of these at φ = 1.04 returned a flame speed of 48.57 cm/s. In the same data set, the similar equivalence ratio of φ = 1.05 was repeated twice, with measured flame speeds of 52.27 cm/s and 52.17 cm/s. While this 7% difference could be within the acceptable scatter in the data, similar scatter was not seen at other equivalence ratios in the study, so therefore the point was rejected. The other point at φ = 1.168 similarly reported a significantly, around 11%, slower laminar flame speed than expected.

It was hoped that the Markstein length correlation would help explain these points that were clearly outliers. As with decane and Jet-A, a strong linear correlation was also seen between the burned-gas Markstein length and the equivalence ratio. The updated Markstein length correlation for RP-1 is shown in Equation 7.2. Due to the stronger linear trend, the uncertainty limits were set at φ = ± 0.05 for RP-1.

$$L_b = -0.3268\varphi + 0.4678 \tag{7.2}$$

The burned-gas Markstein lengths for RP-1 are shown in Figure 48. Most of the 2019 data points fall right on the predicted value. There appears to be slightly more scatter in the Markstein length for the 2018 data. Unfortunately, the Markstein analysis did not provide any clear indication of the problem points discussed above, as the Markstein lengths, while not on the predicted value line, are nonetheless very close to the dashed uncertainty lines. The leaner

of the two points (φ = 1.04) is 1.5% outside the limits whereas the other point (φ = 1.168) is 7.5% outside the limits. Similarly, there were points with reasonable flame speeds that had Markstein lengths that were well outside of the predicted values (greater than 10%). These points were lean mixtures where the linear correlation has shown not to be as strong.

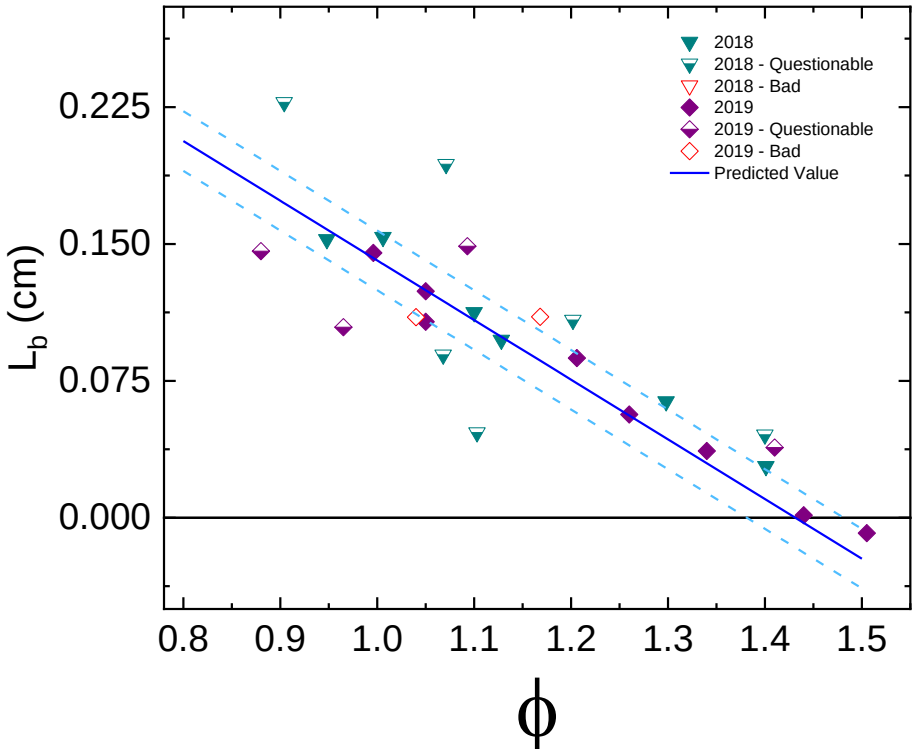

Figure 48. Burned-gas Markstein Lengths for RP-1. Symbols show the experimental results by year, method, and acceptability of the data. Solid line indicates the linear correlation for the Markstein length with dashed lines showing the uncertainty interval.

The consolidated RP-1 data are shown in Figure 49. As can be seen, the peak flame speed occurs around φ = 1.2 using the MW provided by AFRL. Overall, the results for this fuel appear to be more repeatable than Jet-A.

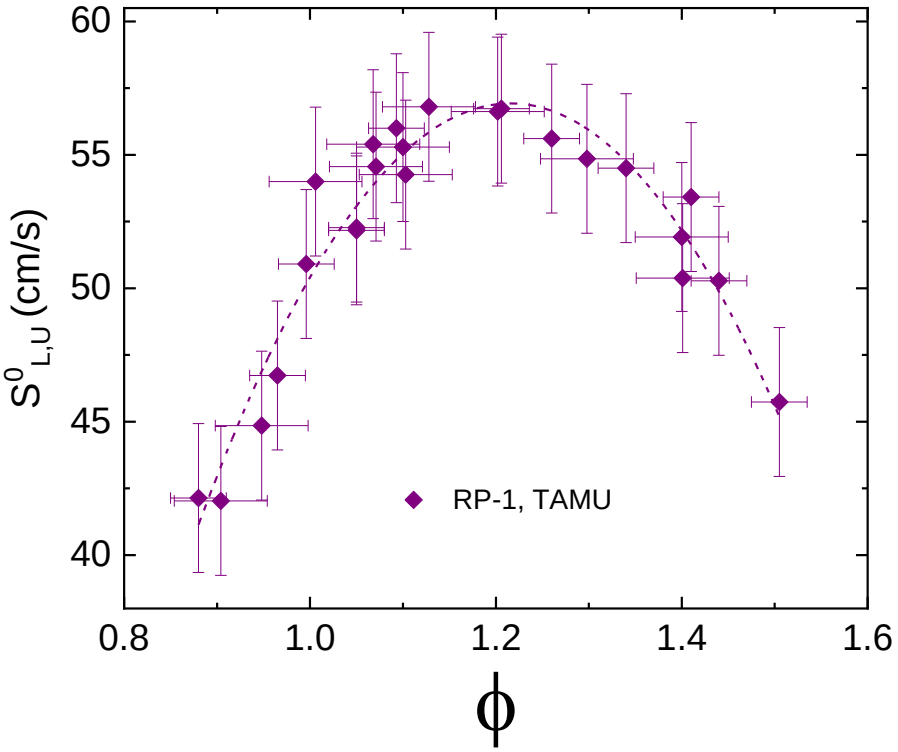

Figure 49. Final data set for RP-1 laminar flame speed. Symbols indicate data points, and the dashed line is a trend line through the data. Phi is based on average molecule ($C_{12}H_{24.1}$) as reported by AFRL.

Diesel Fuel #2

The Diesel Fuel #2 used for all experiments was identified as POSF 12758, with an average molecular formula of $C_{13.1}H_{24}$. This average molecule results in a reported average molecular weight of 181.528 g/mol. The diesel fuel was bright red in color, which is commonly known as off-road diesel. Unlike the other fuels included in this study, the diesel fuel experiments were conducted at a higher temperature. The experimental temperature was

initially raised to 413 K due to large amounts of condensation on the windows when attempting mixtures at 403 K.

The first set of data collected used the partial pressure method; these data are referred to as “413 K PP”. The mass-based data were collected at increasing temperatures. In the graphs that follow, they are referenced as such.

As seen in Figure 50, the initial data produced reasonable results. The measured flame speeds were similar to those seen for Jet-A and RP-1 at the given equivalence ratios. Experiments were limited to lean, stoichiometric, and slightly rich due to obvious condensation on the windows when attempting richer mixtures. At the maximum equivalence ratio shown, $\varphi = 1.161$, only slight condensation was detected on the window. At the slightly richer condition, $\varphi = 1.174$, filling was aborted due to large amounts of condensation.

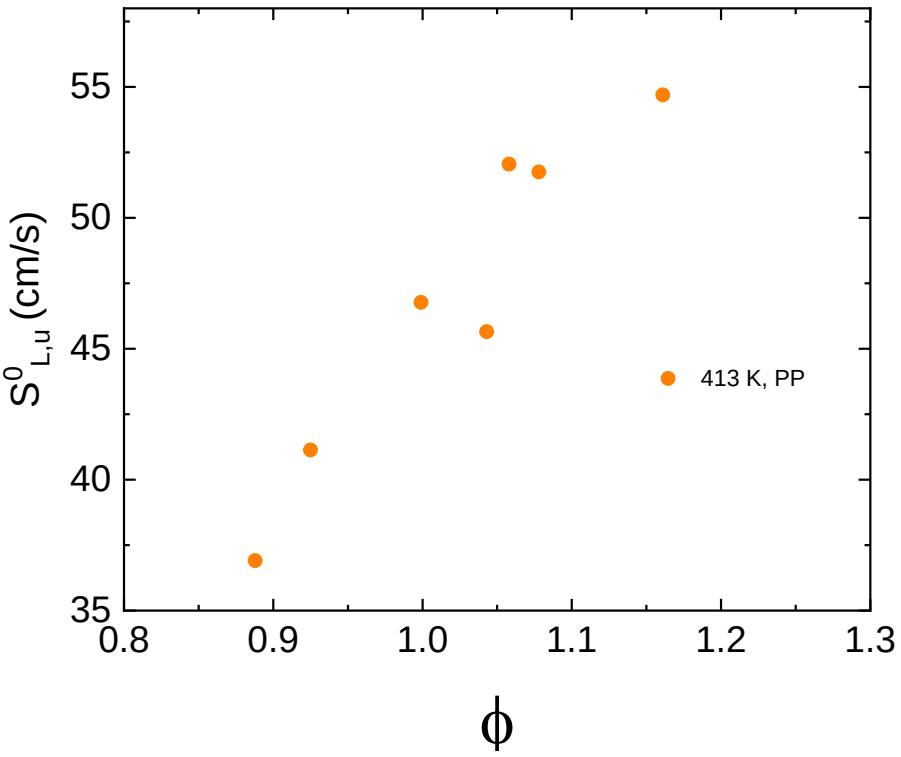

Figure 50. Initial partial pressure data for Diesel Fuel #2 at 1 atm, 413 K.

When these experiments were attempted using the mass-based method, it was quickly noticed that there was something wrong. An initial mass loading of Diesel Fuel #2 of 1.52 grams, which should have resulted in φ = 1.0, proved to be too lean to burn. Based on the corresponding partial pressure, 6.34 Torr, this should have resulted in φ = 0.765. Thus, it is understandable why it might have been too lean to burn. Based on these numbers, the back-calculated molecular weight was MW = 240 g/mol using the method described in Chapter 7.

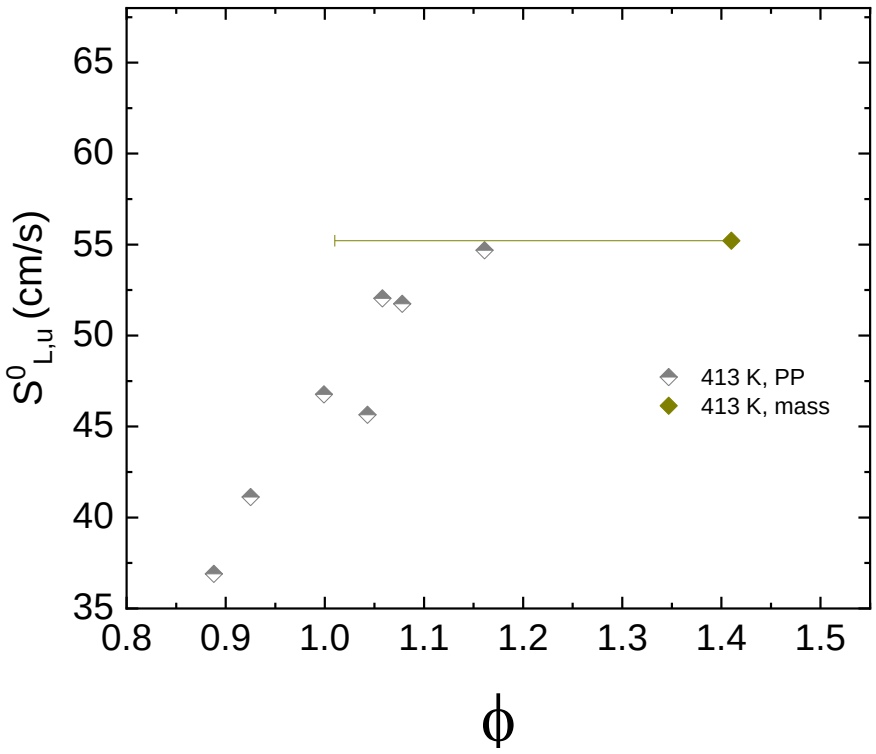

Figure 51. Diesel Fuel #2 Results as 413 K comparing partial pressure method to the mass-based method.

These factors strongly indicated that fuel was pooling somewhere in the vessel, and not entering or remaining in vapor form. To test this hypothesis, an extremely rich mixture, φ = 1.41 was tested with a fuel mass loading of 2.11 grams. The data point, as seen in Figure 51, shows where the loaded mass calculates the equivalence ratio, whereas the error bar extending to the left shows where the measured partial pressure calculates the equivalence ratio. As can be seen, if the partial pressure value were used the resultant flame speed is similar to what had been seen previously. This result verified that fuel was pooling somewhere and not fully

vaporizing. To get the measured partial pressure and mass-based methods results to agree in terms of the equivalence ratio, the temperature of the vessel needed to be raised.

The temperature of the vessel was raised in 5-degree increments to control the leak rate of the vessel, while still finding a temperature that would allow the fuel to fully vaporize. As expected, as the temperature increased, the calculated molecular weight moved closer to the reported value, which resulted in the injected mass and measured partial pressure returning closer equivalence ratios. The increase in temperature also resulted in an increase in laminar flame speed. There was a 16-cm/s difference in flame speed at $\varphi = 1.0$ between 423 K and 448 K. As seen previously, the calculated molecular weight at 448 K, 190.16 g/mol, was 4.75% greater than the value reported by AFRL. However, there was little change in this value between 443 K and 448 K. Also at 448 K, a full curve was able to be collected with a peak value around $\varphi = 1.2$. Therefore, the temperature was not increased any further. Complete results are shown in Figure 52.

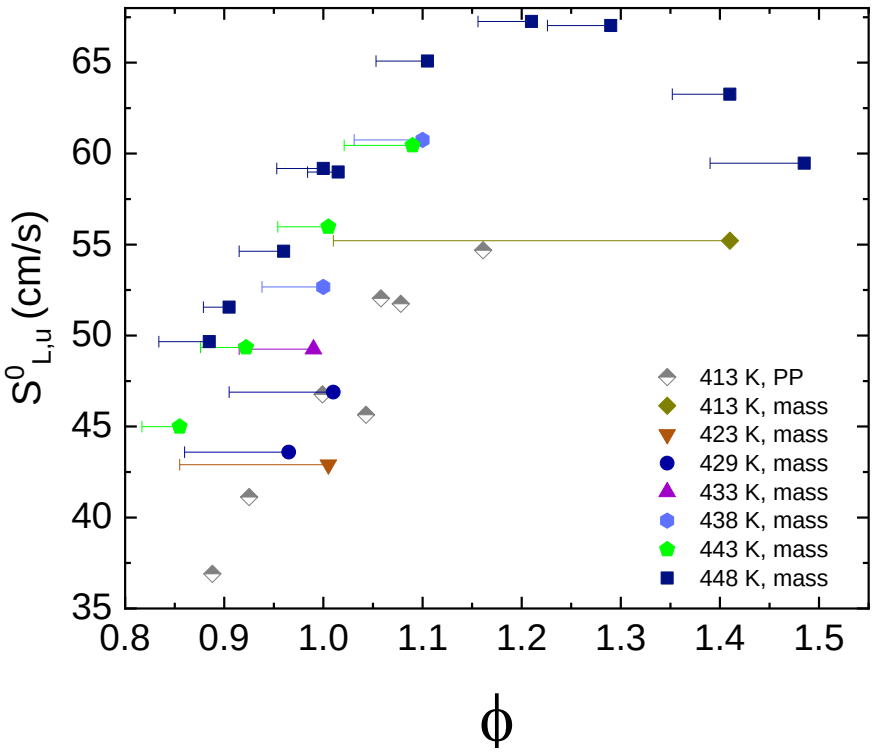

Figure 52. Complete set of results for Diesel Fuel #2, highlighting the temperature increase and the difference in equivalence ratio based on partial pressure and measured mass. Phi is based on average molecule ($C_{13.1}H_{24}$) provided by AFRL.

As with the previous fuels, an analysis of the measured burned-gas Markstein length was conducted. For this analysis, only the data collected at 448 K were used. Once again, a strong linear trend was seen. The correlation found for n-decane was adjusted in accordance with the previously described method. The current equation is shown as Equation 7.3. Based on this analysis, the only point that could be considered questionable is the richest mixture φ = 1.425 tested. The Markstein length results are shown in Figure 53.

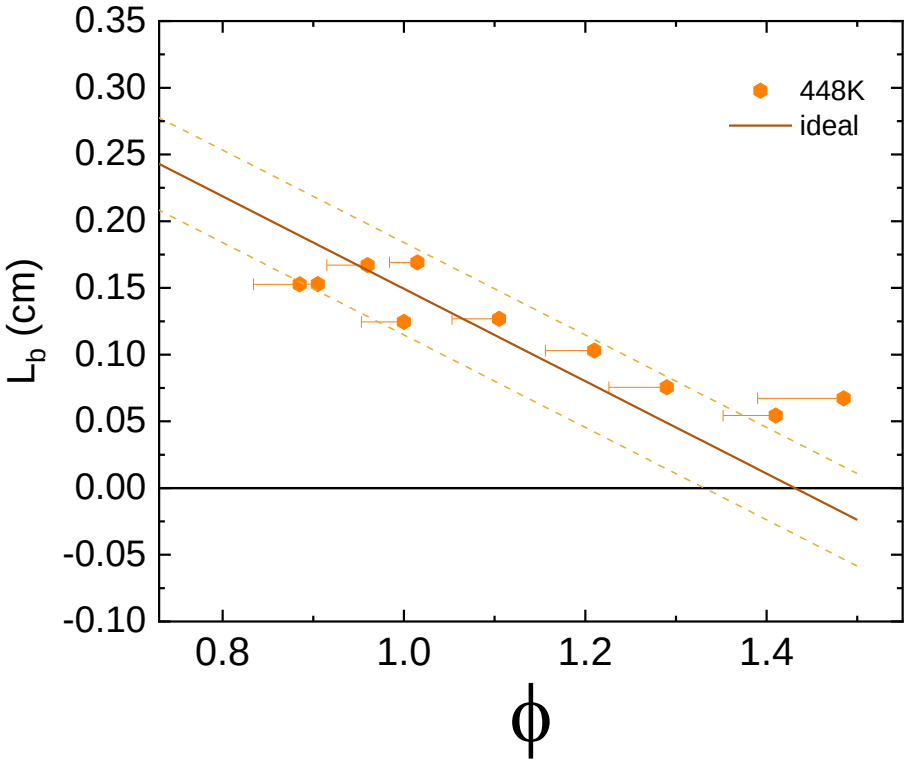

Figure 53. Markstein length data for Diesel Fuel #2 at 448 K and 1 atm.

$$L_b = 0.034633\varphi + 0.4957 \tag{7.3}$$

The final, compiled Diesel Fuel #2 results are shown in Figure 54. At the elevated temperature of 448 K, a full experimental curve was able to be tested. Peak laminar flame speed was found between φ = 1.2 and φ = 1.3, based on the MW provided by the supplier.

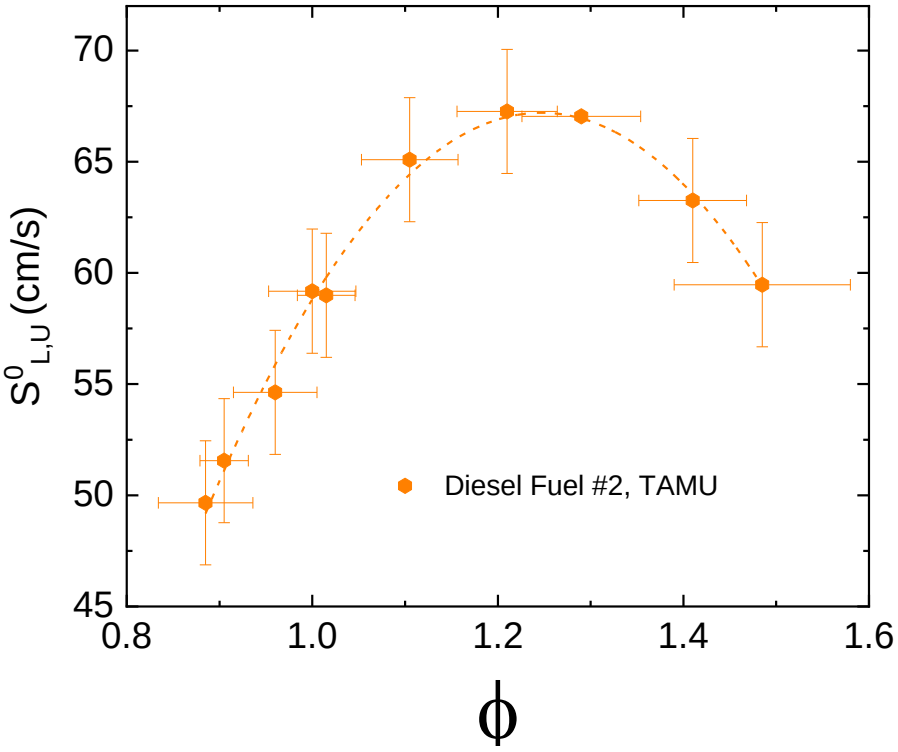

Figure 54. Final, acceptable Diesel Fuel #2 flame speed data at 448 K and 1 atm. Phi is based on average molecule ($C_{13.1}H_{24}$) provided by AFRL.

S-8

The S-8 used in this study was identified as POSF 5018, with an average chemical formula of $C_{11.8}H_{25.6}$ and a Molecular Weight of 168 g/mol. The fuel was a clear liquid. The density at room temperature was 0.757 mL/g.

Two sets of data were collected for S-8. The first of these used the partial pressure method to fill the vessel. These data are identified as the "2018" in the figures below. This data set consisted of 11 points ranging in equivalence ratios from φ = 0.946 to φ = 1.629. The

second set of data used the mass-based method to inject the fuel into the vessel. These data are identified as “2019” below. Similarly, these 11 data points ranged from φ = 0.84 to φ = 1.63

Figure 55 shows the complete experimental results for S-8. Overall, the data produce a very distinct curve with the peak flame speed of 58.4 cm/s occurring around φ = 1.25. A lean flammability limit was found to be below φ = 0.885 as the attempted point at φ = 0.84 was too lean to ignite.

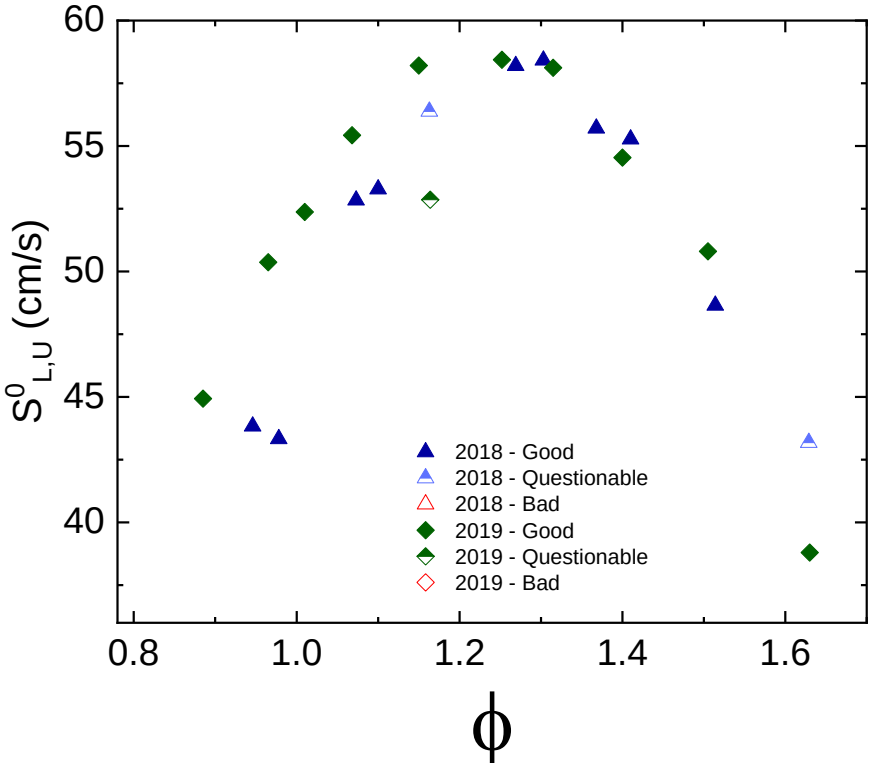

Figure 55. Complete laminar flame speed results for S-8. Data are color coded by year and method with indications on the acceptability of the data. Phi is based on average molecule ($C_{11.8}H_{25.6}$) provided by AFRL.

There appears to be significantly more scatter for mixtures leaner than φ = 1.15 as opposed to the rich mixtures. The most notable of these is the 5.35-cm/s difference in the data points near φ = 1.15.

The Markstein length analysis, shown in Figure 56, shows the same strong linear correlation as seen for the other fuels. The uncertainty limits were set at φ = ± 0.1. Most of the 2019 data fall directly on the predicted value line. Similar to what was seen for decane, for mixtures leaner than about φ = 1.1, it appears that the linear trend is over-predicting the Markstein length. The linear correlation equation is shown in Equation 7.4.

$$L_b = -0.33\varphi + 0.4723 \tag{7.4}$$

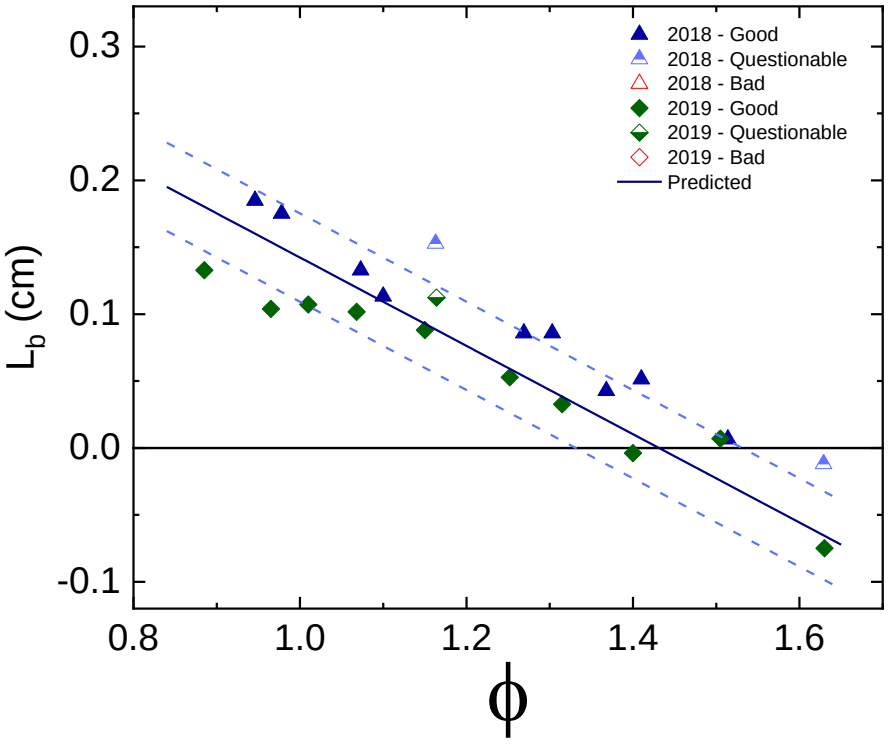

Figure 56. Complete Markstein Length data for S-8. Symbols show the experimental results by year, method, and acceptability of the data. Solid line indicates the linear correlation for the Markstein length with dashed lines showing the uncertainty interval.

The complete set of acceptable results for S-8 is shown in Figure 57. The only data point that was excluded was the "questionable" data point from 2019 near φ = 1.16. While the Markstein length did not flag the point for further investigation, the measured flame speed was around 9% slower than other data points near the same equivalence ratio.

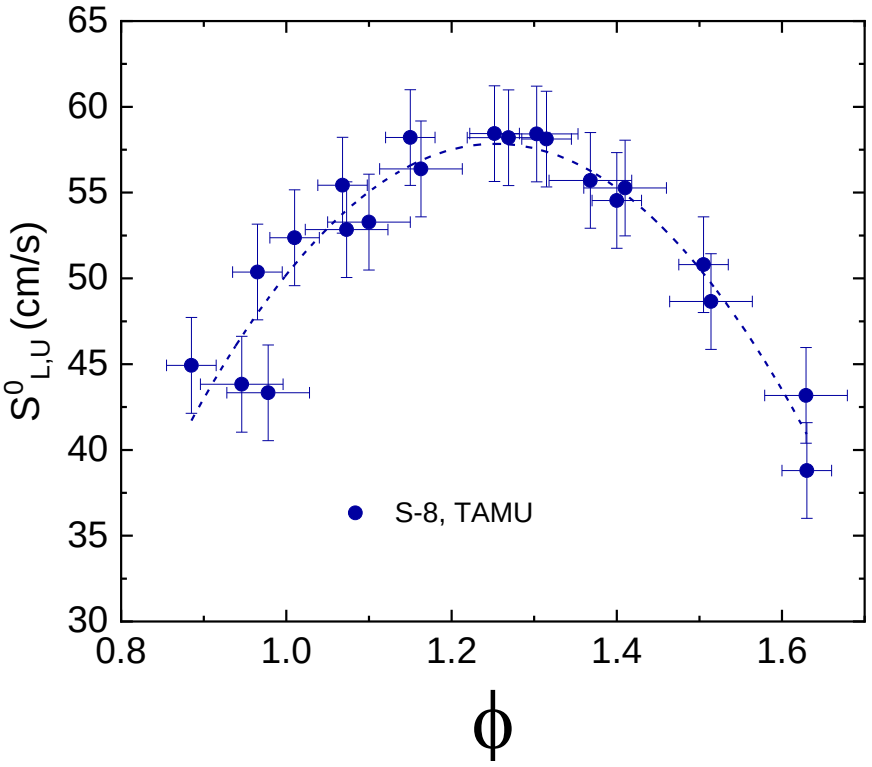

Figure 57. Complete experimental results for S-8 at 403 K and 1 atm. Phi is based on average molecule ($C_{11.8}H_{25.6}$) provided by AFRL.

Shell GTL

As stated previously, the Shell GTL fuel used in this study was identified as POSF 5729. For these measurements, a molecular weight of 144.34 g/mol and an average molecule of $C_{10.15}H_{22.26}$ was calculated based on the GC x GC data provided by AFRL. Data were gathered in two sets using first the partial pressure method (2018 data) and later the injected-

mass method (2019 data) over a range of equivalence ratios from φ = 0.845 to φ = 1.446. All experiments were conducted at initial conditions of 1 atm and 403 K.

Figure 58 shows the complete set of laminar flame speed results for Shell GTL. There appear to be two separate curves, with the mass-based data peaking at a leaner, φ =1.1, equivalence ratio as opposed to φ = 1.15 where the 2018 data peak. Independently, each data set appears to have a very distinct curve.

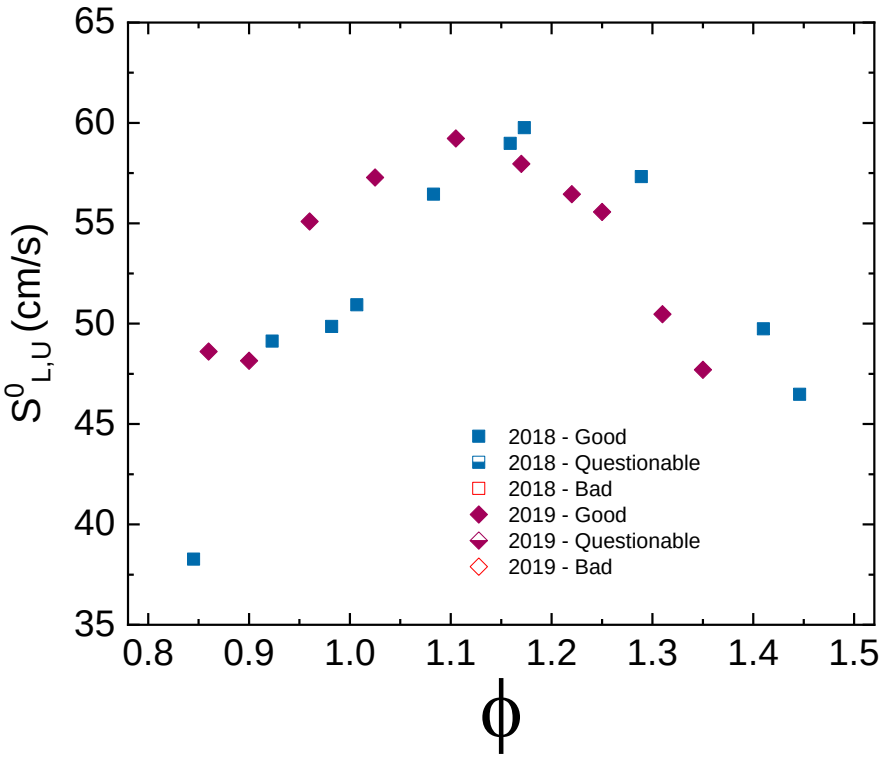

Figure 58. Complete laminar flame speed results for Shell GTL. Data are color coded by year and method with indications on the acceptability of the data. Phi is based on average molecule ($C_{10.15}H_{22.26}$) provided by AFRL.

The mass-based measurements allowed for the back calculation of the molecular weight in the manner previously discussed. While filling the syringes, it was determined that Shell GTL has a room-temperature density of 0.7369 mL/g. This value was similar to the other fuels in the study. The molecular weight was measured to be within 1% of the provided value. This level of agreement indicates that the stated average molecule and molecular weight currently being used are accurate.

As with the previous fuels, additional analysis was performed using the burned-gas Markstein lengths. Once again, a strong linear correlation was seen between the Markstein length and equivalence ratio. As seen in Figure 59, the mass-based data typically produced a slightly smaller Markstein length. Overall, the data appear to be in very good agreement. As such, none of the data were flagged for further investigation or possible removal due to the Markstein length.

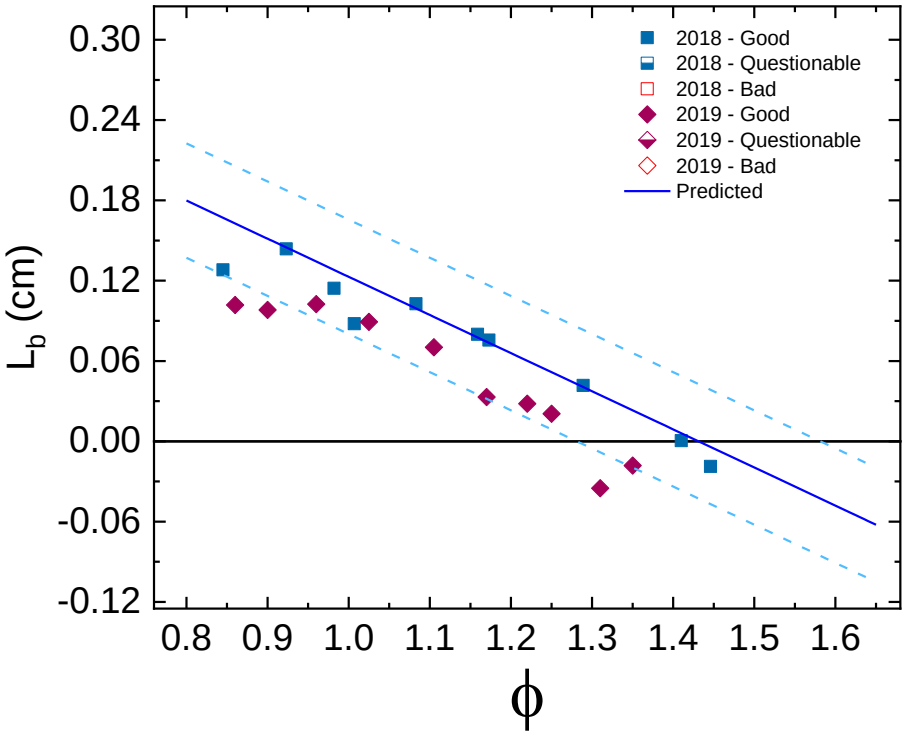

Figure 59. Complete Markstein Length data for Shell GTL. Symbols show the experimental results by year, method, and acceptability of the data. Solid line indicates the linear correlation for the Markstein length with dashed lines showing the uncertainty interval.

The combined Shell GTL data are shown in Figure 60. As can be seen, there were no points considered to be bad data. Therefore, all collected data points were included for analysis. The peak laminar flame speed of 59.76 was found at φ = 1.173.

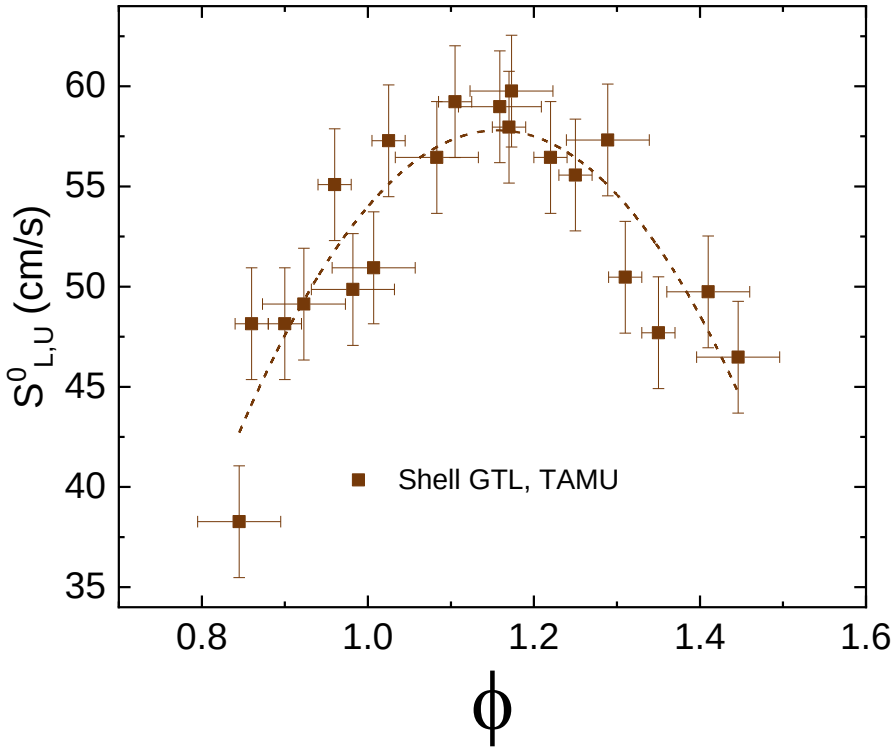

Figure 60. Combined experimental results for Shell GTL data at 1 atm and 403 K. Phi is based on average molecule ($C_{10.15}H_{22.26}$) provided by AFRL.

Conclusions

The experimental data for all of the fuels produced very good results. All fuels showed distinct flame speed curves. This ability to be curve fit is a good indication of overall repeatability of the experimental procedure. Results for the four fuels tested at 403 K are shown in Figure 61. Shell GTL has the fastest peak flame speed, 59.76 cm/s, whereas Jet-A has the slowest peak flame speed, 56.38 cm/s, a difference of just under 6% among all the fuels tested.

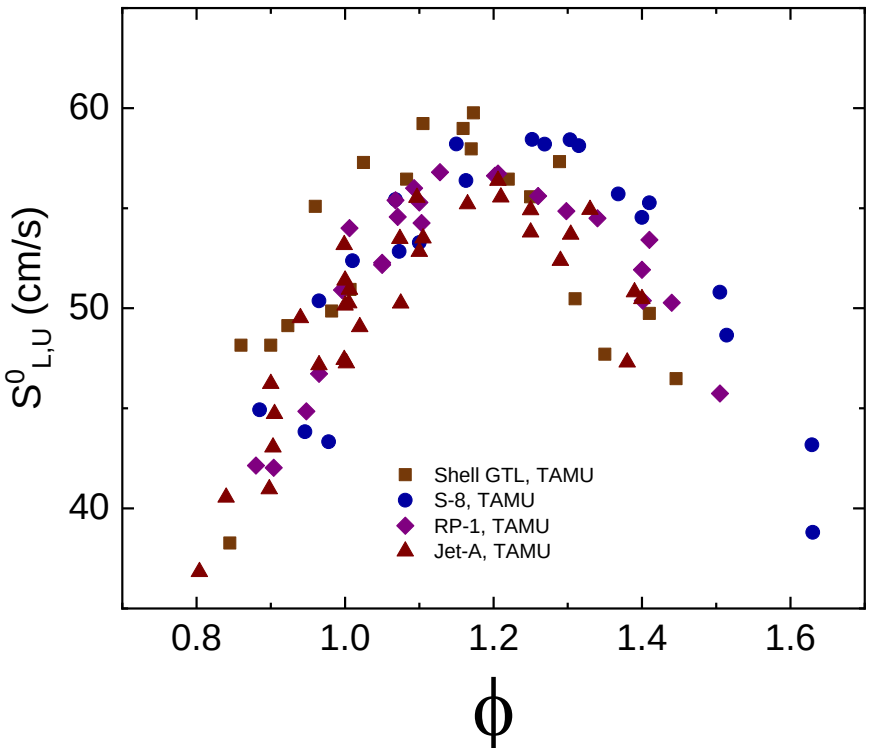

Figure 61. Combined laminar flame speed results for the 4 fuels tested at 403 K. Error bars have been removed for clarity of data.

For most fuels, the peak flame speed occurs around φ = 1.2, based on the MW and average molecules provided by the supplier. This equivalence ratio for the peak flame speed is slightly richer than expected, and it led to a considerable amount of concern regarding the accuracy of the current data. However, the overall consistency of the results indicates that the peak flame speed location is not due to careless experimental error. The worst case this would indicate is a systematic error, such as the same amount of fuel condensing in every experiment. Many of the possible sources of uncertainty were discussed in detail in the previous chapters. There is no indication any fuel is getting lost or condensing in the vessel. Error bars in φ have

been added to help address this uncertainty. Methods for dealing with the main source of uncertainty, especially when comparing additional data sets are discussed in the next chapter.

CHAPTER VIII

EQUIVALENCE RATIO VERSUS MOLE FRACTION

In typical laminar flame speed studies, data are presented as laminar flame speed versus equivalence ratio. Up to this point in this dissertation, this is how the data have been presented. While this method is excellent for single-component fuels, or well-defined mixtures, it is less useful when the fuel is defined by an average molecule that could change, sometimes significantly, from one production batch to the next. It is also less useful when there is some variance or even no information provided at all on the average molecule for a given fuel batch within the scientific community. To better guide future comparisons and interpretations on these fuels, a new method of using the fuel mole fraction rather than the equivalence ratio is now proposed. The justification is presented below.

POSF Numbers

As mentioned earlier, when AFRL receives a shipment of fuel, a POSF identification number is assigned to that fuel. As AFRL is the distributer of liquid fuels to most research groups in the United States this system can be very useful. Unfortunately, it can also lead to significant confusion within the literature when conflicting values are published by researchers for the same batch designations.

For example, when the blended batch of Jet-A known as POSF 4658 was being distributed, the average molecule of $C_{10.17}H_{19.91}$ was initially reported by [19]. This value was subsequently cited in [14, 15]. However, a significantly different value of $C_{11.7}H_{25.3}$ was

reported in [1] for the same POSF 4658. This is a 14.34% difference. The current batch of Jet-A, the one used in the present study, known as POSF 10325, has the average molecule of $C_{11.4}H_{22.1}$ reported by multiple sources [1, 60]. To the best of the authors' knowledge, no other average molecules have been reported for POSF 10325.

Unfortunately, there is similar confusion for different batches of S-8. The current batch of S-8 identified as POSF 5018 has an average molecule reported by AFRL as $C_{11.8}H_{25.6}$, which is the value used in the current study. For the same batch of fuel, Kang et al. [60] reported an average molecule of $C_{10.82}H_{23.7}$. This version represents an 8% difference in molecular weight for the average molecule when compared to the one used for the dissertation work herein.

A similar discrepancy occurred with a previous batch of S-8 identified as POSF 4734. The work of [18] reported an average molecule of $C_{10}H_{22.7,}$ whereas [14] gave an average molecule of $C_{11.847}H_{25.502}$. The most recent value reported by AFRL for POSF 4734 was $C_{11.7}H_{25.3,}$ which unfortunately matches neither of the values reported in the literature. The work of Dooley et al. [61] acknowledges the use of POSF 4734 and identifies that it has a measured molecular weight of 163 ± 15 g/mol. However, they chose to use a 2-component surrogate to determine fuel properties. This surrogate, which consists of 51.9% dodecane and 48.1% iso-octane by moles, has a molecular weight of 143.4 g/mol. This value represents a 12% difference in molecular weight from the reported MW of the actual fuel. Part of the purpose of their study was to validate the surrogate model.

A downside to the POSF number identification system is that it only applies to fuels sourced through AFRL. However, a major benefit of specifying the POSF number is so that everyone will know exactly which fuel was tested. But this system only works if the same

values are used and published by the researchers. In summary, different average molecules and molecular weights specified for the same POSF number leads to some confusion in what was tested and how the numbers were calculated. As shown below, the average MW impacts the calculation of the equivalence ratio, a key variable used when plotting the results of laminar flame speed experiments.

Benefits of Mole Fraction

By definition, the equivalence ratio, φ, is highly dependent on knowing the correct chemical composition of the fuel. Thus, equivalence ratio is a relative parameter, which can lead to significant uncertainty in the actual equivalence ratio being tested. This problem is evident from the wide variation in the average molecules discussed above. It is also important to notice that these different, average molecules will lead to a different amount of fuel being present in mixtures of the same reported equivalence ratio. A much more quantitative parameter is fuel mole fraction, X_{FUEL}, which is solely based on the percentage of fuel, on a molar basis, that is in the mixture.

Figure 62 shows X_{FUEL} plotted against φ, for the three identified batches of Jet-A, POSF 10325, POSF 4658, and the "Singh Surrogate" [5]. As can be seen, the difference of almost 1.5 carbon atoms and 3 hydrogen atoms significantly impacts the amount of fuel at any given equivalence ratio. There is about 11.5% more fuel, by mole, present at any given equivalence ratio with POSF 4658 than POSF 10325. The 12-component surrogate identified by [5] falls between the two tested average molecules. Even though they did not specify the average

molecule of their fuel, it is useful to know how they calculated equivalence ratio (the use of a surrogate) to compare their results with the current results and those from literature.

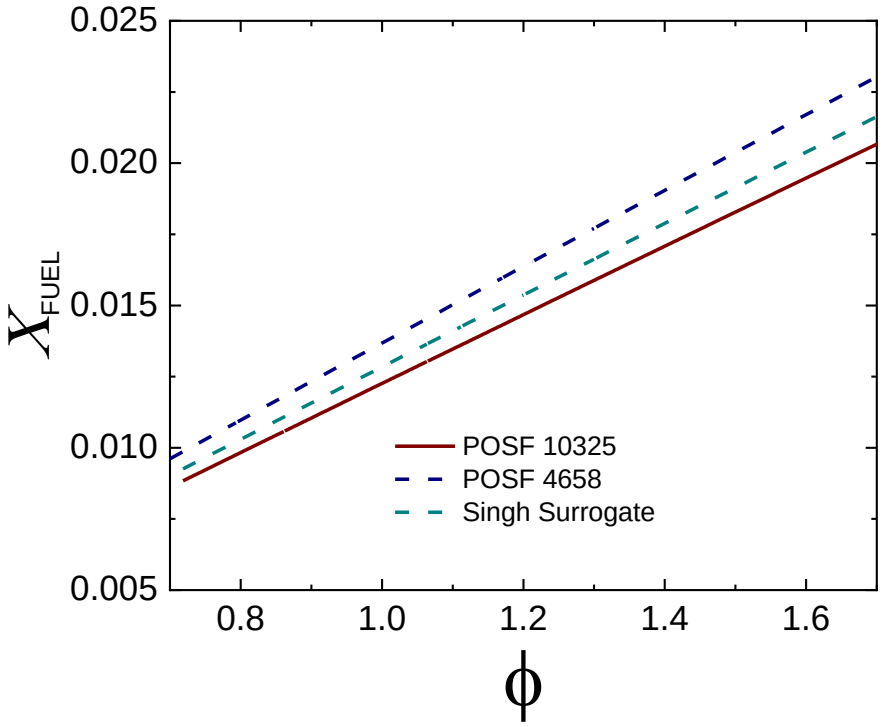

Figure 62. Fuel mole fraction versus equivalence ratio for Jet-A for different identified average molecules.

Similar results are shown for different average molecules of S-8 in Figure 63. As with Jet-A, the study of [5] used a seven-component surrogate with an average molecule of $C_{11.4}H_{24.8}$, whereas the study of [18] stated an average molecule of $C_{10}H_{22.7}$. A value of X_{FUEL} = 0.015 shifts form around φ = 1.2 in the study of [18] to around φ = 1.35 in the current study. This somewhat large shift is most likely due to the almost 2-atom increase in carbon content

in the average molecule being used in the current study. The conversion between φ and fuel mole fraction is shown in Equation 9.1. This equation assumes that primary standard air is being used as the oxidizer.

$$X_{FUEL} = \frac{1}{1 + \frac{N_{O_2,stoic}}{\varphi}(4.76)} \tag{9.1}$$

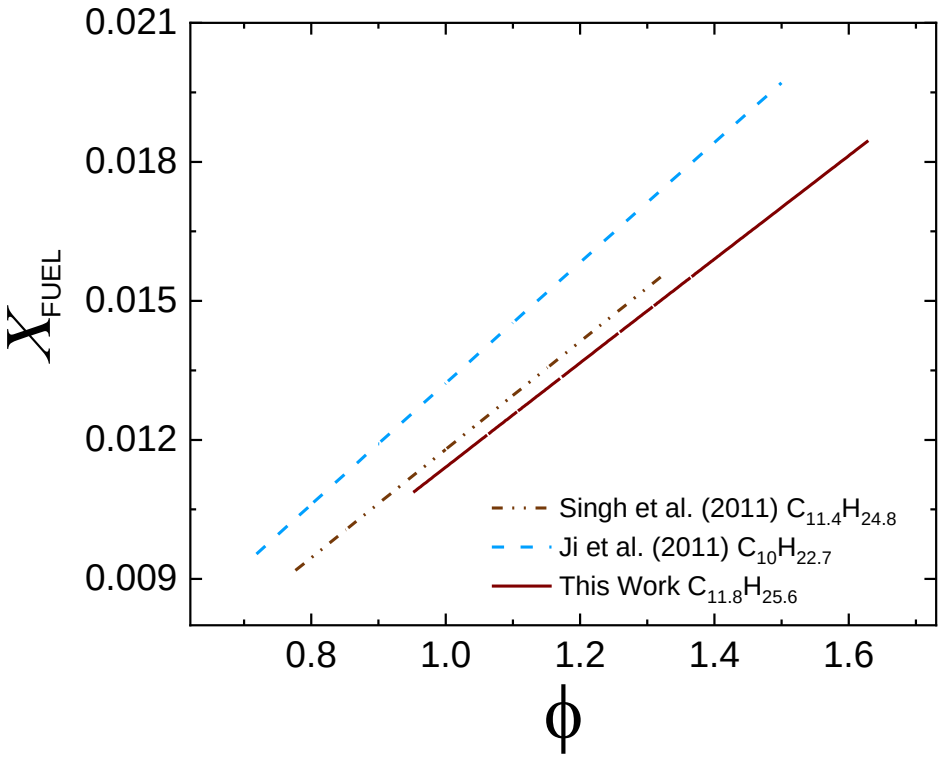

Figure 63. Fuel mole fraction versus equivalence ratio for S-8 for different identified average molecules.

The conversion to X_{FUEL} also shows a significant decrease in uncertainty over φ. As discussed in the previous chapter, the uncertainty in φ = ± 0.03 is based on experimental uncertainties. This equivalence ratio uncertainty corresponds to an uncertainty of around X_{FUEL} = ± 0.0004 for all of the fuels in this study.

Literature Comparisons

For the purpose of comparing to results in the literature, only studies at the same initial conditions are used. Also, direct comparisons are limited to studies that directly specified what average fuel molecule was used. This information allows for easy conversion between equivalence ratio, φ, and fuel mole fraction, X_{FUEL}. Unfortunately, there was no literature data found for direct comparison of RP-1 or Diesel Fuel #2, and very limited data for Shell GTL. Therefore, a majority of the discussion in this chapter focuses on Jet-A and S-8.

Jet-A

Looking at the data for Jet-A when compared to data available in the literature shows an initial problem. As seen in Figure 64, the current data appear to be shifted to the right and peaking at a richer equivalence ratio, around φ = 1.2 instead of closer to φ = 1.1, as expected for hydrocarbon fuels over a wide range of carbon numbers. This apparent discrepancy led to significant confusion and several of the checks discussed earlier in the dissertation to verify the mixing procedure. It is also of note that the current results are on the order of 5 – 10 cm/s slower than the fastest of the results available in the literature.

As discussed in the literature review (Chapter II), the three studies of Dr. C.-J. Sung's group, [13-15] all used POSF 4658, which was just shown to have a significant difference in the mole fraction of fuel for a given equivalence ratio; whereas [5] used a 6-component surrogate to calculate equivalence ratio.

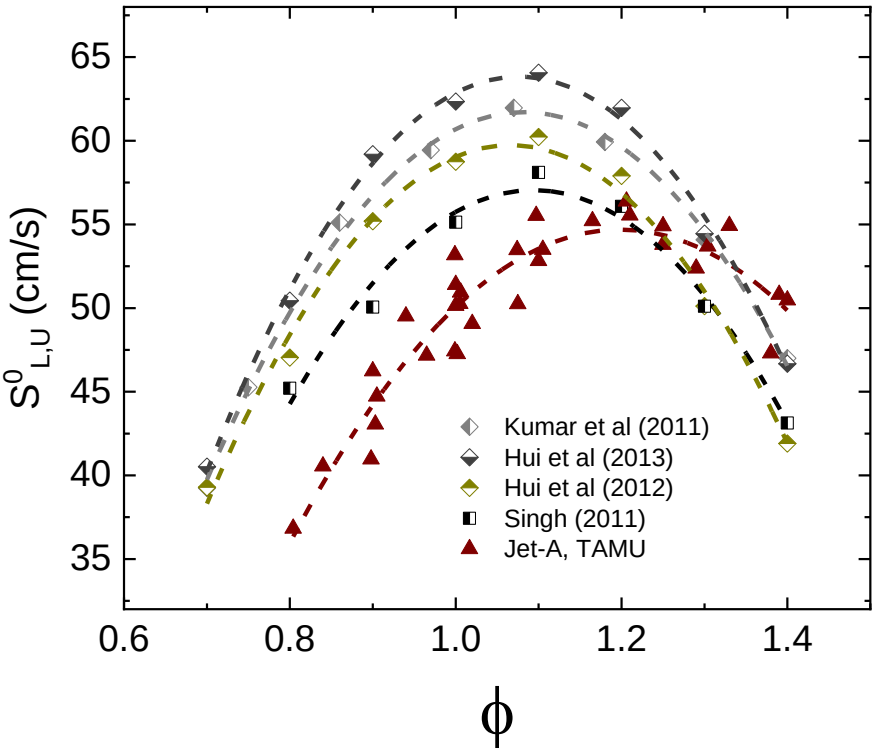

Figure 64. Complete Jet-A data compared to data in the literature. Symbols represent data points using the MW provided by the various sources to calculate equivalence ratio. Dashed lines are trend lines through the data.

Looking now at the same results using fuel mole fraction, X_{FUEL}, on the x-axis instead of φ shows interesting results. As can be seen in Figure 65, the data now show much better agreement in terms of the peak relative to the amount of fuel in the fuel-air mixture. All curves peak around $X_{FUEL} = 0.015$. The data now most closely match the results of [5], which was the only other spherical flame data shown. As discussed earlier, the results of [13-15] were all tested using the counterflow, twin-flame method which is known to produce faster results.

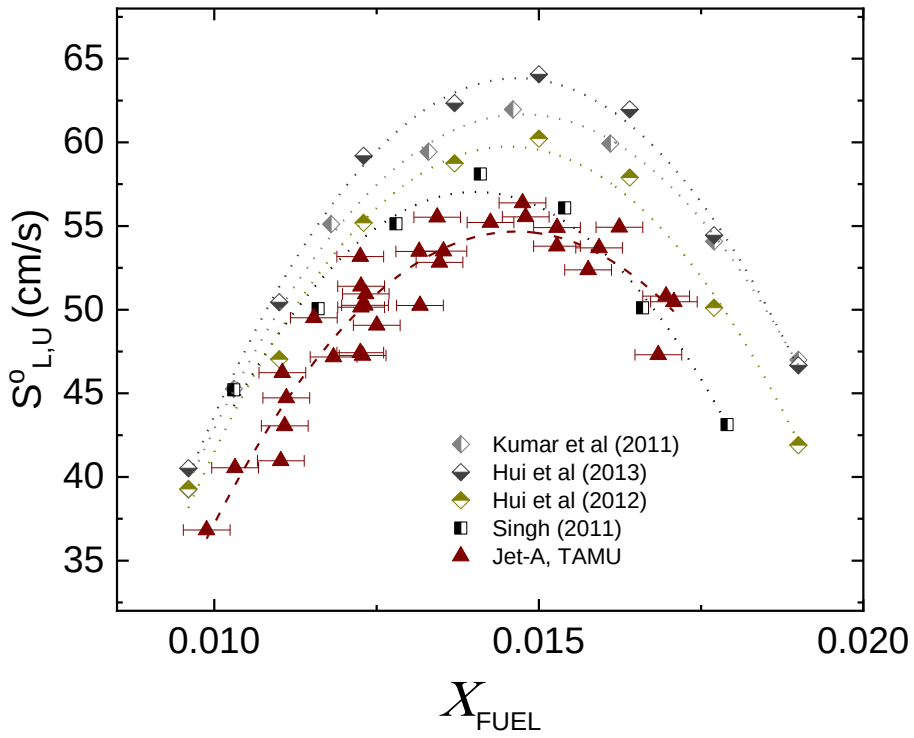

Figure 65. Complete Jet-A data compared to the literature using fuel mole fraction on the x-axis. Symbols represent data points. Dashed lines are trend lines through the various data sets.

S-8

While there were several studies for S-8, the average molecule was not always clearly defined in corresponding papers. The studies of [13-15] all identified using POSF 4734. However, they had a different method of calculating equivalence ratio in each of them. For example, an unspecified, 10-component surrogate was used to calculate equivalence ratio in [13]. While an average molecule was listed in [14], there were no laminar flame speed data presented. Whereas, the follow on study [15] specifically listed an average molecule for Jet-A, one was not listed for S-8. Therefore these studies are excluded from the following analysis.

Similar to the results for Jet-A, there appears to be a significant shift in the current data relative to the literature data. The peak flame speed, 58.4 cm/s appears to be similar to the results of [5], but the shape of the current curve also appears to be slightly broader.

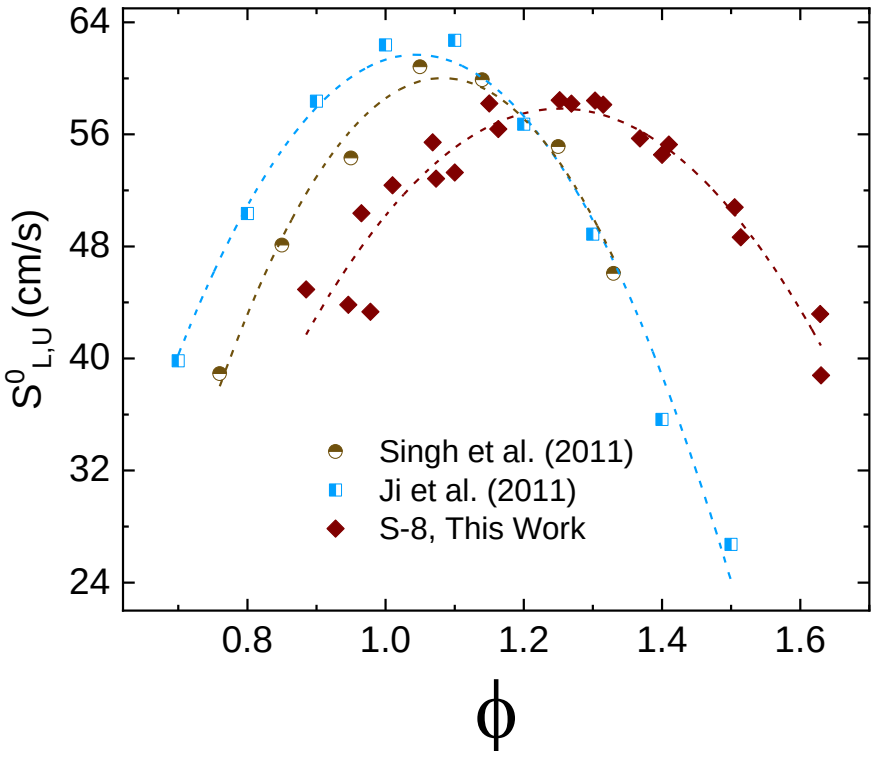

Figure 66. Complete S-8 data compared to available data in the literature. Symbols represent data points using the MW provided by the various sources when calculating the equivalence ratio. Dashed lines are trend lines through the various data sets.

Looking now at the same data in Figure 67, but using X_{FUEL} on the x-axis, there is much better agreement among the data sets. When compared to the study of [18], the shift appears to have mostly disappeared. The study of [5] now appears to be shifted out of place, peaking at a lower X_{FUEL}.

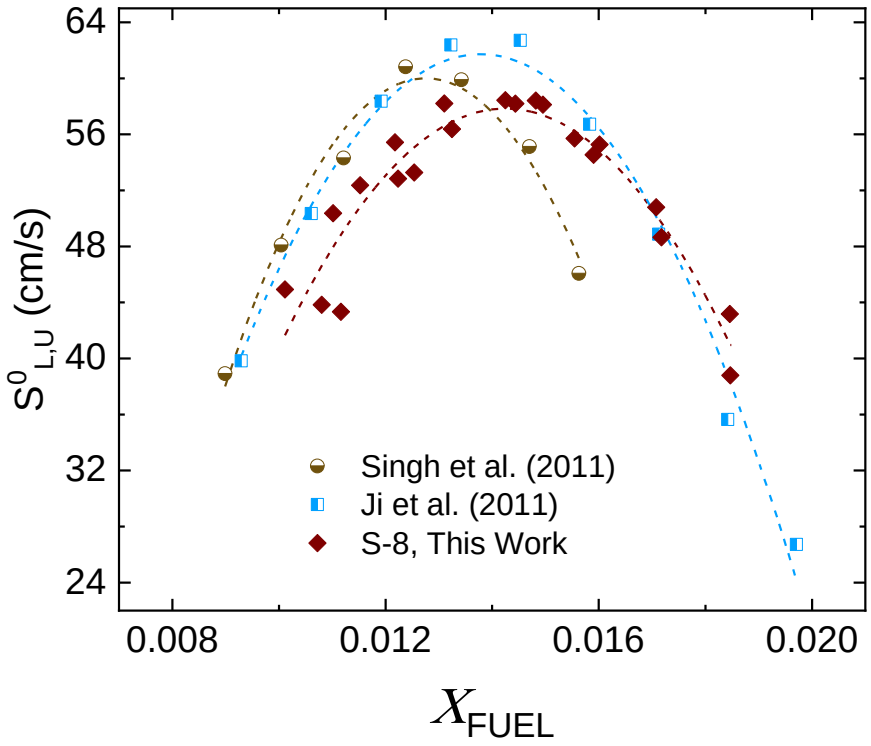

Figure 67. Complete S-8 data compared to the literature using fuel mole fraction on the x-axis. Symbols represent data points. Dashed lines are trend lines through the various data sets.

Shell GTL

There is only one other study [18] that has investigated Shell GTL at similar conditions. A specific average molecule was not given, but it was assumed in that study that the composition was similar to S-8 and therefore the average molecule of S-8, $C_{10}H_{22.7}$ was used herein when interpreting their data. In this case, their molecule is almost identical to the molecule for Shell GTL, $C_{10.15}H_{22.26}$, used in the current study. Hence, there is almost no shift

between the graphs using φ or X_{FUEL} on the x-axis. The comparison using φ on the x-axis is shown in Figure 68, and using X_{FUEL} in Figure 69.

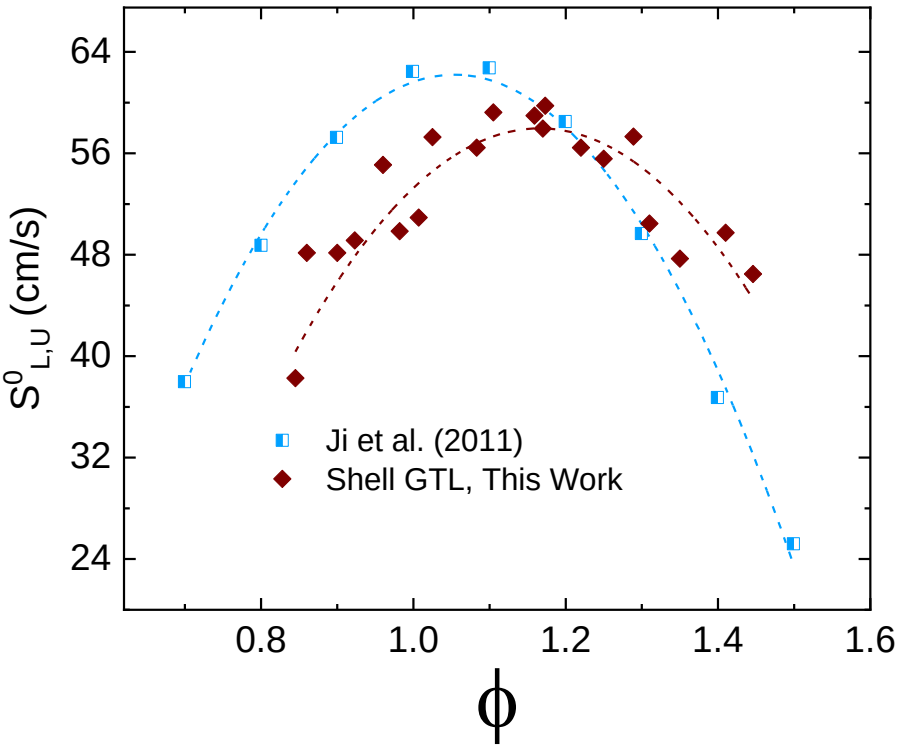

Figure 68. Complete Shell GTL data compared to data in the literature. Symbols represent data points using the corresponding average MW to evaluate the equivalence ratio. Dashed lines are trend lines through the two data sets.

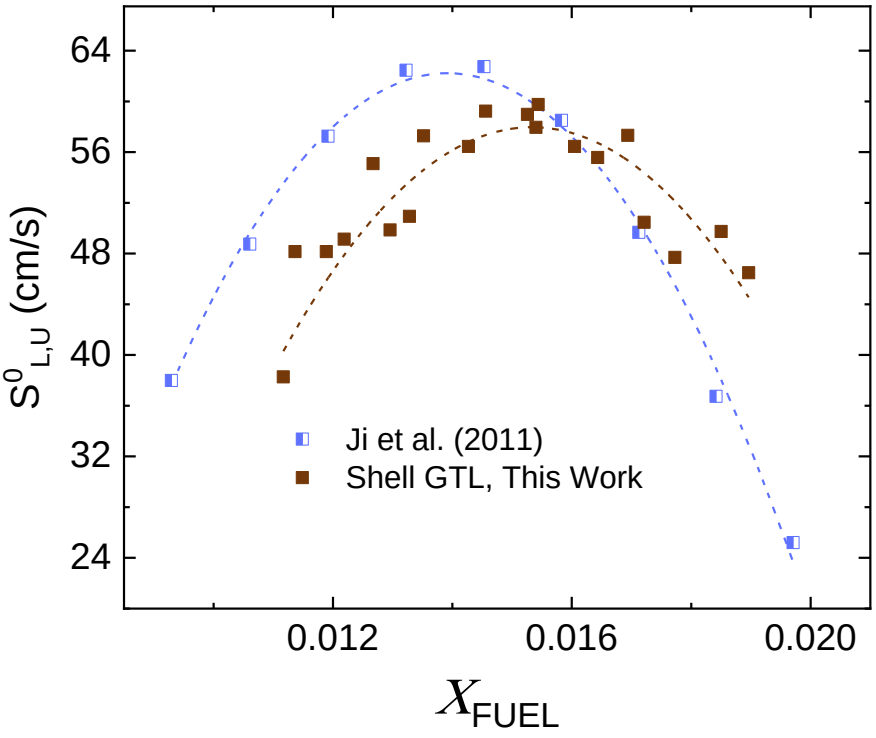

Figure 69. Complete Shell GTL data compared to the literature using fuel mole fraction on the x-axis. Symbols represent data points. Dashed lines are trend lines through the two data sets.

Chemical Kinetics Mechanism Comparisons

When selecting the appropriate chemical kinetics mechanisms, there are several parameters that need to be taken into account. These include, but are not limited to: average chemical formula, H/C ratio, and chemical composition. The average formula of Jet-A, POSF 10325 is $C_{11.4}H_{22.1}$ with an H/C ratio of is 1.938. As reported by [1], the chemical composition of POSF 10325 by volume is: 16.49% aromatics, 52.69% paraffins, and 30.83% naphthenes. Ideally, the more parameters that can be matched the better.

The recent, 3-component "Narayanaswamy surrogate" and accompanying chemical kinetics mechanism of [29] was specifically designed for Jet-A. This model was designed to use one hydrocarbon molecule from each of the major classes of hydrocarbons found in typical jet fuels. As discussed in the literature review chapter, this model includes: 30.3% dodecane, 21.2% m-xylene, and 48.5% MCH to represent paraffins, aromatics, and naphthenes respectively. One of the drawbacks to this mechanism is the limited number of species included. For example, the mechanism does not contain decane, which is frequently used in other jet fuel surrogates. This drawback limits the number of surrogates that can be tested with the mechanism.

Another possible disadvantage of the "Narayanaswamy surrogate" is that it is actually not a very good match for the current batch of Jet-A. The average chemical formula is $C_{8.73}H_{16.79}$ with an H/C ratio of 1.923. While this formula is a fairly close match in term of H/C ratio, with a 0.77% difference, there is actually a difference of almost 3 carbon atoms and 5 hydrogen atoms leading to a difference of 23.5% in the average molecular weight. As can be seen in Figure 70, the chemical composition is not a perfect match either. While the same three major classes of hydrocarbons are present, the ratios are not the same. While paraffins, in this case dodecane, make up just under a third of the "Narayanaswamy surrogate", they account for over 50% of the current Jet-A. Likewise, the naphthene species, MCH, accounts for just under half of the surrogate, while it measures a little under a third of the current batch of Jet-A.

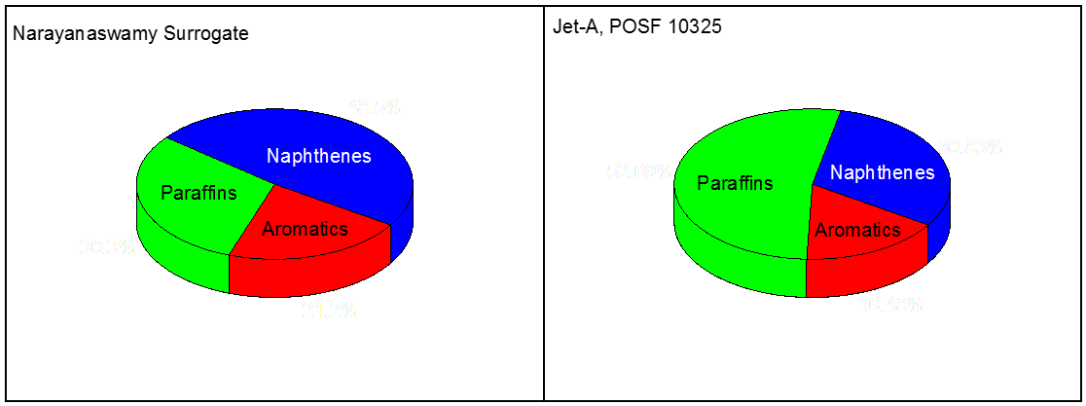

Figure 70. Chemical Composition Comparison of the "Narayanaswamy Surrogate" and the current batch of Jet-A (POSF 10325).

To look at the effect of species concentrations, an adjustment was made to the "Narayanaswamy Surrogate" to make it similar to the composition of POSF 10325. The resultant surrogate has an average molecule of $C_{9.79}H_{19.66}$ with an H/C = 2.006. This compromise average molecule is just under 3.5% greater than the H/C ratio for POSF 10325. It is referred to in the following graphs as "Narayanaswamy Adjusted."

Looking first at the results with φ on the x-axis, as seen in Figure 71, the experimental results are significantly shifted to the right, as expected. Both the baseline surrogate and the adjusted surrogate show peak flame speeds around φ = 1.05, with the adjusted surrogate being slightly faster. The experimental results appear to follow the same general shape for lean mixtures, however the shift is so significant that it is difficult to make any meaningful comparison. The curves intersect around φ = 1.25.

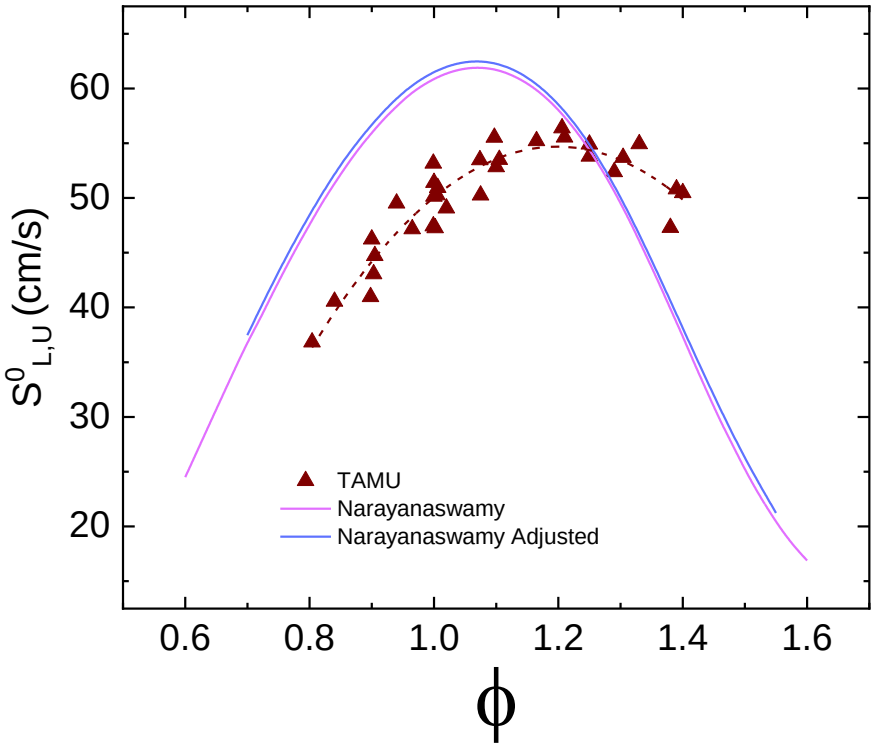

Figure 71. Jet-A laminar flame speed data compared to the "Narayanaswamy Surrogate" at 403 K and 1 atm.

When the x-axis is adjusted from φ to X_{FUEL}, a corresponding shift in the results is clear. For the baseline "Narayanaswamy Surrogate", the data now cross the model on the lean side of the curve, and the data now agree much better with the "Narayanaswamy Adjusted" results. While there appears to still be a slight mismatch in the peak location, it is not as significant as before making it easier to compare the results. The peak flame speed for the model is 62.57 cm/s which is just under 11% faster than the experimental results.

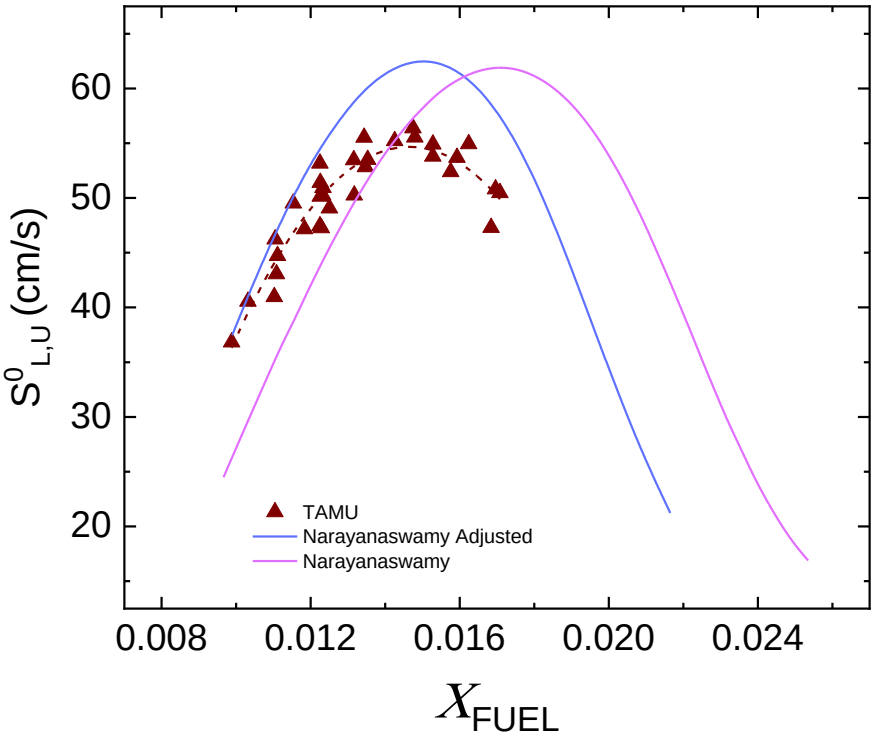

Figure 72. Jet-A laminar Flame Speed data compared to both versions of the Narayanaswamy Surrogate using X_{FUEL} on the x-axis.

The initial surrogate of [4] is labeled "Sur_1" and appears to be a better match to the current Jet-A. When the six components of the surrogate are divided into the three hydrocarbon classes discussed above, as seen in Figure 73, the surrogate appears to be a much better match to POSF 10325 than the "Narayanaswamy Surrogate." The average molecule for the surrogate works out to be $C_{10.3}H_{20.5}$, which is not a perfect match for the current fuel, but it is closer.

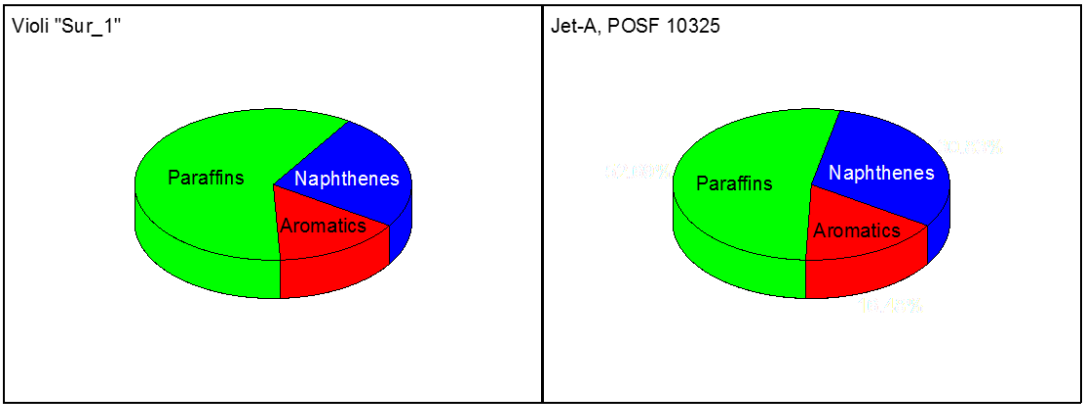

Figure 73. Chemical composition comparison of "Sur_1" [4] to the current Jet-A (POSF 10325).

As expected, because of the difference in average molecule, there is still a mismatch in the data peak when φ is used as the metric for comparison. These results are shown in Figure 74. The peak flame speed for the surrogate is around φ = 1.08 compared to φ = 1.2 of around 11%, which is similar to the difference in the average molecular weight of the surrogate (144 g/mol) compared to POSF 10325 (159 g/mol).

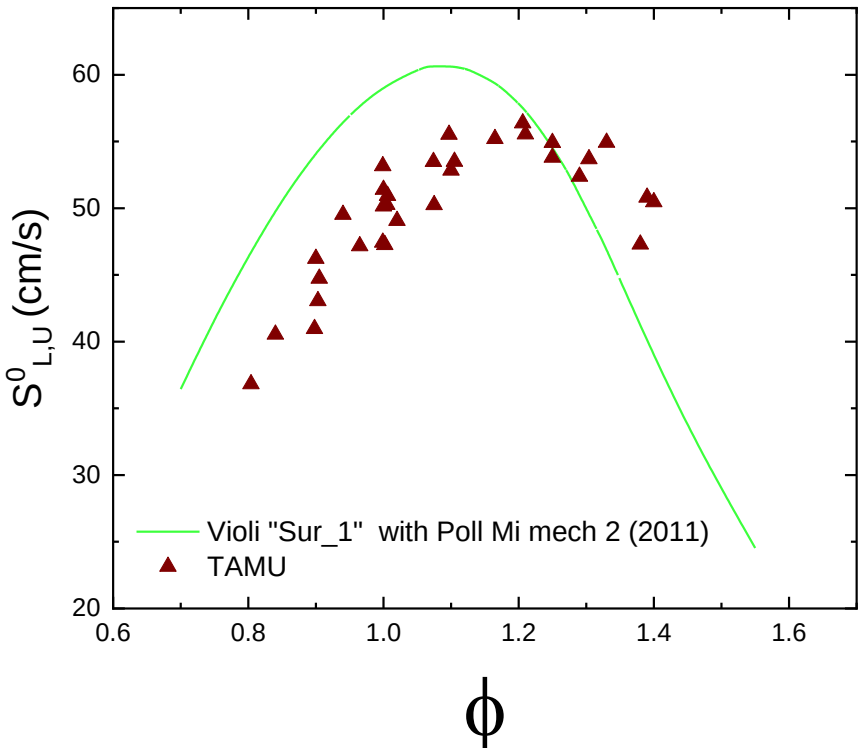

Figure 74. Jet-A experimental data compared to "Sur_1" using the Poll Mi mech 2 [7] chemical kinetics mechanism with φ on the x-axis.

When the x-axis is switched to X_{FUEL}, as seen in Figure 75, the locations of the curves show excellent agreement. The peak flame speed for the surrogate (60.64 cm/s) does end up to be around 7.5% faster than the experimental data (56.38 cm/s).

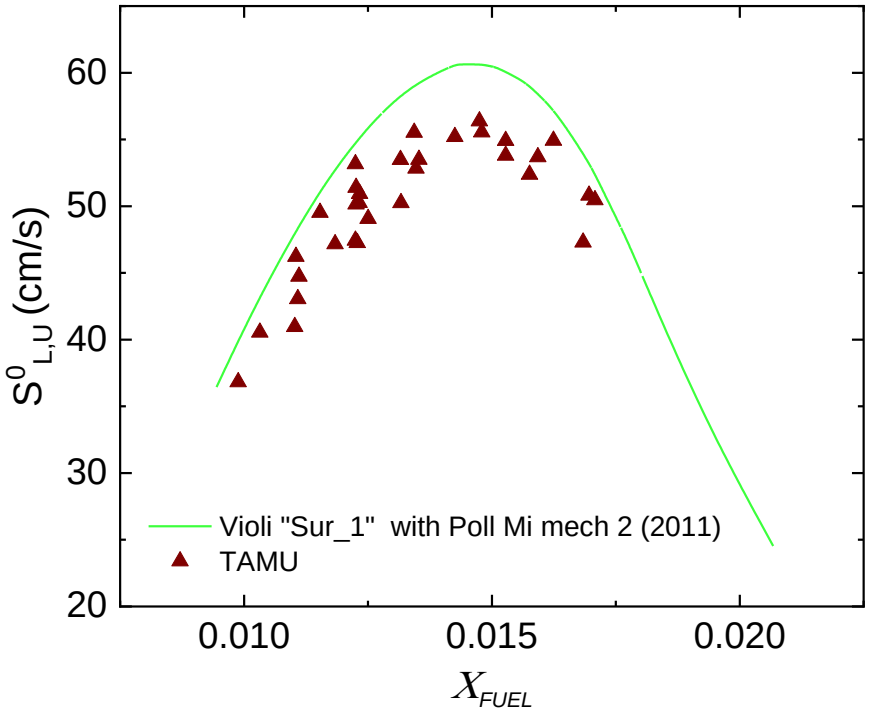

Figure 75. Jet-A experimental data compared to "Sur_1" using the Poll Mi mech 2 [7] chemical kinetics mechanism with X_{FUEL} on the x-axis.

The next mechanism to be considered is one of the surrogates suggested of diesel fuel, the surrogate of Pei et al. [62]. This surrogate and mechanism were developed at the Lawrence Livermore National Laboratory (LLNL). This two-component mechanism was comprised of 77% dodecane and 23% m-xylene by volume. It is believed to be more representative of diesel fuel than pure dodecane because it contains xylene to represent the benzene family. Since the LLNL mechanism is very large (containing over 2900 species), to save computational time

this surrogate is run using the “Narayanaswamy Mechanism” as both species are present in the mechanism.

As seen in Figure 76, the LLNL model does not show very good agreement with the experimental data. Once again, a strong shift is seen relative to the experimental data with a peak flame speed around $\varphi = 1.2$. However, this 2-component surrogate has an average molecule of $C_{11.08}H_{22.32}$ resulting in a molecular weight of 155.57 g/mol. This MW is 14.3 % lower than the stated average molecule of our Diesel Fuel of 181.53 g/mol. As discussed previously, the average MW of the current Diesel Fuel appears to be closer to 190 g/mol. It is reasonable, then, for this surrogate to not line up with the data very well when plotted using equivalence ratio.

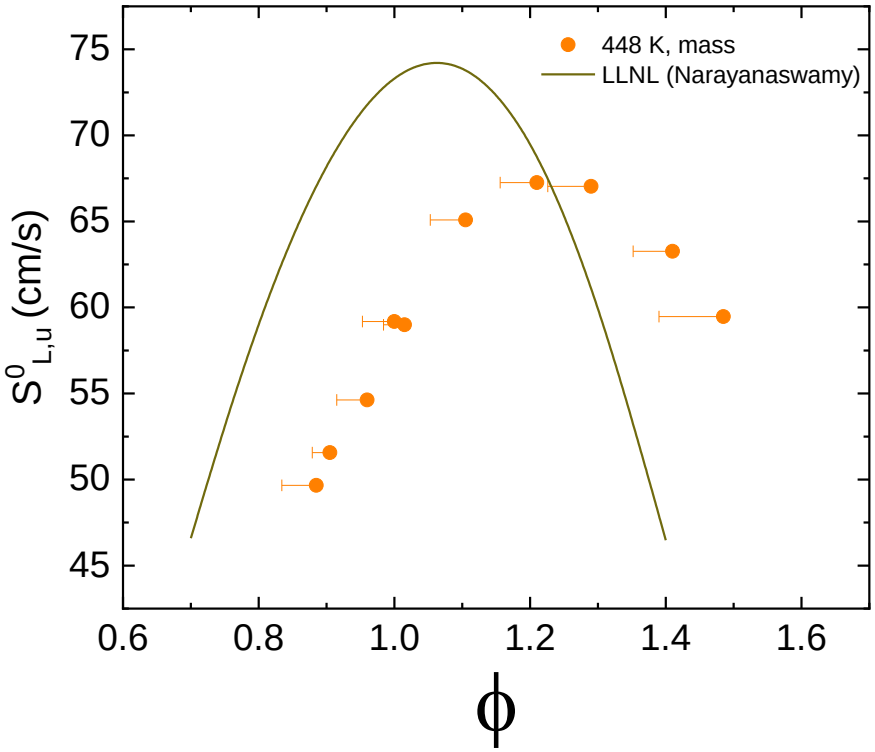

Figure 76. Experimental data for DF #2 compared to model predictions based on the LLNL Surrogate at 448 K.

Looking now at a comparison using X_{FUEL}, in the same manner as previously discussed, the plot is contained in Figure 77. The model prediction now has much better agreement with the experimental data. However, the model over predicts the peak flame speed by 10.6%. The peak flame speed occurs around X_{FUEL} = 0.013, similar to the results with the other fuels.

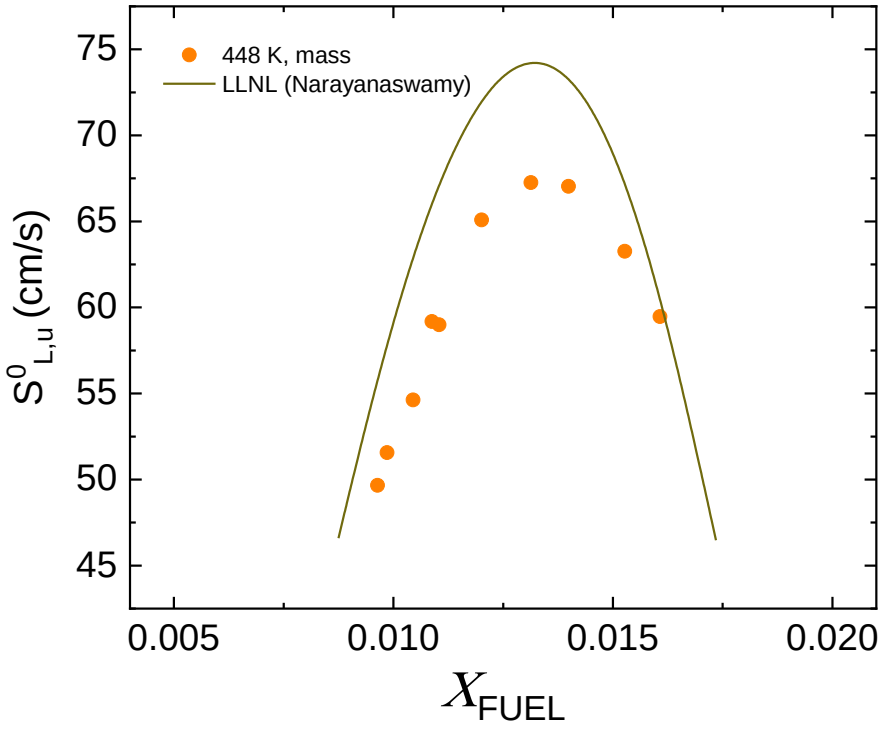

Figure 77. Experimental data for DF #2 compared to model predictions using the LLNL surrogate with X_{FUEL} on the x-axis at 448 K.

Conclusions

Different research groups are defining their fuel and therefore calculating equivalence ratio in different ways. While this can be somewhat problematic and confusing as long as groups specify what average molecule they used and how they arrived at that molecule, adjustments can be made to account for these differences when making comparisons across studies. As shown, the use of X_{FUEL} seems to normalize these values and presents the amount of fuel in the mixture as a percentage.

Similar corrections need to be applied when comparing data to various surrogates using updated chemical kinetics mechanisms. None of these surrogates perfectly match the fuels. As seen with the experimental results, there is better agreement when using fuel mole fraction on the x-axis. To better match all of the properties of the fuels, the chemical kinetics mechanisms need to be updated to include larger naphthenes (cycloalkanes) than MCH. Otherwise, attempting to match other properties will force the average molecule and therefore the average molecular weight to be too small.

CHAPTER IX

CONCLUSIONS

New laminar flame speed data have been collected for five common, kerosene-based fuels: Jet-A, RP-1, Diesel Fuel #2, S-8, and Shell GTL. An additional study was performed on n-decane to verify and improve the experimental procedure for working with these low vapor pressure liquid fuels.

Overall, the fuels had very similar results. All fuels saw a flame speed that peaked between 56 and 60 cm/s between $\varphi = 1.1$ and $\varphi = 1.25$. While this is a richer equivalence ratio than expected, it is believed to be caused by the average molecule used to calculate the equivalence ratio. This observation is in part verified when switching to fuel mole fraction as the parameter to use when comparing results to the data (and models) available in the literature.

Understanding and limiting the uncertainty in the fuel-air mixture being tested (and hence equivalence ratio) was a large portion of this study. The uncertainty is believed to be $\varphi = \pm 0.03$ stemming from a combination of instrumentation and fuel properties. The uncertainty in flame speed is calculated to be on the order of $\pm$ 2.79 cm/s. This value is primarily due to the repeatability of the experimental data.

To help limit the uncertainty to the level stated above, numerous improvements were made to the experimental procedure. These became necessary due to the low vapor pressure nature of the fuel. The first of these improvements was switching from the partial pressure method to add the fuel to the vessel to an alternate method that required measuring out the mass of the fuel that was injected into the vessel. Additional valves and fittings were removed

from the septum configuration, hence reducing the number of possible cold spots that fuel could condense. Finally, better syringes with airtight barrels and 10-inch needles were used to inject the fuel. This modification allowed for the operator to actually see the fuel entering the chamber as it left the tip of the syringe, removing any doubt that the fuel made it all the way into the vessel.

During the data analysis, a strong linear correlation was noticed for the burned-gas Markstein length for these fuels. This trend appears to be stronger for stoichiometric and rich mixtures. Fortunately, this correlation appears useful as a tool to help identify potentially inaccurate data points. More research should be conducted in this area to improve the correlation for lean mixtures and determine the application to other fuels.

When initially compared to data in the literature, the experimental results seemed to be shifted toward richer equivalence ratios. However, this is apparent shift was due to the difference in the average molecule used to calculate φ. Since there is no standard average molecule generally accepted for all batches of kerosene, and it appears that calculated molecular weights, usually derived using some form of mass spectroscopy analysis, are accurate to only within about 15%, a different parameter was suggested. It is proposed that fuel mole fraction, X_{FUEL}, be used as opposed to φ. This alternate way of presenting the flame speed data avoids any uncertainty in average mixture MW and corresponding equivalence ratio since it is only dependent on the actual mass of fuel in the mixture. The amount of fuel in the mixture can be definitively measured.

When adjusted to X_{FUEL}, direct comparisons to surrogates through chemical kinetics mechanisms and other experimental data are possible. The proposed surrogates also appear to

be predicting slightly faster laminar flame speeds than the current experimental results suggest. However, many of these surrogates, such as the "Narayanaswamy Surrogate" [29] were all tuned using the experimental results from counterflow configurations [13-15, 18]. As previously mentioned, the counterflow configuration is known to produce slightly faster results [16]. Therefore, the current spherical flame data should be used to develop and tune improved surrogates and chemical kinetics mechanisms.

However, experimentally, the largest source of uncertainty is with the fuel itself. With 15% uncertainty in the fuel average molecule, it becomes difficult to fully know with what chemical composition anyone is actually working. Surrogate mixtures are frequently used to model these real fuels, and they also have well-defined and known average molecules. However, when comparing the model results to experimental data, it is important to know if the surrogate has been chosen to match the fuel, or if the fuel composition has been artificially adjusted to match the surrogate.

For the liquid fuel community, it would be helpful if some standards were put into place to ease the comparison of results and facilitate future collaboration. Examples include things as simple as the way surrogates are defined. From the literature, the general trend is by mole fraction. However, there are still a few published surrogates that are defined by mass fraction or liquid volume. While good attention to detail will catch this, and adjust accordingly for it, it still leads to additional confusion to future researchers and users. While X_{FUEL} is clearly a better parameter to use when comparing different data sets, tradition favors the continued us of φ. If this preference is to continue, then there should be an agreed upon standard average molecule for Jet-A and other kerosene-based fuels that needs to be used.

REFERENCES

[1] Edwards, J. T., 2017. "Reference Jet Fuels for Combustion Testing," Proc. 55th AIAA SciTech Forum, Grapevine, TX.

[2] Ji, C., Dames, E., Wang, Y. L., Wang, H., and Egolfopoulos, F. N., 2010. "Propagation and extinction of premixed C5–C12n-alkane flames," Combustion and Flame, **157**(2), pp. 277-287.

[3] Edwards, T., and Maurice, L. Q., 2001. "Surrogate Mixtures to Represent Complex Aviation and Rocket Fuels," Journal of Propulsion and Power, **17**(2), pp. 461-466.

[4] Violi, A., Yan, S., Eddings, E. G., Sarofim, A. F., Granata, S., Faravelli, T., and Ranzi, E., 2002. "Experimental formulation and kinetic model for JP-8 surrogate mixtures," Combustion Science and Technology, **174**(11-12), pp. 399-417.

[5] Singh, D., Nishiie, T., and Qiao, L., 2011. "Experimental and Kinetic Modeling Study of the Combustion of n-Decane, Jet-A, and S-8 in Laminar Premixed Flames," Combustion Science and Technology, **183**(10), pp. 1002-1026.

[6] Ranzi, E., 2005. "Wide-range kinetic modeling study of the pyrolysis, partial oxidation, and combustion of heavy n-alkanes," Industrial & engineering chemistry research, **44**(14), pp. 5170-5183.

[7] Ranzi, E., Frassoldati, A., Grana, R., Cuoci, A., Faravelli, T., Kelley, A. P., and Law, C. K., 2012. "Hierarchical and comparative kinetic modeling of laminar flame speeds of hydrocarbon and oxygenated fuels," Progress in Energy and Combustion Science, **38**(4), pp. 468-501.

[8] Kim, D., Martz, J., and Violi, A., 2014. "A surrogate for emulating the physical and chemical properties of conventional jet fuel," Combustion and Flame, **161**(6), pp. 1489-1498.

[9] Kim, D., Martz, J., Abdul-Nour, A., Yu, X., Jansons, M., and Violi, A., 2017. "A six-component surrogate for emulating the physical and chemical characteristics of conventional and alternative jet fuels and their blends," Combustion and Flame, **179**, pp. 86-94.

[10] Kim, D., and Violi, A., 2018. "Hydrocarbons for the next generation of jet fuel surrogates," Fuel, **228**, pp. 438-444.

[11] Honnet, S., Seshadri, K., Niemann, U., and Peters, N., 2009. "A surrogate fuel for kerosene," Proceedings of the Combustion Institute, **32**(1), pp. 485-492.

[12] Bikas, G., and Peters, N., 2001. "Kinetic modelling of n-decane combustion and autoignition: Modeling combustion of n-decanem," Combustion and Flame, **126**(1), pp. 1456-1475.

[13] Kumar, K., Sung, C.-J., and Hui, X., 2011. "Laminar flame speeds and extinction limits of conventional and alternative jet fuels," Fuel, **90**(3), pp. 1004-1011.

[14] Hui, X., Kumar, K., Sung, C.-J., Edwards, T., and Gardner, D., 2012. "Experimental studies on the combustion characteristics of alternative jet fuels," Fuel, **98**, pp. 176-182.

[15] Hui, X., and Sung, C.-J., 2013. "Laminar flame speeds of transportation-relevant hydrocarbons and jet fuels at elevated temperatures and pressures," Fuel, **109**, pp. 191-200.

[16] Konnov, A. A., Mohammad, A., Kishore, V. R., Kim, N. I., Prathap, C., and Kumar, S., 2018. "A comprehensive review of measurements and data analysis of laminar burning velocities for various fuel+air mixtures," Progress in Energy and Combustion Science, **68**, pp. 197-267.

[17] Kumar, K., and Sung, C.-J., 2007. "Laminar flame speeds and extinction limits of preheated n-decane/O2/N2 and n-dodecane/O2/N2 mixtures," Combustion and Flame, **151**(1), pp. 209-224.

[18] Ji, C., Wang, Y. L., and Egolfopoulos, F. N., 2011. "Flame Studies of Conventional and Alternative Jet Fuels," Journal of Propulsion and Power, **27**(4), pp. 856-863.

[19] Dooley, S., Won, S. H., Chaos, M., Heyne, J., Ju, Y., Dryer, F. L., Kumar, K., Sung, C.-J., Wang, H., Oehlschlaeger, M. A., Santoro, R. J., and Litzinger, T. A., 2010. "A jet fuel surrogate formulated by real fuel properties," Combustion and Flame, **157**(12), pp. 2333-2339.

[20] Dooley, S., Won, S. H., Heyne, J., Farouk, T. I., Ju, Y., Dryer, F. L., Kumar, K., Hui, X., Sung, C.-J., Wang, H., Oehlschlaeger, M. A., Iyer, V., Iyer, S., Litzinger, T. A., Santoro, R. J., Malewicki, T., and Brezinsky, K., 2012. "The experimental evaluation of a methodology for surrogate fuel formulation to emulate gas phase combustion kinetic phenomena," Combustion and Flame, **159**(4), pp. 1444-1466.

[21] Malewicki, T., Gudiyella, S., and Brezinsky, K., 2013. "Experimental and modeling study on the oxidation of Jet A and the n-dodecane/iso-octane/n-propylbenzene/1,3,5-trimethylbenzene surrogate fuel," Combustion and Flame, **160**(1), pp. 17-30.

[22] Chong, C. T., and Hochgreb, S., 2011. "Measurements of laminar flame speeds of liquid fuels: Jet-A1, diesel, palm methyl esters and blends using particle imaging velocimetry (PIV)," Proceedings of the Combustion Institute, **33**(1), pp. 979-986.

[23] Colket, M., Edwards, T., Cernansky, N., Dryer, F., Egolfopoulos, F., Friend, D., Law, E., Lenhert, D., Lindstedt, P., Pitsch, H., Sarofim, A., Seshadri, K., Smooke, M., Tsang, W., and Williams, S., 2007, "Development of an Experimental Database and Kinetic Models for Surrogate Jet Fuels," 45th AIAA Aerospace Sciences Meeting and Exhibit, American Institute of Aeronautics and Astronautics.

[24] Denman, B. M., Munzar, J. D., and Bergthorson, J. M., 2012. "An Experimental and Numerical Study of the Laminar Flame Speed of Jet Fuel Surrogate Blends," ASME Paper GT2012-69917.

[25] Moghaddas, A., Eisazadeh-Far, K., and Metghalchi, H., 2012. "Laminar burning speed measurement of premixed n-decane/air mixtures using spherically expanding flames at high temperatures and pressures," Combustion and Flame, **159**(4), pp. 1437-1443.

[26] Comandini, A., Dubois, T., and Chaumeix, N., 2015. "Laminar flame speeds of n-decane, n-butylbenzene, and n-propylcyclohexane mixtures," Proceedings of the Combustion Institute, **35**(1), pp. 671-678.

[27] Kick, T., Herbst, J., Kathrotia, T., Marquetand, J., Braun-Unkhoff, M., Naumann, C., and Riedel, U., 2012. "An experimental and modeling study of burning velocities of possible future synthetic jet fuels," Energy, **43**(1), pp. 111-123.

[28] Dagaut, P., Karsenty, F., Dayma, G., Diévart, P., Hadj-Ali, K., Mzé-Ahmed, A., Braun-Unkhoff, M., Herzler, J., Kathrotia, T., Kick, T., Naumann, C., Riedel, U., and Thomas, L., 2014. "Experimental and detailed kinetic model for the oxidation of a Gas to Liquid (GtL) jet fuel," Combustion and Flame, **161**(3), pp. 835-847.

[29] Narayanaswamy, K., Pitsch, H., and Pepiot, P., 2016. "A component library framework for deriving kinetic mechanisms for multi-component fuel surrogates: Application for jet fuel surrogates," Combustion and Flame, **165**, pp. 288-309.

[30] Narayanaswamy, K., Blanquart, G., and Pitsch, H., 2010. "A consistent chemical mechanism for oxidation of substituted aromatic species," Combustion and Flame, **157**(10), pp. 1879-1898.

[31] Narayanaswamy, K., Pepiot, P., and Pitsch, H., 2014. "A chemical mechanism for low to high temperature oxidation of n-dodecane as a component of transportation fuel surrogates," Combustion and Flame, **161**(4), pp. 866-884.

[32] Narayanaswamy, K., Pitsch, H., and Pepiot, P., 2015. "A chemical mechanism for low to high temperature oxidation of methylcyclohexane as a component of transportation fuel surrogates," Combustion and Flame, **162**(4), pp. 1193-1213.

[33] Koniavitis, P., Rigopoulos, S., and Jones, W. P., 2018. "Reduction of a detailed chemical mechanism for a kerosene surrogate via RCCE-CSP," Combustion and Flame, **194**, pp. 85-106.

[34] Alekseev, V. A., Soloviova-Sokolova, J. V., Matveev, S. S., Chechet, I. V., Matveev, S. G., and Konnov, A. A., 2017. "Laminar burning velocities of n-decane and binary kerosene surrogate mixture," Fuel, **187**, pp. 429-434.

[35] Wu, Y., Modica, V., Yu, X., and Grisch, F., 2018. "Experimental Investigation of Laminar Flame Speed Measurement for Kerosene Fuels: Jet A-1, Surrogate Fuel, and Its Pure Components," Energy & Fuels, **32**(2), pp. 2332-2343.

[36] Dagaut, P., El Bakali, A., and Ristori, A., 2006. "The combustion of kerosene: Experimental results and kinetic modelling using 1- to 3-component surrogate model fuels," Fuel, **85**(7), pp. 944-956.

[37] Szymkowicz, P. G., and Benajes, J., 2018. "Development of a Diesel Surrogate Fuel Library," Fuel, **222**, pp. 21-34.

[38] Edwards, T., 2003. "Liquid Fuels and Propellants for Aerospace Propulsion: 1903-2003," Journal of Propulsion and Power, **19**(6), pp. 1089-1107.

[39] Turns, S. R., 2012, An Introduction to Combustion: Concepts and Applications, McGraw Hill, New York.

[40] Çengel, Y. A. B., Michael A. , 2002, Thermodynamics: An Engineering Approach, McGraw-Hill Higher Education.

[41] Widegren, J. A., and Bruno, T. J., 2008. "Thermal Decomposition Kinetics of the Aviation Turbine Fuel Jet A," Industrial & Engineering Chemistry Research, **47**(13), pp. 4342-4348.

[42] Andersen, P. C., and Bruno, T. J., 2005. "Thermal Decomposition Kinetics of RP-1 Rocket Propellant," Industrial & Engineering Chemistry Research, **44**(6), pp. 1670-1676.

[43] Krejci, M. C., Mathieu, O., Vissotski, A. J., Ravi, S., Sikes, T. G., Petersen, E. L., Kérmonès, A., Metcalfe, W., and Curran, H. J., 2013. "Laminar Flame Speed and Ignition Delay Time Data for the Kinetic Modeling of Hydrogen and Syngas Fuel Blends," Journal of Engineering for Gas Turbines and Power, **135**(2), pp. 021503-021503-021509.

[44] Singh, D., 2010, "Study of Surrogates For Conventional And Synthetic Aviation Fuels," Master of Science in Engineering, Purdue University.

[45] Sikes, T., Mannan, M. S., and Petersen, E. L., 2018. "An experimental study: laminar flame speed sensitivity from spherical flames in stoichiometric CH4–air mixtures," Combustion Science and Technology, **190**(9), pp. 1594-1613.

[46] Chen, Z., 2011. "On the extraction of laminar flame speed and Markstein length from outwardly propagating spherical flames," Combustion and Flame, **158**(2), pp. 291-300.

[47] Monteiro, E., Bellenoue, M., Sotton, J., Moreira, N. A., and Malheiro, S., 2010. "Laminar burning velocities and Markstein numbers of syngas–air mixtures," Fuel, **89**(8), pp. 1985-1991.

[48] Burke, M. P., Chen, Z., Ju, Y., and Dryer, F. L., 2009. "Effect of cylindrical confinement on the determination of laminar flame speeds using outwardly propagating flames," Combustion and Flame, **156**(4), pp. 771-779.

[49] Maxwell, J. B., 1950, Data Book on Hydrocarbons: Application to Process Engineering, D. Van Nostrand Company, INC, New York.

[50] Munzar, J. D., Akih-Kumgeh, B., Denman, B. M., Zia, A., and Bergthorson, J. M., 2013. "An experimental and reduced modeling study of the laminar flame speed of jet fuel surrogate components," Fuel, **113**, pp. 586-597.

[51] Kim, H. H., Won, S. H., Santner, J., Chen, Z., and Ju, Y., 2013. "Measurements of the critical initiation radius and unsteady propagation of n-decane/air premixed flames," Proceedings of the Combustion Institute, **34**(1), pp. 929-936.

[52] Singh, D., Nishiie, T., and Qiao, l., 2010, "Laminar Burning Speeds and Markstein Lengths of n-Decane/Air, n-Decane/O2/He, Jet-A/Air and S-8/Air Flames," 48th AIAA Aerospace Sciences Meeting Including the New Horizons Forum and Aerospace Exposition, American Institute of Aeronautics and Astronautics.

[53] Keesee, C. L., Petersen, E. L., Zhang, K., and Curran, H. J., 2015. "Laminar Flame Speed Measurements of Synthetic Gas Blends With Hydrocarbon Impurities," ASME Paper GT2015-42905.

[54] Burke, S. M., Burke, U., Mc Donagh, R., Mathieu, O., Osorio, I., Keesee, C., Morones, A., Petersen, E. L., Wang, W., DeVerter, T. A., Oehlschlaeger, M. A., Rhodes, B., Hanson, R. K., Davidson, D. F., Weber, B. W., Sung, C.-J., Santner, J., Ju, Y., Haas, F. M., Dryer, F. L., Volkov, E. N., Nilsson, E. J. K., Konnov, A. A., Alrefae, M., Khaled, F., Farooq, A., Dirrenberger, P., Glaude, P.-A., Battin-Leclerc, F., and Curran, H. J., 2015. "An experimental and modeling study of propene oxidation. Part 2: Ignition delay time and flame speed measurements," Combustion and Flame, **162**(2), pp. 296-314.

[55] Zhou, C.-W., Li, Y., O'Connor, E., Somers, K. P., Thion, S., Keesee, C., Mathieu, O., Petersen, E. L., DeVerter, T. A., Oehlschlaeger, M. A., Kukkadapu, G., Sung, C.-J., Alrefae, M., Khaled, F., Farooq, A., Dirrenberger, P., Glaude, P.-A., Battin-Leclerc, F., Santner, J., Ju, Y., Held, T., Haas, F. M., Dryer, F. L., and Curran, H. J., 2016. "A comprehensive experimental and modeling study of isobutene oxidation," Combustion and Flame, **167**, pp. 353-379.

[56] Lowry, W., de Vries, J., Krejci, M., Petersen, E., Serinyel, Z., Metcalfe, W., Curran, H., and Bourque, G., 2010. "Laminar Flame Speed Measurements and Modeling of Pure Alkanes and Alkane Blends at Elevated Pressures," ASME Paper GT2010-23050.

[57] Klingbeil, A. E. J., J.B. and R.K. Hanson, 2006. "Temperature- and pressure-dependent absorption cross sections of gaseous hydrocarbons at 3.39 μm," Measurement science & technology, **17**(7), pp. 1950-1957.

[58] MacDonald, M. E., 2012, "Decomposition Kinetics of The Rocket Propellant RP-1 and its Chemical Kinetic Surrogates," PHD, Stanford University.

[59] Moffat, R. J., 1988. "Describing the uncertainties in experimental results," Experimental Thermal and Fluid Science, **1**(1), pp. 3-17.

[60] Kang, D., Kim, D., Kalaskar, V., Violi, A., and Boehman, A. L., 2019. "Experimental characterization of jet fuels under engine relevant conditions – Part 1: Effect of chemical composition on autoignition of conventional and alternative jet fuels," Fuel, **239**, pp. 1388-1404.

[61] Dooley, S. W., Sang Hee; Jahangirian, Saeed; Ju, Yiguahg; Dryer, Frederick L., 2012, "An Experimentally Validated Surrogate Fuel for the Combustion Kinetics of S-8, a Synthetic Paraffinic Jet Aviation Fuel," AIAA Aerospace Sciences Meeting Nashville, TN.

[62] Pei, Y., Mehl, M., Liu, W., Lu, T., Pitz, W. J., and Som, S., 2015. "A Multicomponent Blend as a Diesel Fuel Surrogate for Compression Ignition Engine Applications," Journal of Engineering for Gas Turbines and Power, **137**(11), pp. 111502-111502-111509.

APPENDIX A

EQUIVALENCE RATIO CALCULATION

Traditional Method

One of the key parameters used in laminar flame is the equivalence ratio, φ. This is used to determine how lean or rich a mixture is. An equivalence ratio that is less than 1 indicates a fuel lean mixture, whereas an equivalence ratio greater than one indicates a fuel rich mixture. An equivalence ratio of one means that there is just enough oxygen present to convert all of the hydrogen and carbon in the fuel to either H_2O or CO_2 respectively. Therefore, knowing the stoichiometric amount of O_2 necessary is very important. For pure fuels, this calculation is very straightforward, as can be seen for decane ($C_{10}H_{22}$) in Figure A 1.A 1.

Typically, when doing these calculations it is assumed that one mole of fuel is present. Once the stoichiometric amount of O_2 is determined, the total moles in the mixture can be determined. From the total number of moles, N_{TOT}, mole fractions, X_i, and thus partial pressures can be calculated.

This process is complicated somewhat when dealing with real fuels because the molecule used to calculate stoichiometric O_2, and therefore φ, is an average molecule. For example, the average molecule used in this study for Jet-A is $C_{11.4}H_{22.1.}$ Other studies have used different average molecules. As with all averages, there is some distribution of the blend around this average. This distribution and its repeatability have currently not been studied. This leads to an inherent uncertainty in determining what φ actually is.

Decane: $C_{10}H_{22}$

$$C_{10}H_{22} + a(O_2 + 3.76N_2) \rightarrow bCO_2 + dH_2O + 3.76aN_2$$

Carbon:

$10 \rightarrow b$

Hydrogen:

$22 \rightarrow 2d$

$11 \rightarrow d$

Oxygen:

$2a \rightarrow 2b + d$

$2a = 2(10) + 11$

$2a = 31$

$a = 15.5$

Calculate total number of Moles:

$$C_{10}H_{22} + \frac{15.5}{\varphi}(O_2 + 3.76N_2) \rightarrow Products$$

Figure A 1. Calculation of Stoichiometric O_2 for Decane/Air mixture.

Molecular Weight Method

An alternative method to calculating φ relies more on approximations. This method as shown in Figure A 2 calculates an average ratio of the mass of O_2 to the mass of fuel. The ratio is then used as the approximate stoichiometric ratio for all fuels.

Calculate mass of fuel and O_2:

$$mass_{FUEL} = 10(12.0107) + 22(1.00794) = 142.282$$

$$mass_{O_2} = 15.5(31.998) = 495.969$$

Determine Mass Ratio of Oxygen to Fuel:

$$\frac{mass_{O_2}}{mass_{FUEL}} = 3.486$$

Figure A 2. Molecular Weight method to determine Equivalence Ratio.

APPENDIX B

MARKSTEIN LENGTH CORRELATION

A correlation to predict the value of the Markstein length was found during this study. This linear trend was found for decane and then adjusted to more accurately apply to the other kerosene-based fuels included in this study. The linear fit for decane, shown in Equation AB.1, is based on a linear fit through the experimental results.

$$L_b = -0.28105\varphi + 0.40227 \qquad \text{AB.1}$$

Adjustments were then made to this equation to apply to the other fuels. This adjustment was done by multiplying equation AB.1 by the ratio of the stoichiometric coefficient for the fuel to that of decane, a_r, as shown in **Error! Reference source not found.**A 3. Dashed intervals used as indicators of accuracy in this measurement were based off of an uncertainty in equivalence ratio ranging from $\varphi = \pm 0.05$ to ± 0.15 based on the overall scatter of the data. The resultant equations for all fuels are shown in Table A 1.

Decane: $C_{10}H_{22}$

$$C_{10}H_{22} + a(O_2 + 3.76N_2) \rightarrow bCO_2 + dH_2O + 3.76aN_2$$

At Stoichiometric the stoichiometric coefficient, a, is 15.5 (see Appendix 1).

Jet-A (POSF 10325): $C_{11.4}H_{22.1}$

$$C_{11.4}H_{22.1} + a(O_2 + 3.76N_2) \rightarrow bCO_2 + dH_2O + 3.76aN_2$$

a = 16.925

$$a_r = \frac{a_{fuel}}{a_{decane}} = \frac{16.925}{15.5}$$

Figure A 3. Example calculation for stoichiometric coefficient ratio.

Table A 1. Markstein Length correlation equations for kerosene-based fuels.

FUEL	a_r	Equation
JET-A (POSF 10325)	1.0919	$L_b = -0.30688\varphi + 0.43925$
RP-1 (POSF 5235)	1.1629	$L_b = -0.3268\varphi + 0.4678$
DF #2	1.2323	$L_b = 0.34633\varphi + 0.4957$
S-8 (POSF 5018)	1.1742	$L_b = -0.33\varphi + 0.4723$
Shell GTL (POSF 5729)	1.0139	$L_b = -0.285\varphi + 0.40785$

APPENDIX C

TDI BROOKS FUEL ANALYSIS

Table A 2. TDI Brooks analysis for Jet-A (POSF 10325).

Jet-A (POSF 10325)					
Compound	**AFRL % Weight**	**TDI Brooks Run #1**	**% Diff**	**TDI Brooks Run #2**	**% Diff**
n-C9	1.42	1.23	13.39	1.28	10.19
n-C10	3.26	3.08	5.50	3.29	-0.92
n-C11	4.29	3.75	12.70	4.11	4.14
n-C12	3.74	3.18	15.06	3.30	11.65
n-C13	2.80	2.63	5.96	2.70	3.64
i-C15	NA	0.40	NA	0.41	NA
n-C14	2.02	1.63	19.20	1.63	19.41
i-C16	NA	0.42	NA	0.42	NA
n-C15	1.03	0.87	15.81	0.87	15.59
n-C16	0.43	0.33	23.44	0.33	24.16
i-C18	NA	0.06	NA	0.06	NA
n-C17	0.21	0.11	46.67	0.12	41.38
Pristane	NA	0.05	NA	0.06	NA
n-C18	0.05	0.03	35.80	0.04	27.20
Phytane	NA	0.02	NA	0.02	NA
n-C19	0.01	0.01	-33.00	0.01	-14.00
n-C20	ND	0.01	NA	0.00	NA
n-C21	ND	0.00	NA	0.00	NA

Table A 3. TDI Brooks analysis for RP-1 (POSF 5235).

RP-1 (POSF 5235)					
Compound	**AFRL % Weight**	**TDI Brooks Run #1**	**% Diff**	**TDI Brooks Run #2**	**% Diff**
n-C9	0.00	0.0095	-0.67	0.010	-0.725
n-C10	0.05	0.2509	-6.16	0.267	-6.644
n-C11	0.15	0.8971	-17.41	1.055	-21.100
n-C12	0.19	0.7081	-13.85	0.762	-15.305
n-C13	0.04	0.0614	-0.76	0.264	-8.000
i-C15	NA	0.5353	NA	0.598	NA
n-C14	0.01	0.0664	-2.79	0.076	-3.272
i-C16	NA	0.2808	NA	0.319	NA
n-C15	ND	0.0208	NA	0.026	NA
n-C16	ND	0.0085	NA	0.002	NA
i-C18	NA	0.0101	NA	0.007	NA
n-C17	ND	0.0011	NA	0.001	NA
Pristane	ND	0.0034	NA	0.004	NA
n-C18	ND	NA	NA	0.000	NA
Phytane	ND	NA	NA	0.001	NA

Table A 4. TDI Brooks analysis for Diesel Fuel #2 (POSF 12758).

Diesel Fuel #2 (POSF 12758)					
Compound	AFRL % Weight	TDI Brooks Run #1	% Diff	TDI Brooks Run #2	% Diff
n-C9	0.37	0.249	32.649	0.23	37.51
n-C10	1.07	0.810	24.327	0.78	26.94
n-C11	1.67	1.176	29.587	1.18	29.15
n-C12	1.55	1.112	28.232	1.05	32.55
n-C13	1.42	1.042	26.641	0.97	31.65
i-C15	NA	0.233	NA	0.22	NA
n-C14	1.39	0.986	29.101	0.89	35.67
i-C16	NA	0.352	NA	0.31	NA
n-C15	1.21	0.887	26.727	0.79	34.40
n-C16	0.96	0.649	32.354	0.58	39.36
i-C18	NA	0.195	NA	0.19	NA
n-C17	0.95	0.558	41.232	0.58	39.21
Pristane	NA	0.323	NA	0.33	NA
n-C18	0.62	0.421	32.065	0.42	32.85
Phytane	NA	0.197	NA	0.18	NA
n-C19	0.58	0.400	31.017	0.36	38.07
n-C20	0.43	0.269	37.488	0.27	36.63
n-C21	ND	0.182	NA	0.19	NA
n-C22	0.20	0.120	39.850	0.12	37.90
n-C23	0.12	0.073	38.917	0.07	37.67
n-C24	0.08	0.039	50.750	0.04	48.63
n-C25	0.04	0.021	47.000	0.02	47.00
n-C26	0.02	0.011	46.500	0.01	50.50
n-C27	ND	0.005	NA	0.00	NA

APPENDIX D

COMPLETE EXPERIMENTAL RESULTS

Table A 5. Complete experimental results for decane.

FM Run	ϕ	X_{FUEL}	$mass_{FUEL}$	$S_{L,u}^0$	L_b	Initial Temp	Needle Length	¼ Turn	Comments
1101	0.98	0.01311	-	53.17	0.1107	129.7	2 inch	YES	
1102	1.079	0.01441	-	57.76	0.0968	127.4	2 inch	YES	
1103	1.3	0.01731	-	57.18	0.0334	131.8	2 inch	YES	
1104	1.193	0.01591	-	60.65	0.0757	131.8	2 inch	YES	
1105	0.84	0.01126	-	43.44	0.1479	129.5	2 inch	YES	
1106	1.155	0.01541	-	60.47	0.0841	130.2	2 inch	YES	
1107	1.092	0.01458	-	59.42	0.1008	130.8	2 inch	YES	
1108	0.996	0.01332	-	55.17	0.135	130	2 inch	YES	
1109	1.119	0.01494	-	59.64	0.0861	130.9	2 inch	YES	
1110	1.36	0.01810	-	53.75	0.0036	132.5	2 inch	YES	
1111	1.495	0.01986	-	46.14	-0.0069	132.6	2 inch	YES	
1118	0.87	0.01165	1.51	46.4	0.1209	131.0	2 inch	YES	PP & mass, Bad?
1119	0.92	0.01232	1.47	48.39	0.1765	130.0	2 inch	YES	PP & mass, Bad?
1120	1.005	0.01344	1.49	55.92	0.1322	130.3	2 inch	YES	
1121	1.3	0.01731	1.92	56.36	0.0276	130.2	2 inch	YES	
1122	1.12	0.01495	1.66	59.98	0.0955	129.3	2 inch	YES	
1123	1.49	0.01980	2.2	43.09	-0.0297	129.9	2 inch	YES	
1124	0.875	0.01172	1.3	36.44	0.2621	130.0	2 inch	YES	Bad?
1125	0.92	0.01232	1.37	50.08	0.1313	130	2 inch	YES	
1126	1.23	0.01640	1.82	60.58	0.0813	130.1	2 inch	YES	
1128	1.215	0.01620	1.8	59.87	0.05	134.4	6 inch	YES	
1129	1.01	0.01350	1.5	58.23	0.1039	129.9	2 inch	NO	
1130	1.1	0.01469	1.64	61.04	0.0901	130.8	6 inch	NO	
1131	0.95	0.01271	1.41	56.64	0.1717	130.1	6 inch	NO	
1132	1.44	0.01914	2.13	44.87	-0.0155	130.3	6 inch	NO	
1133	0.915	0.01225	1.36	43.24	0.2233	130.1	6 inch	NO	Bad?
1134	1.31	0.01745	1.94	54.13	0.019	130.1	6 inch	NO	
1135	0.81	0.01086	1.21	47.04	0.2176	130.0	6 inch	NO	
1136	1.16	0.01548	1.72	59.44	0.0333	130.0	6 inch	NO	

1137	1.14	0.01522	1.69	59.48	0.0644	130.3	6 inch	NO	
1138	0.94	0.01258	1.4	57.93	0.1301	130.5	2 inch	NO	New Decane Here forward
1139	1.18	0.01574	1.75	61.95	0.0943	130.2	2 inch	NO	
1140	1.22	0.01627	1.81	60.13	0.0425	130.5	2 inch	NO	
1141	1.0	0.01337	1.48	57.29	0.2072	130.6	2 inch	NO	
1142	1.135	0.01515	1.68	61.14	0.0768	130.3	2 inch	NO	
1143	1.355	0.01803	2.0	53.57	0.0245	131.1	2 inch	NO	
144	0.855	0.01146	1.27	51.25	0.1968	131.0	2 inch	NO	
1145	1.46	0.01940	2.15	45.41	-0.0132	131.0	4 inch	NO	
1146	1.025	0.01370	1.52	60.41	0.1341	130.7	4 inch	NO	
1147	1.575	0.02090	2.32	35.08	-0.0606	130.9	4 inch	NO	
1148	1.105	0.01476	1.64	62.63	0.1220	131.2	10 inch	NO	
1149	1.31	0.01745	1.94	54.44	0.0213	129.8	10 inch	NO	
1150	0.79	0.01059	1.18	43.46	0.1133	130.1	10 inch	NO	
1151	1.46	0.01940	2.15	43.88	0.0044	130.0	10 inch	NO	
1152	0.89	0.01192	1.32	43.21	0.1282	130.3	10 inch	NO	Bad?
1153	0.895	0.01199	1.33	47.1	0.1184	130.2	10 inch	NO	Bad?
1154	1.3	0.01731	1.92	57.76	-0.0114	129.8	10 inch	NO	Split Air (400 Torr) Fuel Condensed ?
1155	1.435	0.01908	2.12	56.81	0.0328	129.9	10 inch	NO	Split Air (400 Torr) Fuel Condensed ?
1156	0.94	0.01258	1.4	44.65	0.1621	130.0	10 inch	NO	Split Air (400 Torr) Fuel Condensed due to vapor Pressure?
1157	1.08	0.01443	1.6	54.62	0.0027	130.1	10 inch	NO	Split Air (400 Torr) Fuel Condensed ?

1158	1.08	0.01443	1.6	61.96	0.1023	130.0	10 inch	NO	Split Air (125 Torr)
1159	1.46	0.01940	2.15	42.02	-0.0072	130.1	10 inch	NO	Split Air (125 Torr)
1160	0.875	0.01172	1.3	44.4	0.1277	130.1	10 inch	NO	Split Air (125 Torr), Bad?
1161	0.9	0.01205	1.34	55.4	0.0944	129.9	10 inch	NO	Split Air (125 Torr
1162	0.84	0.01126	1.25	51.94	0.1565	130.0	10 inch	NO	Split Air (125 Torr)
1163	1.00	0.01337	1.48	55.53	0.0966	130.0	10 inch	NO	Split Air (125 Torr)
1164	1.01	0.01350	1.5	57.02	0.1033	129.8	10 inch	NO	Split Air (125 Torr)
1165	1.29	0.01718	1.91	54.49	0.0003	129.9	10 inch	NO	Split Air (125 Torr)

Table A 6. Jet-A (POSF 10325) complete experimental results.

FM Run	ϕ	X_{FUEL}	$mass_{FUEL}$	$S_{L,u}^0$	L_b	Initial Temp	Method	Comments
856	1.04	0.0127	-	55.81	0.0395	130	PP (0 - 1000 Torr)	
857	1.2	0.0147	-	50.57	-0.0189	129.9	PP (0 - 1000 Torr)	Bad?
858	0.94	0.0115	-	49.52	0.0805	130.0	PP (0 - 1000 Torr)	
859	1.14	0.0140	-	54.19	0.0199	130.3	PP (0 - 1000 Torr)	
860	1.25	0.0153	-	53.8	0.0071	130.4	PP (0 - 1000 Torr)	
861	0.84	0.0103	-	40.55	0.1106	130.4	PP (0 - 1000 Torr)	
863	1.1	0.0135	-	52.83	0.0488	130.6	PP (0 - 1000 Torr)	
864	1.0	0.0123	-	50.15	0.078	130.5	PP (0 - 1000 Torr)	
865	0.9	0.0110	-	46.23	0.1027	130.3	PP (0 - 1000 Torr)	
866	1.29	0.0158	-	52.38	0.0151	130.2	PP (0 - 1000 Torr)	
867	1.38	0.0168	-	47.3	-0.0083	130.2	PP (0 - 1000 Torr)	
868	1.0	0.0123	-	51.4	0.0927	130.9	PP (0 - 1000 Torr)	
983	1.0	0.0123	-	53.17	0.1492	131.2	PP (0-100 Torr)	
984	1.2	0.0147	-	56.38	0.0749	130.5	PP (0-100 Torr)	
985	1.4	0.0171	-			130.9	PP (0-100 Torr)	Some Condensation on Window
986	0.8	0.0098	-	36.83	0.1581	130.9	PP (0-100 Torr)	
988	0.9	0.0110	-	43.06	0.1449	131	PP (0-100 Torr)	
990	1.1	0.0135	-	55.53	0.0584	131.6	PP (0-100 Torr)	
991	1.3	0.0159	-	44.68	0.0943	131.0	PP (0-100 Torr)	Bad?
992	1.2	0.0147	-	57.77	0.1189	134.3	PP (0-100 Torr)	
993	0.9	0.0110	-	40.97	0.1772	130.1	PP (0-100 Torr)	
995	1.4	0.0171	-	50.47	0.0375	130.8	PP (0-100 Torr)	
996	1.3	0.0159	-	53.69	0.0250	131.5	PP (0-100 Torr)	
1009	1.0	0.0123	-	47.43	0.1454	131.7	PP (0-100 Torr)	Bad?
1010	1.0	0.0123	-	47.26	0.1374	131.1	PP (0-100 Torr)	
1012	1.0	0.0123	-	43.48	0.2484	132.0	PP (0-100 Torr)	Bad?
1013	1.07	0.0131	-	53.48	0.0783	131.0	PP (0-100 Torr)	
1014	1.0	0.0123	-	52.85	0.1258	133.9	PP (0-100 Torr)	
1015	1.0	0.0123	-	50.94	0.0024	128.8	PP (0-100 Torr)	Let mixture sit for 1 hour
1023	1.2	0.0147	-	55.85	0.0676	134.6	PP (0-100 Torr)	
1024	1.34	0.0164	-	50.22	-0.0143	135.6	PP (0-100 Torr)	
1025	1.4	0.0171	-	46.89	-0.0068	136.0	PP (0-100 Torr)	
1026	0.85	0.0104	-	41.57	0.0122	136.0	PP (0-100 Torr)	
1027	1.3	0.0159	-	49.83	-0.0047	139.6	PP (0-100 Torr)	

1166	1.185	0.0145	1.8	50.07	0.18	129.8	Mass: split air (125 Torr)	Bad?
1168	0.995	0.0122	1.51	45.5	0.2137	129.8	Mass: split air (75 Torr)	
1170	1.075	0.0132	1.63	50.25	0.1071	129.8	Mass: split air (10 Torr)	Some Fuel hit window during fill
1171	1.105	0.0135	1.68	53.5	0.1208	129.9	Mass: split air (10 Torr)	
1172	1.21	0.0148	1.84	55.55	0.0689	129.7	Mass: split air (10 Torr)	
1173	1.02	0.0125	1.55	47.15	0.1832	129.8	Mass: split air (10 Torr)	fuel hitting endcap during fill
1174	1.33	0.0162	2.01	54.93	0.0589	129.7	Mass: split air (10 Torr)	
1175	0.965	0.0118	1.47	47.17	0.1276	127.7	Mass: split air (10 Torr)	
1176	1.39	0.0170	2.1	50.81	-0.0054	129.9	Mass: split air (10 Torr)	
1177	1.02	0.0125	1.55	49.07	0.1056	129.7	Mass: split air (10 Torr)	
1178	1.165	0.0143	1.77	55.21	0.079	129.8	Mass: split air (10 Torr)	
1179	0.905	0.0111	1.38	44.73	0.1271	129.6	Mass: split air (10 Torr)	Failed at 10 minutes, success at 20 minutes
1180	1.005	0.01232	1.53	50.26	0.1076	129.7	Mass: split air (10 Torr)	Wait 20 minutes to ignite

Table A 7. RP-1 (POSF 5235) complete experimental results.

FM Run	ϕ	X_{FUEL}	$mass_{FUEL}$	$S_{L,u}^0$	L_b	Initial Temp	Method	Comments
999	1.006	0.01159	-	54.00	0.15374	131.3	PP (0-100 Torr)	
1000	1.1	0.01266	-	55.29	0.1125	131.5	PP (0-100 Torr)	
1001	0.904	0.01043	-	42.03	0.22764	131.7	PP (0-100 Torr)	
1002	1.298	0.01490	-	54.85	0.06365	131.8	PP (0-100 Torr)	
1003	0.948	0.01093	-	44.85	0.1525	131.7	PP (0-100 Torr)	
1004	1.202	0.01382	-	56.62	0.10834	131.8	PP (0-100 Torr)	
1005	1.4	0.01606	-	51.92	0.04549	131.6	PP (0-100 Torr)	
1006	1.071	0.01233	-	54.56	0.19371	131.6	PP (0-100 Torr)	
1007	1.401	0.01607	-	50.38	0.02819	131.0	PP (0-100 Torr)	
1016	1.103	0.01269	-	54.26	0.0467	134.7	PP (0-100 Torr)	
1017	1.093	0.01258	-	-	-	135.8	PP (0-100 Torr)	No Images, Cammra failed to trigger
1018	1.128	0.01298	-	56.80	0.09739	135.9	PP (0-100 Torr)	
1019	1.068	0.01229	-	55.40	0.08923	136.0	PP (0-100 Torr)	
1182	1.04	0.01198	1.57	48.57	0.1099	~ 130	Mass: split air (10 Torr), 0 - 100 Torr	Bad?
1183	1.206	0.01386	1.82	56.73	0.0875	130.3	Mass: split air (10 Torr), 0 - 100 Torr	
1184	1.093	0.01258	1.65	56.00	0.1488	130.4	Mass: split air (10 Torr), 0 - 100 Torr	Questionable?
1185	1.41	0.01617	2.12	53.42	0.0385	130.5	Mass: split air (10 Torr), 0 - 100 Torr	Questionable?
1186	0.88	0.01015	1.33	42.14	0.1461	130.2	Mass: split air (10 Torr), 0 - 100 Torr	Questionable?
1187	1.505	0.01724	2.26	45.74	-0.0084	130.3	Mass: split air (10 Torr), 0 - 100 Torr	
1188	0.996	0.01148	1.50	50.91	0.1451	130.2	Mass: split air (10 Torr), 0 - 100 Torr	
1189	0.965	0.01112	1.46	46.73	0.1044	130.4	Mass: split air (10 Torr), 0 - 100 Torr	Questionable?

1190	1.05	0.01209	1.58	52.27	0.1241	130.2	Mass: split air (10 Torr), 0 - 100 Torr	
1191	1.168	0.01343	1.76	50.05	0.1101	130.3	Mass: split air (10 Torr), 0 - 100 Torr	Bad?
1192	1.34	0.01538	2.02	54.5	0.0366	130.3	Mass: split air (10 Torr), 0 - 100 Torr	
1193	1.05	0.01209	1.58	52.17	0.1074	130.3	Mass: split air (10 Torr), 0 - 100 Torr	
1194	1.44	0.01651	2.16	50.28	0.0014	130.3	Mass: split air (10 Torr), 0 - 100 Torr	
1195	1.26	0.01447	1.90	55.61	0.0565	130.3	Mass: split air (10 Torr), 0 - 100 Torr	

Table A 8. Diesel Fuel #2 (POSF 12758) complete experimental results.

FM Run	ϕ	X_{FUEL}	$mass_{FUEL}$	$S_{L,u}^0$	L_b	Initial Temp	Method	Comments
1028	0.888	0.0097	-	36.91	0.1129	412.45	PP (0 - 100 Torr)	
1029	1.161	0.0126	-	54.69	0.1233	413.95	PP (0 - 100 Torr)	slight condensation
1030	1.043	0.0113	-	45.65	0.087	411.45	PP (0 - 100 Torr)	slight condensation
1031	0.925	0.0101	-	41.13	0.1134	412.75	PP (0 - 100 Torr)	no condensation
1032	1.174	0.0127	-				PP (0 - 100 Torr)	Lots of condensation
1033	0.999	0.0109	-	46.77	0.1113	413.15	PP (0 - 100 Torr)	no condensation
1035	1.058	0.0115	-	52.05	0.2399	412.15	PP (0 - 100 Torr)	no condensation
1036	1.078	0.0117	-	51.75	0.1387	412.45	PP (0 - 100 Torr)	no condensation
1218	1.1	0.0120	1.52	-	-	413.85	Mass: split air (10 Torr), 0 - 100 Torr	DNI
1219	1.41	0.0153	2.11	55.21	0.1593	415.35	Mass: split air (10 Torr), 0 - 100 Torr	
1220	1.005	0.0109	1.49	-	-	419.25	Mass: split air (5 Torr), 0 - 100 Torr	DNI
1221	1.005	0.0109	1.47	42.9	0.1466	423.45	Mass: split air (5 Torr), 0 - 100 Torr	
1222	1.01	0.0110	1.46	46.89	0.1171	429.45	Mass: split air (5 Torr), 0 - 100 Torr	
1223	0.965	0.0105	1.4	43.59	0.1423	429.05	Mass: split air (5 Torr), 0 - 100 Torr	
1224	0.99	0.0108	1.42	49.25	0.126	434.05	Mass: split air (5 Torr), 0 - 100 Torr	
1225	1.0	0.0109	1.42	52.67	0.1157	438.45	Mass: split air (5 Torr), 0 - 100 Torr	
1226	1.1	0.0120	1.56	60.75	0.1427	438.65	Mass: split air (5 Torr), 0 - 100 Torr	
1227	1.005	0.0109	1.41	55.98	0.1097	443.65	Mass: split air (5 Torr), 0 - 100 Torr	
1228	1.09	0.0118	1.53	60.45	0.1109	443.55	Mass: split air (5 Torr), 0 - 100 Torr	
1229	0.922	0.0100	1.29	49.35	0.1361	443.35	Mass: split air (5 Torr), 0 - 100 Torr	

1230	0.855	0.0093	1.20	44.99	0.2067	444.05	Mass: split air (5 Torr), 0 - 100 Torr	
1231	1.0	0.0109	1.39	59.18	0.1245	448.15	Mass: split air (5 Torr), 0 - 100 Torr	
1232	0.885	0.0096	1.23	49.66	0.1527	448.25	Mass: split air (5 Torr), 0 - 100 Torr	
1233	0.96	0.0104	1.33	54.63	0.1671	448.05	Mass: split air (5 Torr), 0 - 100 Torr	
1234	1.105	0.0120	1.53	65.09	0.1269	448.05	Mass: split air (5 Torr), 0 - 100 Torr	
1235	1.21	0.0131	1.67	67.26	0.1030	447.95	Mass: split air (5 Torr), 0 - 100 Torr	
1236	1.29	0.0140	1.79	67.04	0.0755	448.95	Mass: split air (5 Torr), 0 - 100 Torr	
1237	0.905	0.0099	1.26	51.56	0.1528	448.65	Mass: split air (5 Torr), 0 - 100 Torr	
1238	1.405	0.0152	1.94	-	-	448.85	Mass: split air (5 Torr), 0 - 100 Torr	No Images, Cammra failed to trigger
1239	1.41	0.0153	1.95	63.26	0.0544	449.15	Mass: split air (5 Torr), 0 - 100 Torr	
1240	1.015	0.0110	1.41	58.99	0.1691	448.45	Mass: split air (5 Torr), 0 - 100 Torr	
1241	1.425	0.0154	2.05	59.47	0.0672	447.55	Mass: split air (5 Torr), 0 - 100 Torr	

Table A 9. Syntroleum S-8 (POSF 5018) complete experimental results.

FM Run	ϕ	X_{FUEL}	$mass_{FUEL}$	$S_{L,u}^0$	L_b	Initial Temp	Method	Comments
1080	1.368	0.01555	-	55.71	0.0428	129.7	PP (0 - 100 Torr)	
1081	1.1	0.01254	-	53.28	0.1133	131.1	PP (0 - 100 Torr)	
1082	0.946	0.01080	-	43.83	0.1849	129.3	PP (0 - 100 Torr)	
1083	1.073	0.01223	-	52.84	0.1328	132.5	PP (0 - 100 Torr)	
1084	1.629	0.01846	-	43.18	-0.0119	133.5	PP (0 - 100 Torr)	
1085	0.978	0.01116	-	43.33	0.1753	134.9	PP (0 - 100 Torr)	
1086	1.41	0.01602	-	55.27	0.0515	133.9	PP (0 - 100 Torr)	
1087	1.303	0.01482	-	58.42	0.0858	133.4	PP (0 - 100 Torr)	
1088	1.269	0.01444	-	58.2	0.0858	134.1	PP (0 - 100 Torr)	
1089	1.163	0.01325	-	56.38	0.1528	-	PP (0 - 100 Torr)	
1090	1.514	0.01718	-	48.65	0.0066	132.9	PP (0 - 100 Torr)	
1196	1.01	0.01152	1.51	52.37	0.1072	130.2	Mass: split air (10 Torr), 0 -100 Torr	
1197	1.315	0.01495	1.96	58.12	0.0327	130.2	Mass: split air (10 Torr), 0 -100 Torr	
1198	1.164	0.01326	1.74	52.86	0.1123	130.3	Mass: split air (10 Torr), 0 -100 Torr	Questionable?
1199	0.84	0.00960	1.25	-	-	130.4	Mass: split air (10 Torr), 0 -100 Torr	DNI, Too Lean
1200	1.15	0.01310	1.72	58.21	0.0881	130.2	Mass: split air (10 Torr), 0 -100 Torr	
1201	1.505	0.01708	2.24	50.8	0.007	130.4	Mass: split air (10 Torr), 0 -100 Torr	
1202	0.885	0.01011	1.33	44.93	0.1328	130.4	Mass: split air (10 Torr), 0 -100 Torr	Took 2 tries to ignite
1203	0.965	0.01102	1.44	50.37	0.1039	130.3	Mass: split air (10 Torr), 0 -100 Torr	
1204	1.4	0.01590	2.09	54.54	-0.0038	130.4	Mass: split air (10 Torr), 0 -100 Torr	Syringe finger hold Broke
1205	1.068	0.01218	1.6	55.43	0.1017	130.2	Mass: split air (10 Torr), 0 -100 Torr	

1206	1.63	0.01847	2.42	38.8	-0.0749	130.3	Mass: split air (10 Torr), 0 -100 Torr	
1207	1.252	0.01425	1.87	58.44	0.0528	130.4	Mass: split air (10 Torr), 0 -100 Torr	

Table A 10. Shell GTL (POSF 5729) Complete Experimental Results

FM Run	ϕ	X_{FUEL}	$mass_{FUEL}$	$S_{L,u}^0$	L_b	Initial Temp	Notes
1091	1.007	0.0133	-	50.94	0.0878	405.15	PP (0 - 100 Torr)
1092	0.845	0.0112	-	38.27	0.1281	405.95	PP (0 - 100 Torr)
1093	1.289	0.0169	-	57.32	0.0417	404.85	PP (0 - 100 Torr)
1094	1.159	0.0153	-	58.98	0.08	405.75	PP (0 - 100 Torr)
1095	1.446	0.0190	-	46.48	-0.0188	405.75	PP (0 - 100 Torr)
1096	0.982	0.0130	-	49.86	0.1143	403.55	PP (0 - 100 Torr)
1097	1.083	0.0143	-	56.45	0.1028	403.75	PP (0 - 100 Torr)
1098	1.173	0.0154	-	59.76	0.0756	404.55	PP (0 - 100 Torr)
1099	1.41	0.0185	-	44.74	0.0004	404.75	PP (0 - 100 Torr)
1100	0.923	0.0122	-	49.13	0.1438	407.95	PP (0 - 100 Torr)
1208	1.025	0.0135	1.52	57.28	0.0892	403.45	Mass: split air (10 Torr), 0 - 100 Torr
1209	1.17	0.0154	1.73	57.96	0.0331	403.35	Mass: split air (10 Torr), 0 - 100 Torr
1210	0.9	0.0119	1.34	48.15	0.0981	403.55	Mass: split air (10 Torr), 0 - 100 Torr
1211	1.35	0.0177	2.00	47.7	-0.0181	403.45	Mass: split air (10 Torr), 0 - 100 Torr
1212	1.105	0.0146	1.64	59.23	0.0702	403.55	Mass: split air (10 Torr), 0 - 100 Torr
1213	1.22	0.0160	1.81	56.45	0.0281	403.45	Mass: split air (10 Torr), 0 - 100 Torr
1214	1.31	0.0172	1.94	50.47	-0.0351	403.55	Mass: split air (10 Torr), 0 - 100 Torr
1215	0.96	0.0127	1.43	55.09	0.1025	403.35	Mass: split air (10 Torr), 0 - 100 Torr
1216	1.25	0.0164	1.85	55.57	0.0206	403.55	Mass: split air (10 Torr), 0 - 100 Torr
1217	0.85	0.0112	1.28	48.61	0.1018	403.65	Mass: split air (10 Torr), 0 - 100 Torr

APPENDIX E

SAMPLE FLAME IMAGE ANALYSIS

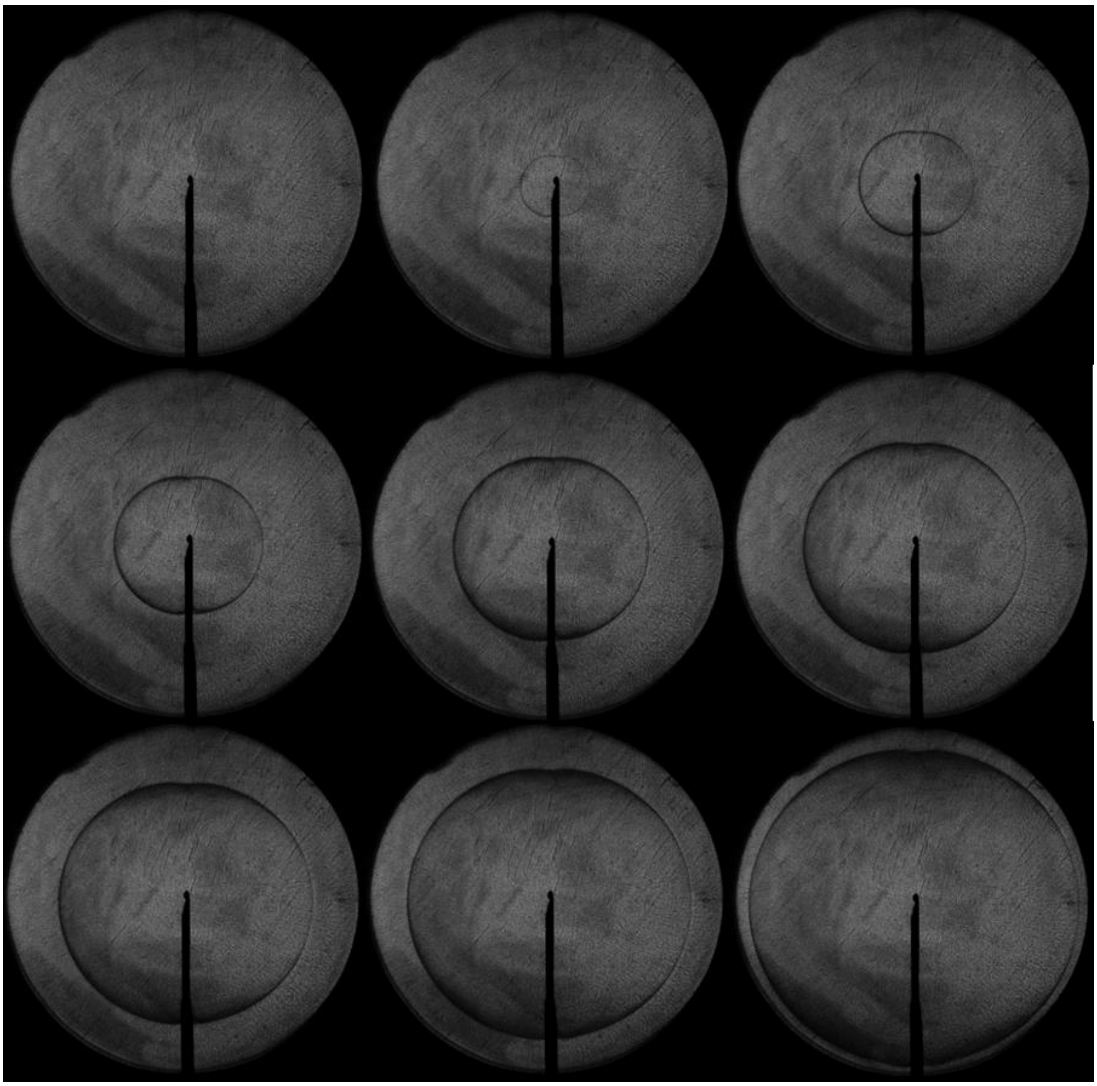

Figure A 4. Sample Flame Images for n-Decane taken from FM 1163, φ = 1.0. Image progression is from left to right top to bottom. The edge of the flame is very faint in the first two images and becomes more distinct as the flame grows.

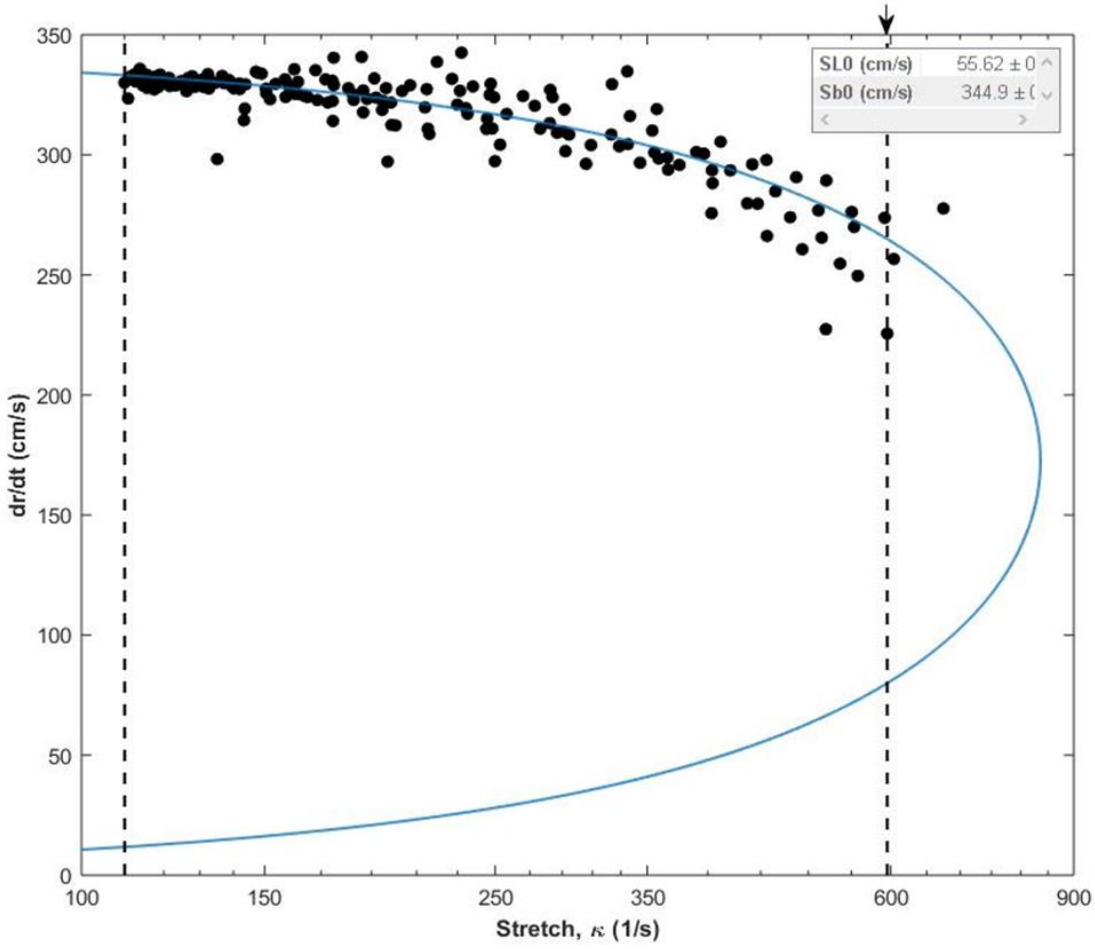

Figure A 5. S_b versus stretch plot for FM 1163 prior to removal of wall and ignition affects. The blue line indicates nonlinear method I, since the Markstein length is positive. Black dots indicate the change in radius of the flame between two frames.

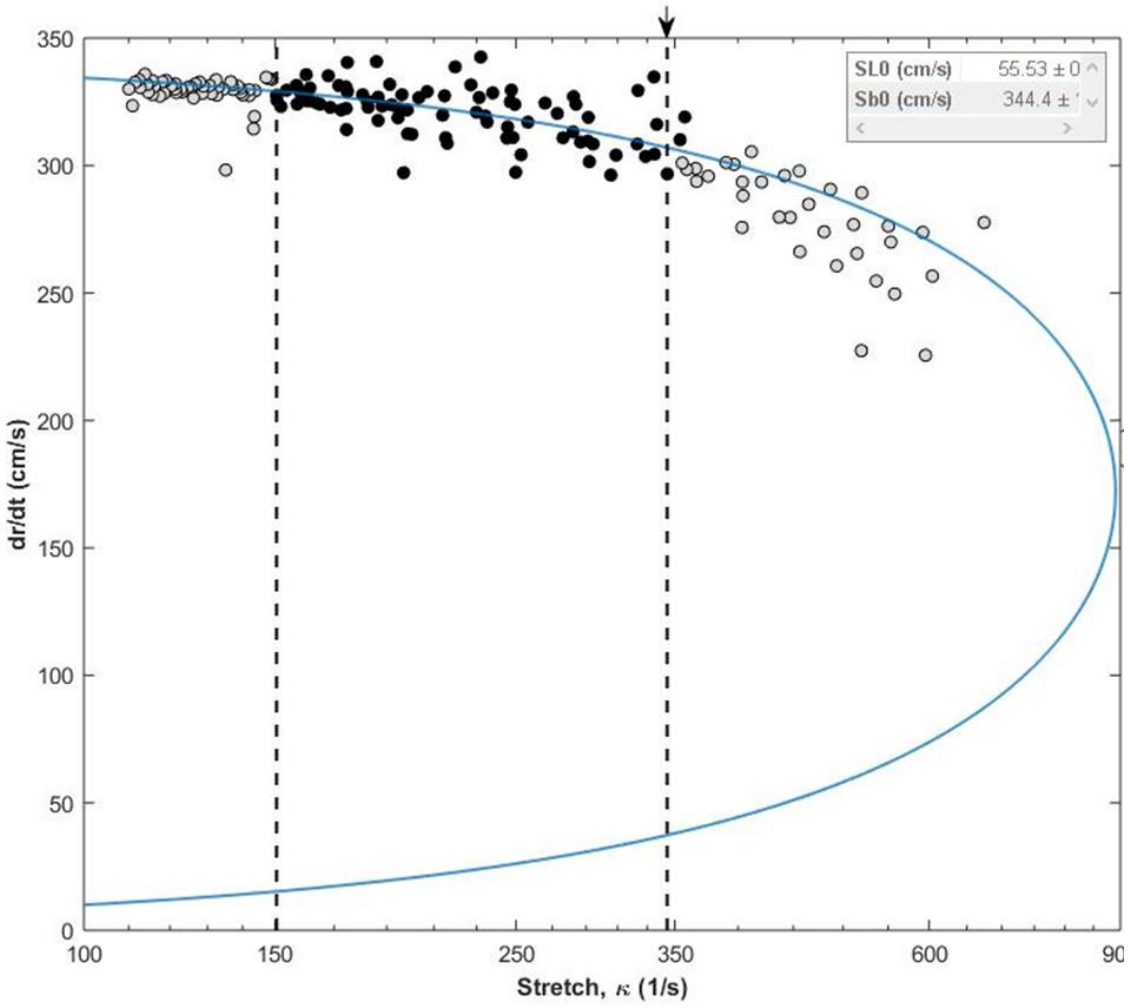

Figure A 6. S_b versus Stretch plot for FM 1163 following the removal of wall and ignition affects. The blue curve is still nonlinear method I. The open points are the points that have been excluded. The black dots are the data still included in the analysis.

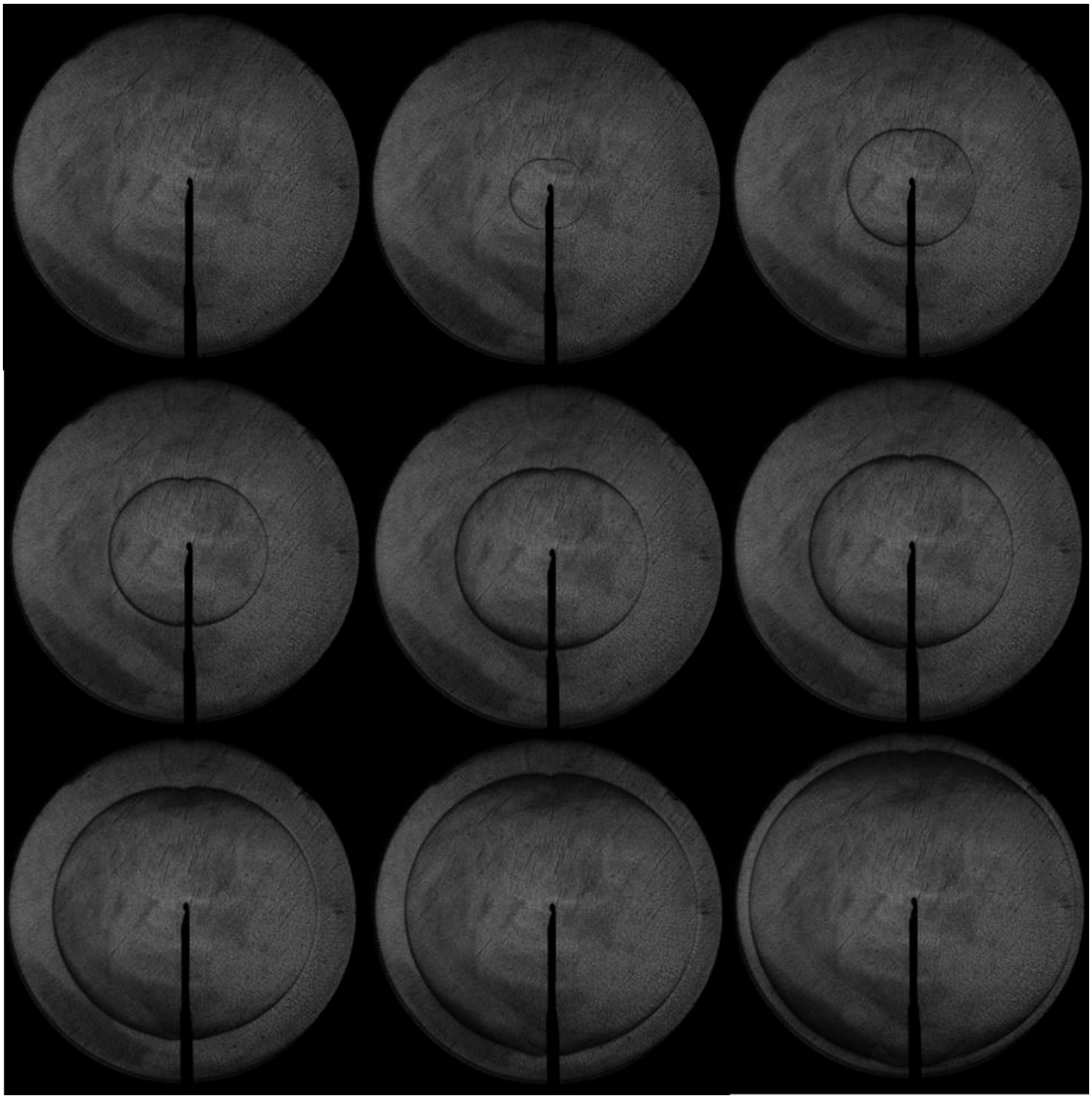

Figure A 7. Sample Flame Images for Jet-A taken from FM 1172, φ = 1.21. Image progression is from left to right top to bottom. This flame has a positive Markstein length (0.1832 cm) resulting in a very smooth edge with no wrinkles detected.

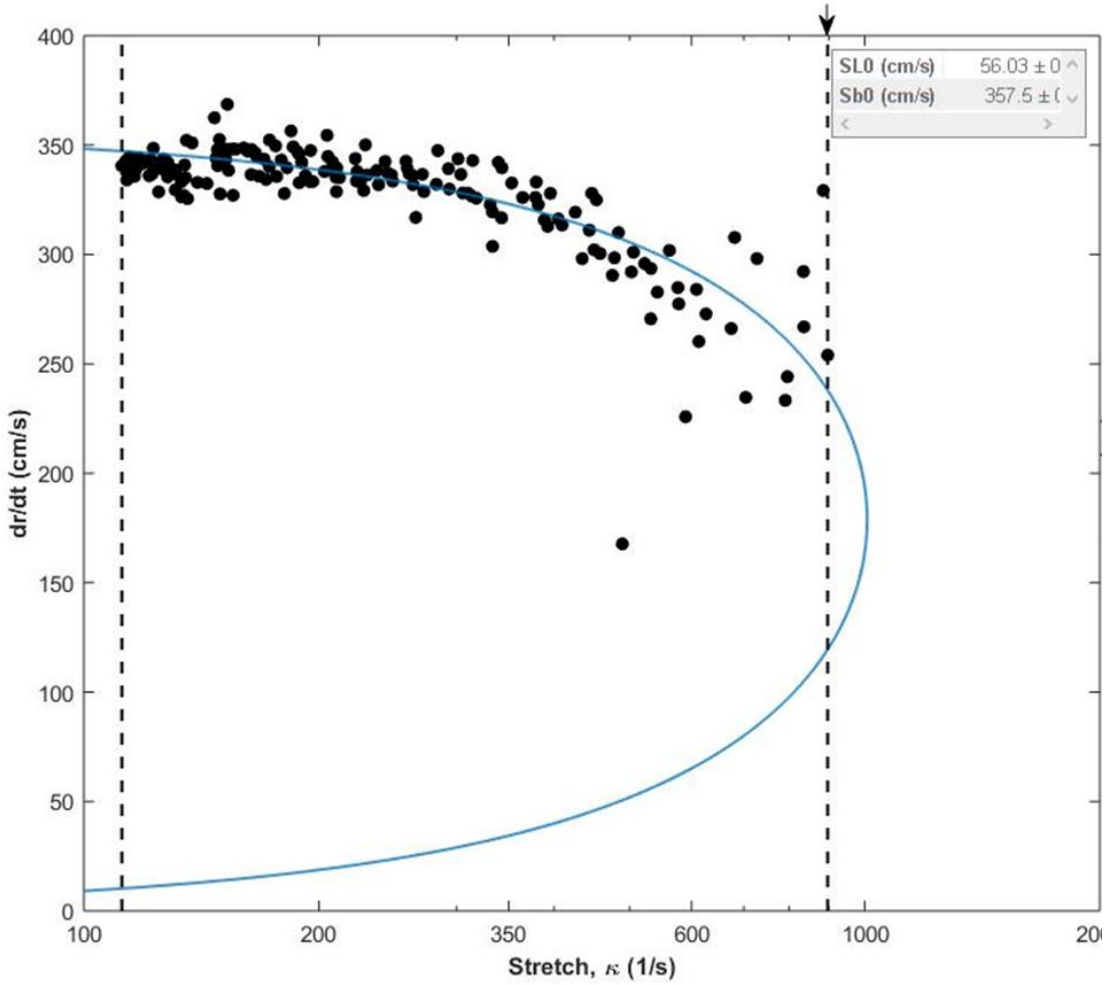

Figure A 8. Initial S_b versus stretch plot for Jet-A (FM 1172) prior to the removal of wall and ignition affects. Since the Markstein length is positive, nonlinear method I was used for analysis as indicated by the blue curve.

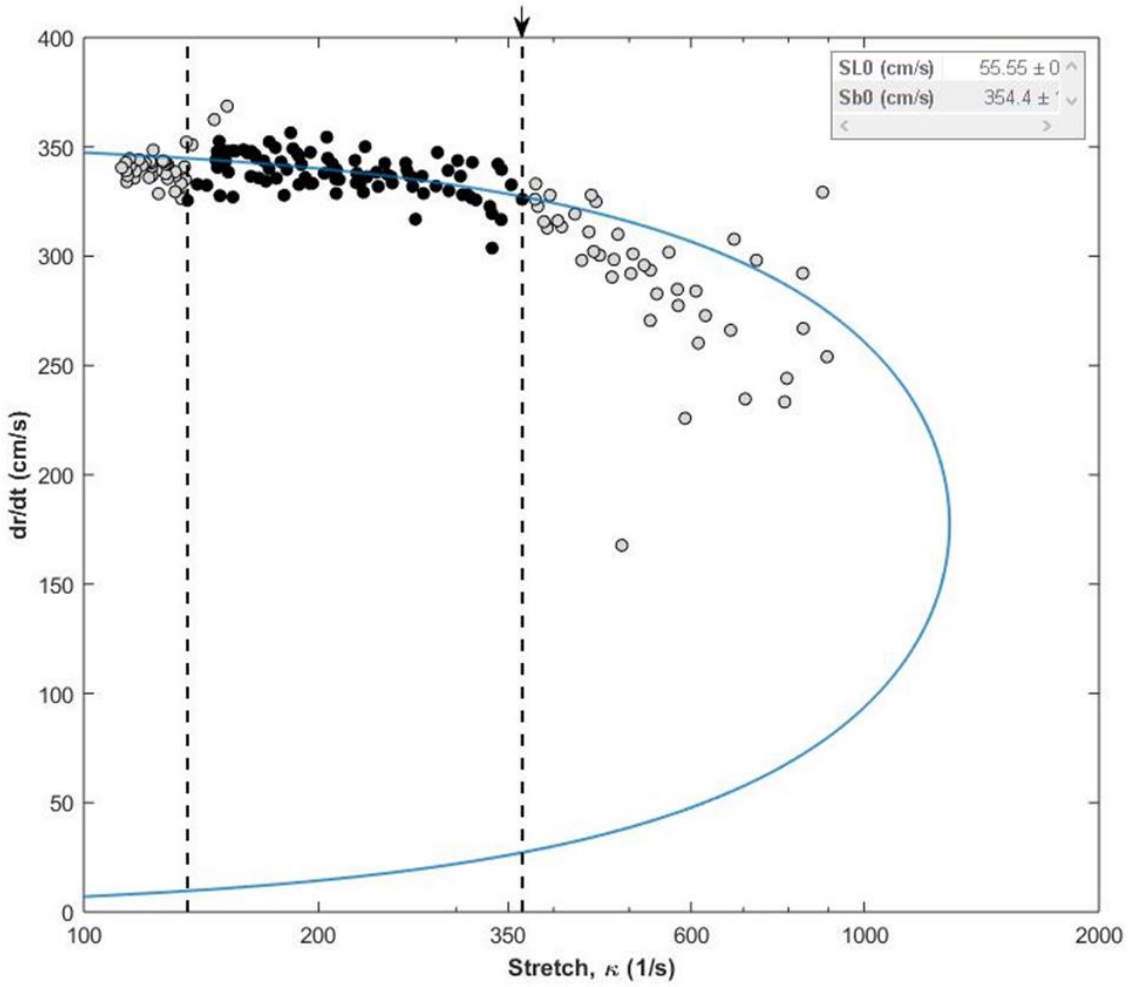

Figure A 9. Final S_b versus stretch plot for FM 1172 following the removal of wall and ignition affects. The open points are the points that have been excluded. The black dots are the data still included in the analysis.

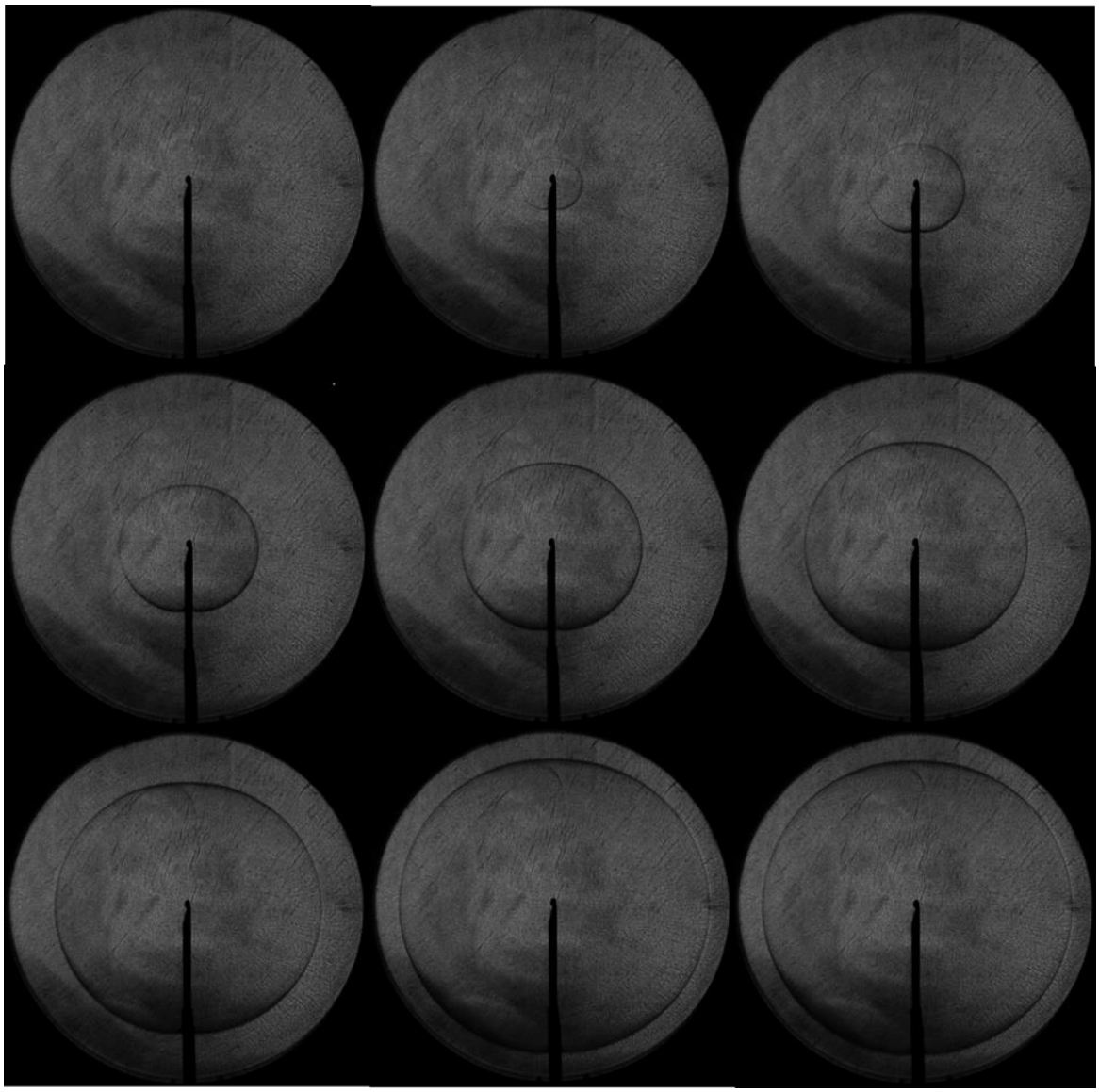

Figure A 10. Sample images for RP-1, taken from FM 1188, φ = 0.996. Image progression is from left to right top to bottom. This flame has a positive Markstein length (0.1451 cm).

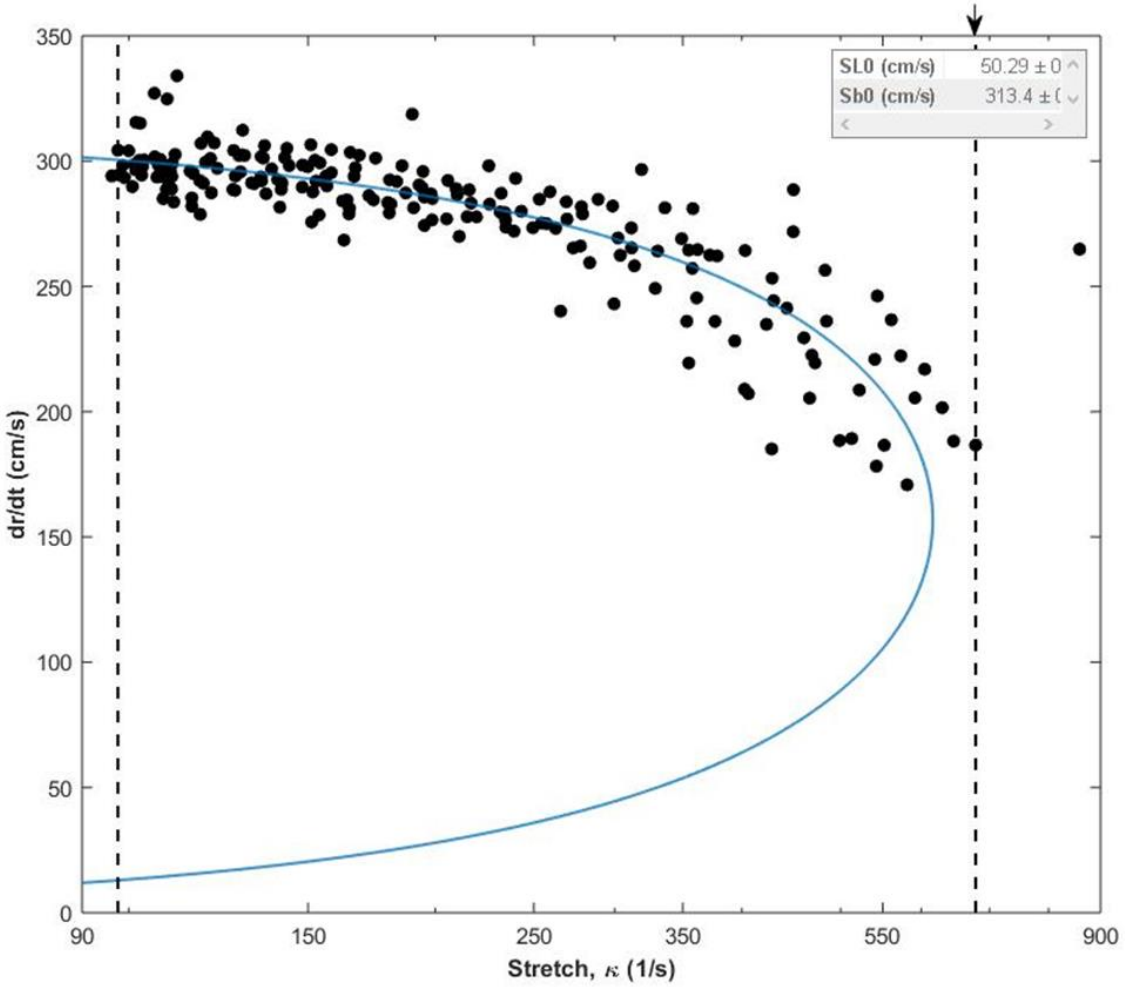

Figure A 11. Initial S_b versus stretch plot for RP-1 taken from FM 1188, prior to the removal of wall and ignition affects. Since the Markstein length is positive, nonlinear method I was used for analysis as indicated by the blue curve.

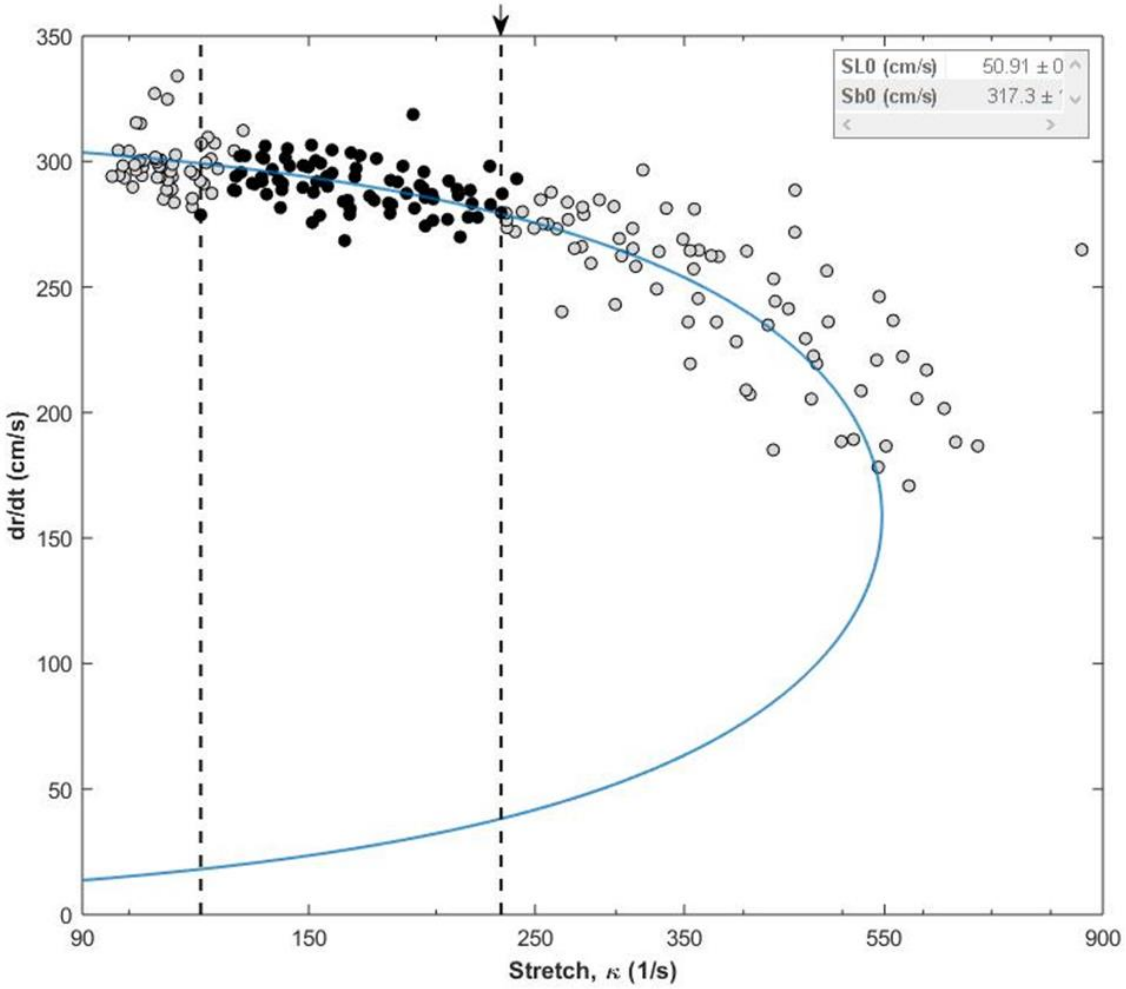

Figure A 12. Final S_b versus stretch plot for RP-1 (FM 1188) with wall and ignition affects removed. The open points are the points that have been excluded. The black dots are the data still included in the analysis.

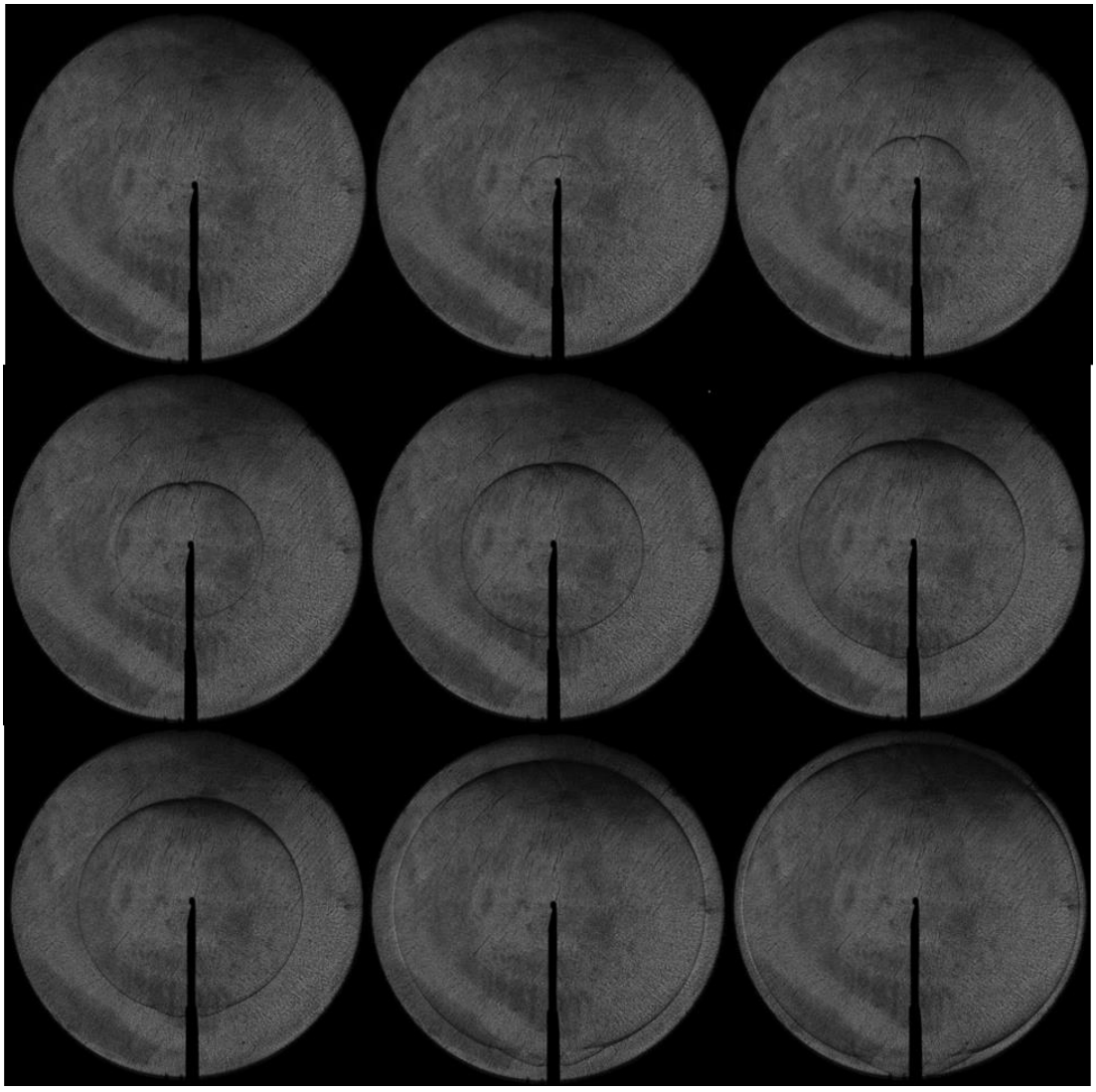

Figure A 13. Selected images for Diesel Fuel #2 (FM RUN 1239) at φ = 1.41. Image progression is from left to right top to bottom. This flame has a positive Markstein length (0.0544 cm). Early flame images the edge is very faint.

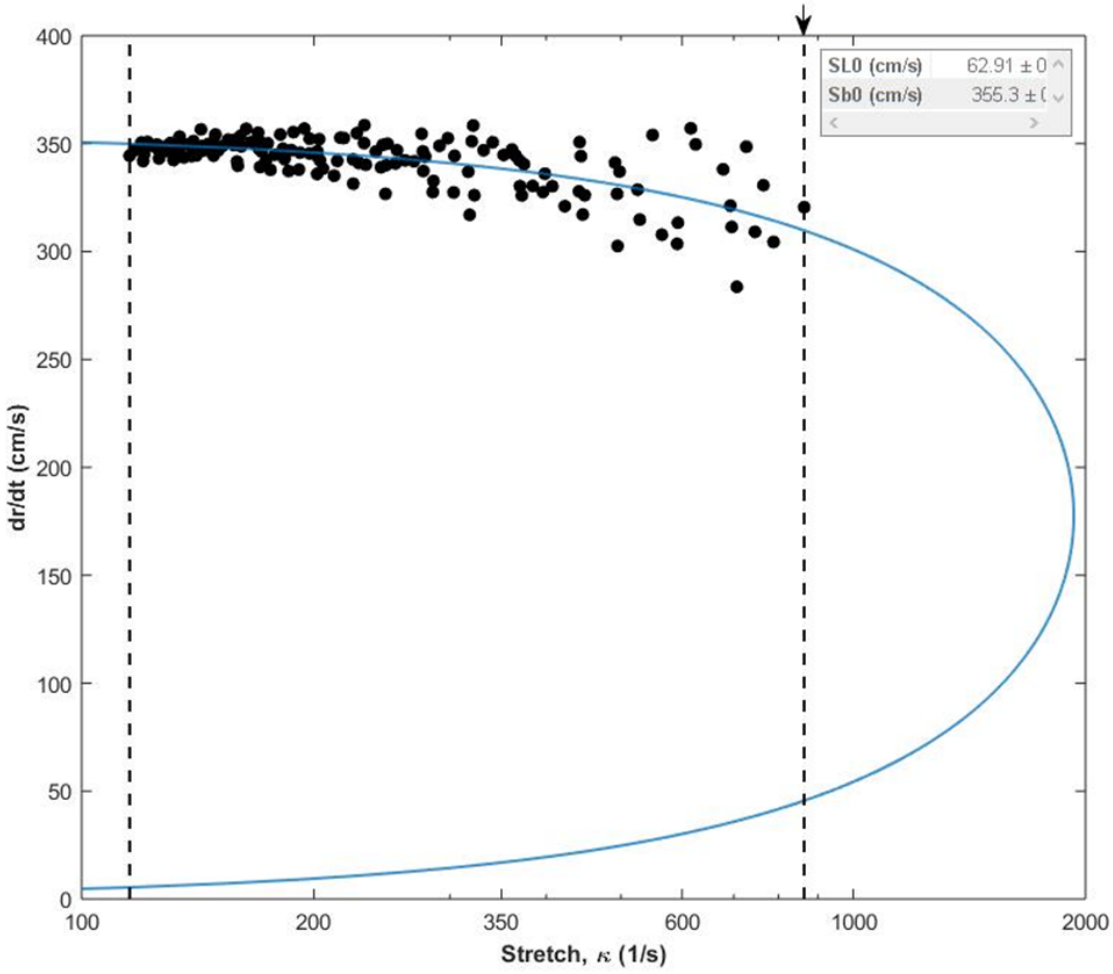

Figure A 14. S_b versus stretch plot for Diesel Fuel #2 (FM Run 1239) at φ = 1.41, prior to the removal of wall and ignition affects. Since the Markstein length is positive, nonlinear method I was used for analysis as indicated by the blue curve.

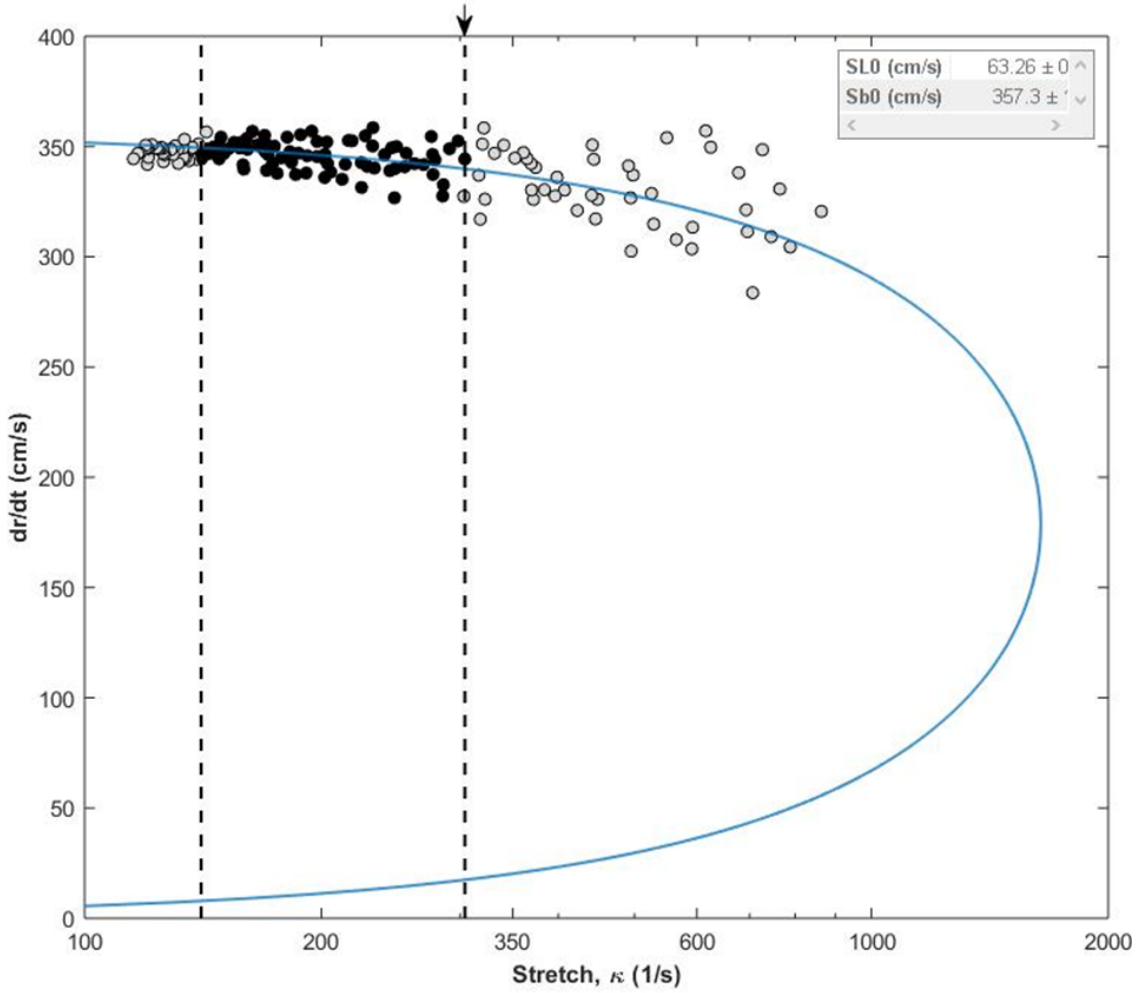

Figure A 15. Final S_b versus stretch plot for Diesel Fuel #2 (FM RUN 1239) following the removal of wall and ignition affects. The open points are the points that have been excluded. The black dots are the data still included in the analysis.

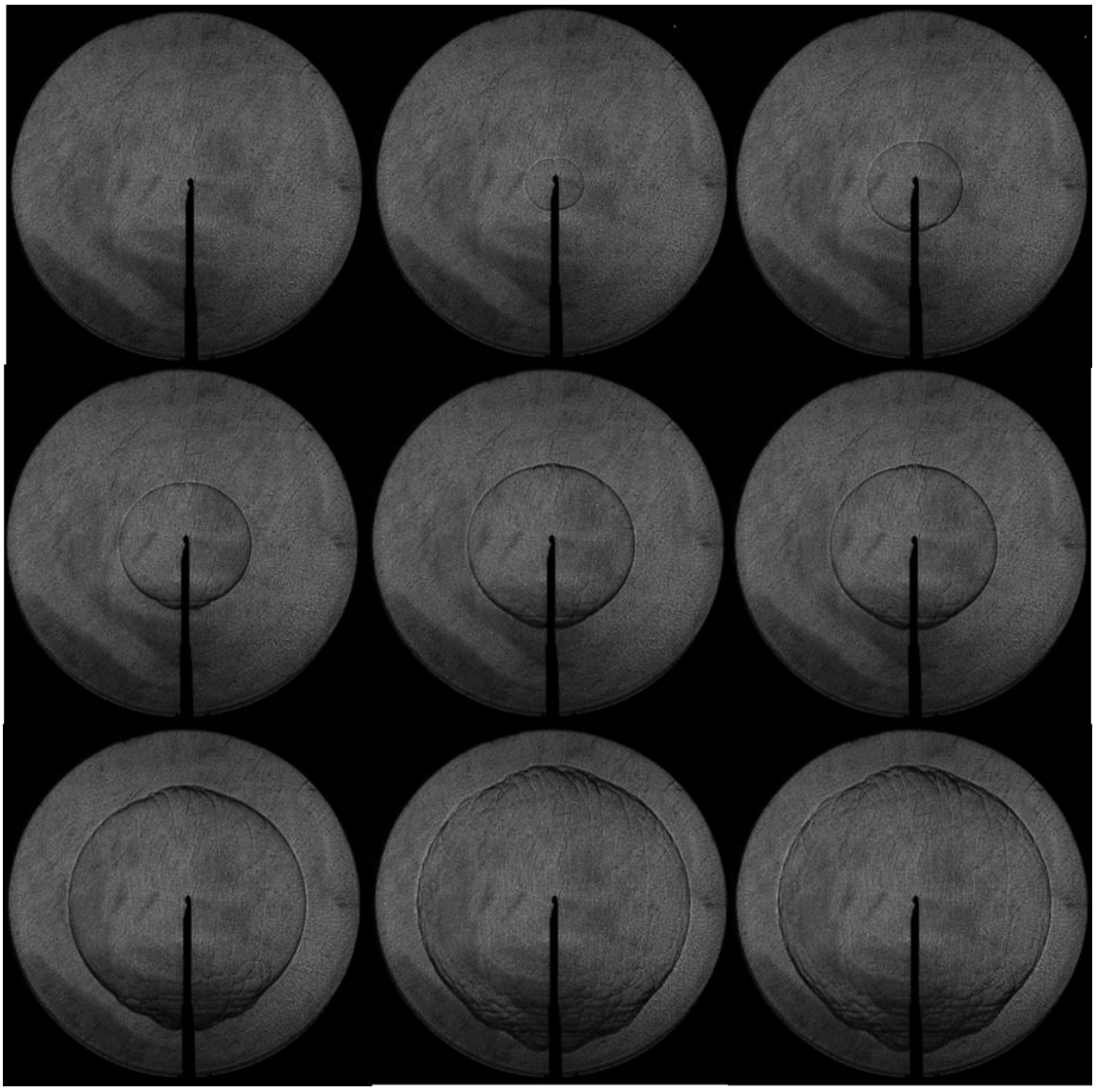

Figure A 16. Flame images for S-8 (FM 1206) at φ = 1.63. Image progress left to right top to bottom. This flame had a negative Markstein length, as indicated by the wrinkles developing in the later flame images.

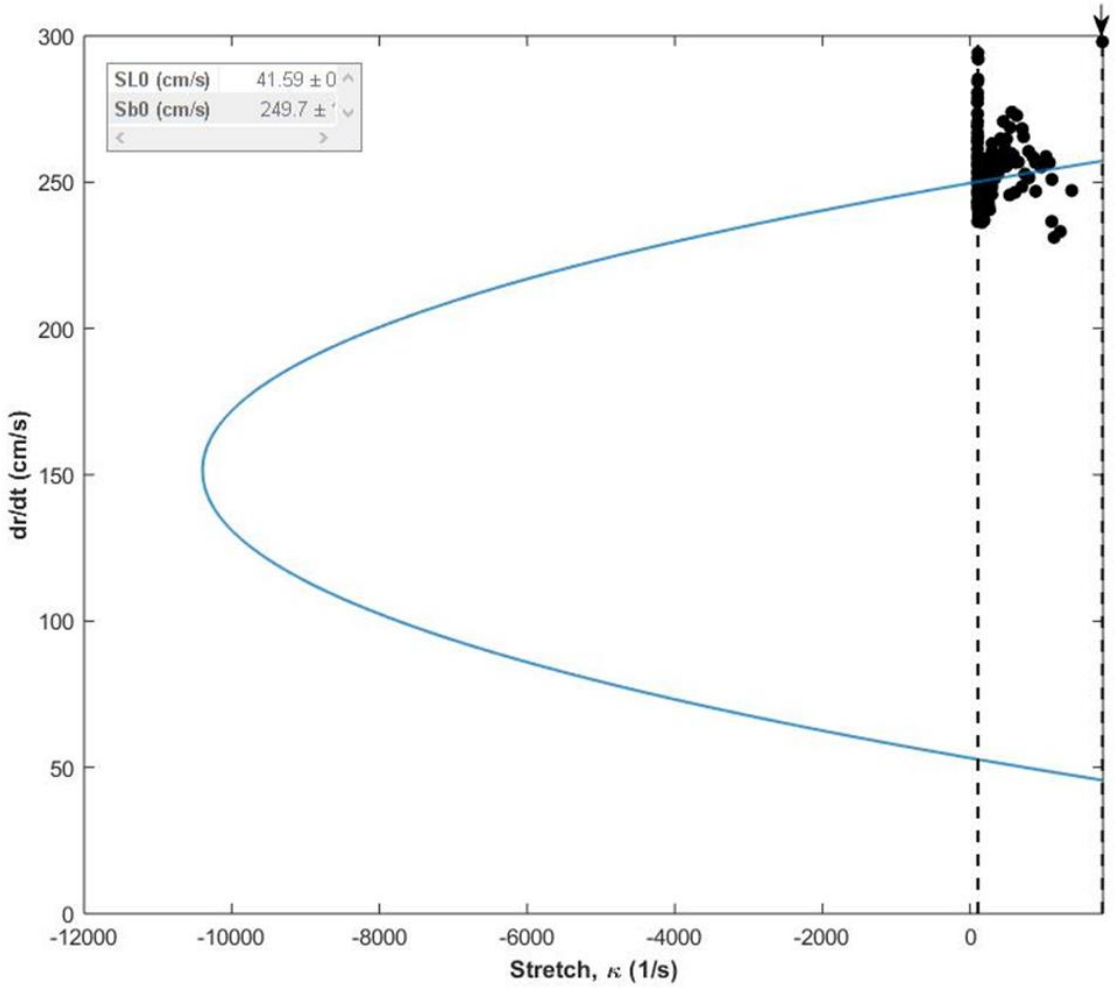

Figure A 17. Initial S_b versus stretch plot for S-8 (FM 1206) including wall and ignition affects. Since the Markstein length is negative the graph appears very different. The blue curve indicates the nonlinear method II values.

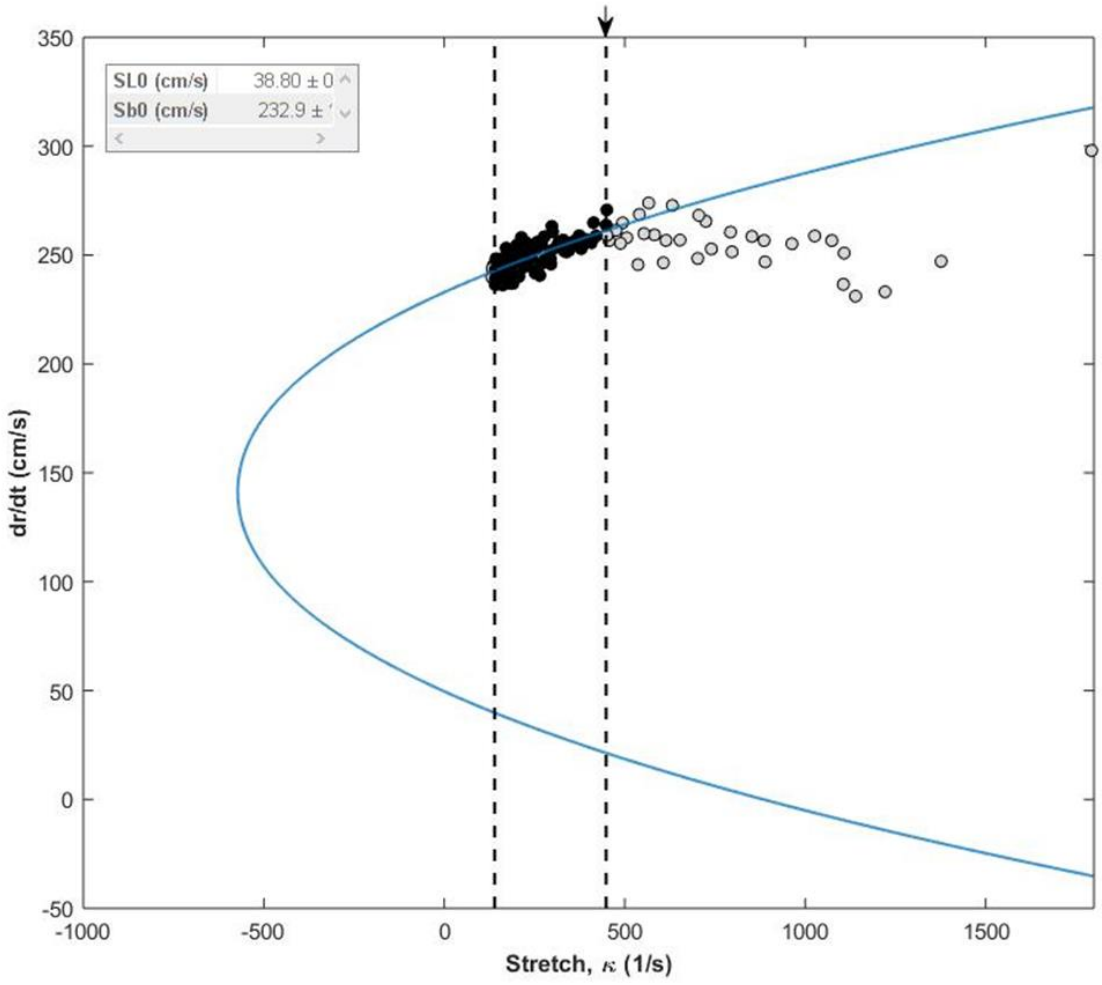

Figure A 18. Final Sb versus stretch plot for S-8 (FM 1206). The open points are the points that have been excluded. The black dots are the data still included in the analysis.

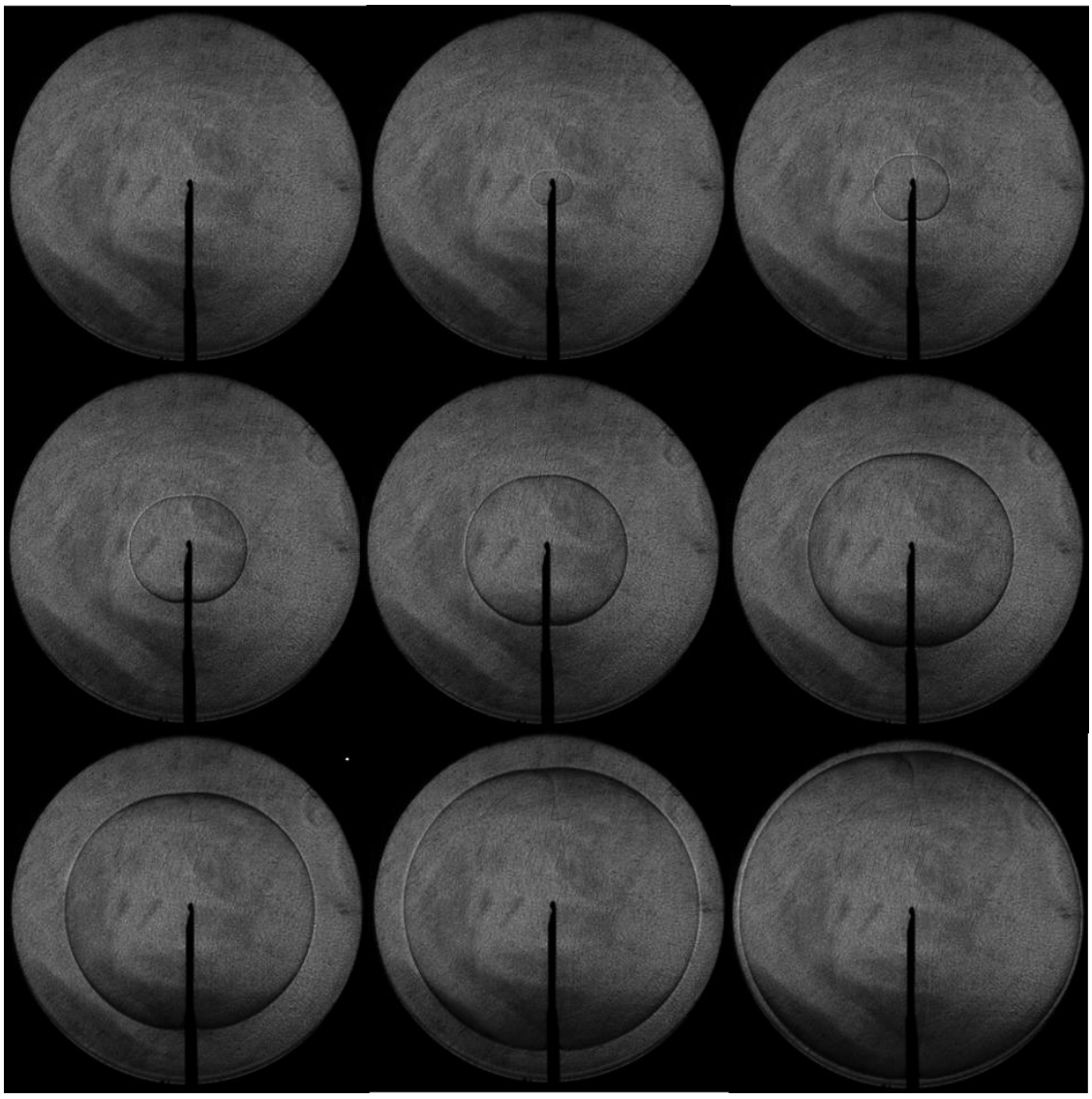

Figure A 19. Flame Images for Shell GTL (FM 1217) at φ = 0.85. Images progress left to right and top to bottom. Since this flame has a positive Markstein length the edge of the flame is very smooth.

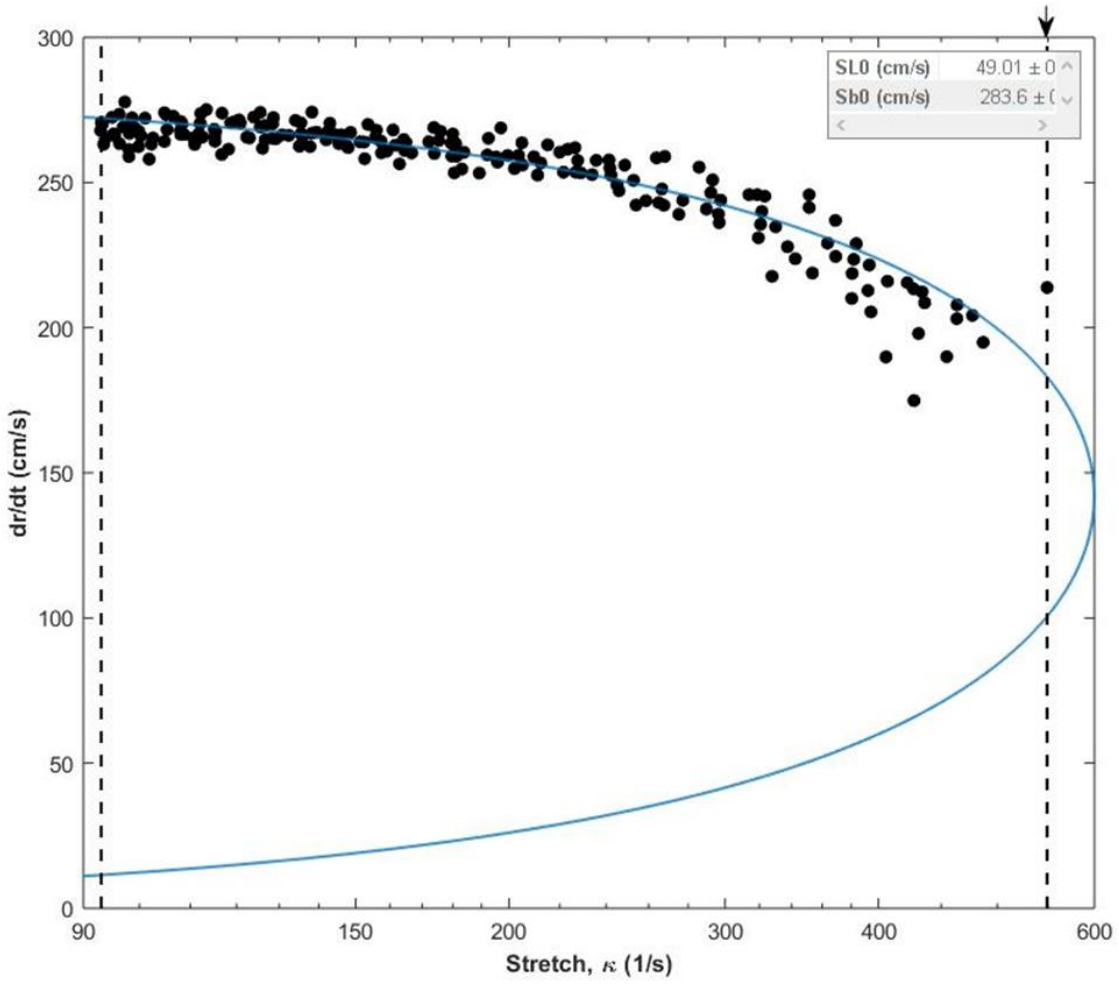

Figure A 20. Initial S_b versus stretch plot for Shell GTL (FM 1217), prior to the removal of wall and ignition affects. Since the Markstein length is positive, nonlinear method I was used for analysis as indicated by the blue curve.

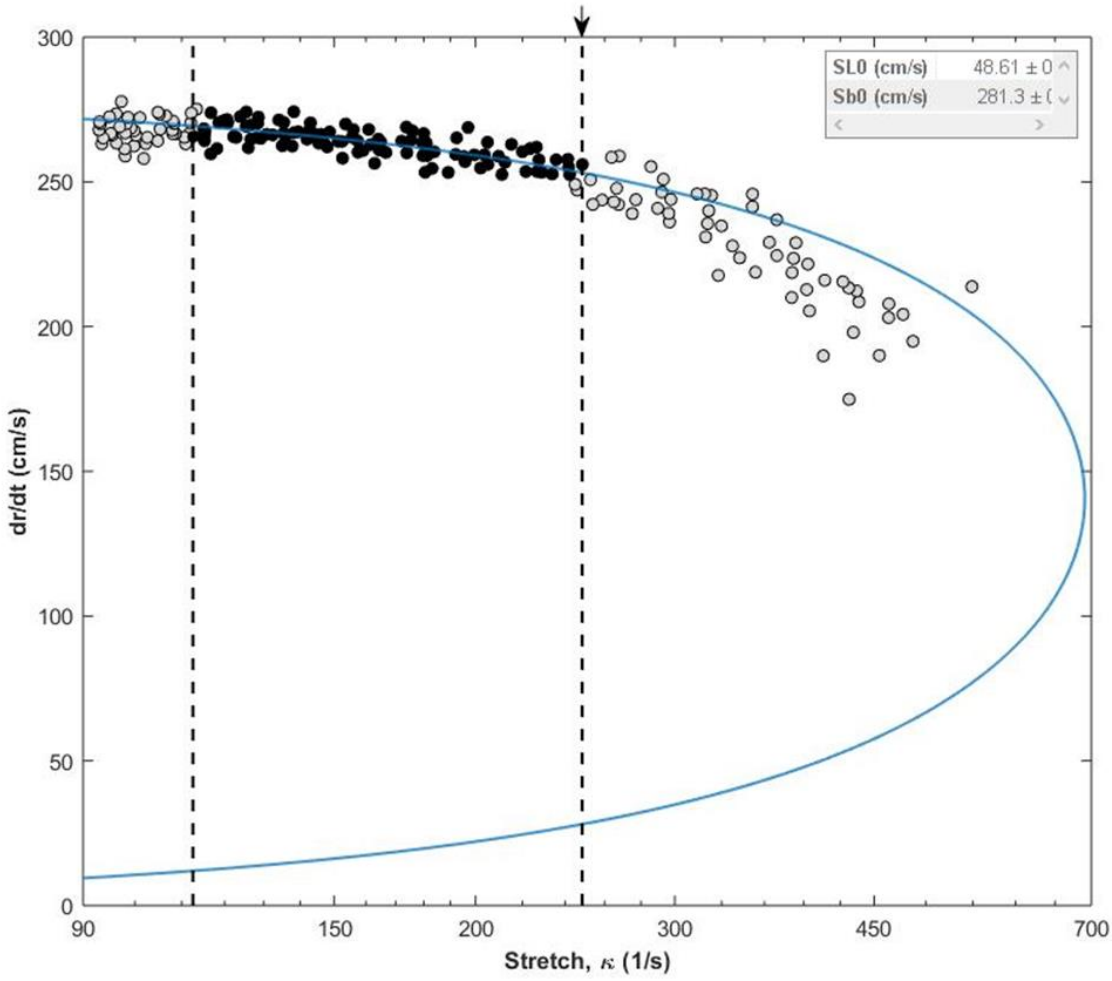

Figure A 21. Final Sb versus stretch plot for, with wall and ignition affects removed, for Shell GTL (FM 1217). The open points are the points that have been excluded. The black dots are the data still included in the analysis.